

**ANALYSIS AND COMPENSATION OF PMD EFFECTS IN HIGH
SPEED FIBER-OPTIC TRANSMISSION SYSTEMS USING
DIFFERENT MODULATION AND DETECTION SCHEMES**

by

MD. SAIFUL ISLAM

DOCTOR OF PHILOSOPHY



#105883#

**DEPARTMENT OF ELECTRICAL AND ELECTRONIC ENGINEERING
BANGLADESH UNIVERSITY OF ENGINEERING AND TECHNOLOGY**

May 2008

Analysis and Compensation of PMD Effects in High Speed Fiber-
Optic Transmission Systems Using Different Modulation and
Detection Schemes

A thesis submitted to the Department of Electrical and Electronic Engineering of
Bangladesh University of Engineering and Technology in partial fulfillment of the
requirement for the degree of

DOCTOR OF PHILOSOPHY IN ELECTRICAL AND ELECTRONIC
ENGINEERING

by

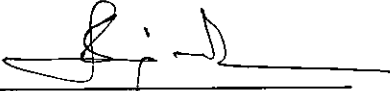

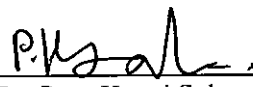
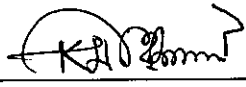

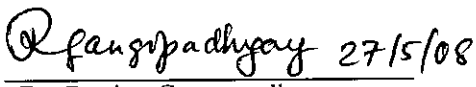
Md. Saiful Islam

DEPARTMENT OF ELECTRICAL AND ELECTRONIC ENGINEERING
BANGLADESH UNIVERSITY OF ENGINEERING AND TECHNOLOGY

May 2008

The thesis titled “**Analysis and Compensation of PMD Effects in High Speed Fiber-Optic Transmission Systems Using Different Modulation and Detection Schemes**” submitted by Md. Saiful Islam (Roll No.: P04040604P, Session: April/2004) has been accepted as satisfactory in partial fulfillment of the requirement for the degree of DOCTOR OF PHILOSOPHY IN ELECTRICAL AND ELECTRONIC ENGINEERING on May 27, 2008.

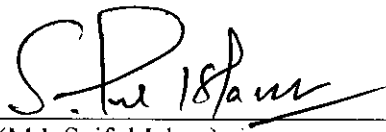
BORAD OF EXAMINERS

1. 
Dr. Satya Prasad Majumder
Professor & Head
Department of Electrical and Electrical Engineering
BUET, Dhaka-1000, Bangladesh
Chairman
(Supervisor & Ex-Officio)
2. 
Dr. A. B. M. Siddique Hossain
Professor
Department of Electrical and Electrical Engineering
BUET, Dhaka-1000, Bangladesh
Member
3. 
Dr. Pran Kanai Saha
Professor
Department of Electrical and Electrical Engineering
BUET, Dhaka-1000, Bangladesh
Member
4. 
Dr. Md. Kamrul Hasan
Professor
Department of Electrical and Electrical Engineering
BUET, Dhaka-1000, Bangladesh
Member
5. 
Dr. Md. Shah Alam
Associate Professor
Department of Electrical and Electrical Engineering
BUET, Dhaka-1000, Bangladesh
Member
6. 
Dr. Ranjan Gangopadhyay
Professor
Department of Electronics and Electrical
Communication Engineering, Indian Institute of
Technology (IIT), Kharagpur – 721302, India
Member (External)

DECLARATION

It is hereby declared that this thesis or any part of it has not been submitted elsewhere for the award of any degree or diploma.

Signature of the candidate


(Md. Saiful Islam)

DEDICATION

To my parents

ACKNOWLEDGEMENTS

I wish to express my sincere gratitude to my supervisor Prof. Satya Prasad Majumder for providing me the opportunity to work with him in the field of optical communication system. I would like to thank him for his constant guidance, encouragement and kind cooperation for my education and research over the past four and half years.

I would then like to thank my Ph. D program committee members, Prof. A. B. M. Siddique Hossain, Prof. Pran Kanai Saha, Prof. Md. Kamrul Hasan and Dr. Md. Shah Alam, for their generous help and numerous advices during every stage of my program. I have learned from them not only the knowledge but also the invaluable methodologies to solve problems.

My full-hearted thanks should go to my parents for their priceless and unconditional love to me. I will forever remain indebted to them. My full-hearted thanks should also go to my parents-in-law for their understanding, love and faith in me.

My deepest thanks from the bottom of my heart, of course, must go to my wife, Sanjida Islam for her love, mental support, constant encouragement and outmost patience without which nothing would have been possible. I sincerely would like to express my endless love to my two sons Sakib and Saif, who are my wish and always make me vital, confident and happy.

Finally, I express my highest gratitude to Almighty Allah Sub-ha-nu-tala for giving me the ability to explore the unknown world of fiber-optic of communications and to complete the Ph. D. degree in BUET.

ABSTRACT

Polarization Mode Dispersion (PMD) is a serious barrier that limits high-speed optical fiber telecommunication systems. PMD is the result of random birefringence in single-mode fibers along the transmission path. This leads to wavelength-dependent polarization states and phases at the output that eventually results in inter-symbol interference and system performance degradation.

In this thesis work, analytical models have been developed to assess and compensate for the effect of PMD considering different modulation and detection schemes; such as, intensity modulation-direct detection (IM-DD), continuous phase frequency shift keying (CPFSK) direct- and heterodyne detection. Based on the analytical model, the average BER performance of an IM-DD optical transmission system is evaluated considering Maxwellian distribution for the differential group delay (DGD). The probability density functions (pdfs) of the random output signal phase fluctuation due to PMD in a CPFSK direct- and heterodyne detection system are analytically developed. The pdf of the signal phase fluctuation is used to evaluate the average BER as a function of mean DGD. As the passive PMD mitigation techniques do not require any dynamically adjusted components and are bit rate independent, an analytical model of PMD compensation technique is also developed with several linecoding to make the single channel optical transmission system more tolerant to PMD.

The impact and compensation of PMD in multi-channel optical transmission system is also analytically investigated considering the interaction of cross-phase modulation (XPM) and PMD. XPM changes the state-of-polarization (SOP) of the channels through nonlinear polarization rotation and induces nonlinear time dependent phase shift for polarization components that leads to amplitude modulation of the propagating waves in a wavelength division multiplexing (WDM) system. The angle between the SOP changes randomly and as a result PMD causes XPM modulation amplitude fluctuation random in the perturbed channel. The pdf of the random angle fluctuation between the SOP of pump and probe due to PMD is determined analytically and the impact of PMD on XPM in a two channel pump-probe configuration is evaluated. To mitigate the PMD in a multi-channel transmission system, a high-birefringent adjustable linear chirped Bragg grating (LCFBG) based PMD compensation scheme is developed and its performance is evaluated using the optimum system parameters.

The results of this research work will find applications in the design of WDM transmission systems in presence of fiber nonlinear effects and PMD.

Table of Contents

Title page	i
Approval page	iii
Declaration	iv
Dedication	v
Acknowledgements	vi
Abstract	vii
Table of contents	viii
List of Tables	xiii
List Figures	xiv
List of symbols	xv
List of abbreviations and acronyms	xxi

Chapter 1 Introduction	1
1.1 Historical perspective of fiber optic communication system	1
1.2 Evolution of PMD and its characterization	3
1.2.1 Definition of PMD, birefringence and PMD vector	4
1.2.2 PMD in short and long fibers	8
1.2.3 The statistical nature of PMD	9
1.3 Literature review, motivation and research objectives	11
1.4 Outline of the thesis	16

Chapter 2	Bit error rate and effect of PMD in IM-DD transmission system	19
	2.1 Intensity modulation and optical coherent system	19
	2.2 Quantifying optical system penalty: BER expression	21
	2.2.1 Q-factor	23
	2.3 System model of IM-DD transmission system	26
	2.4 Theoretical analysis	26
	2.5 Results and discussion	30
	2.5.1 Analytical results and discussion	30
	2.5.2 Simulation results and discussion	32
	2.6 Summary	35
Chapter 3	Effect of PMD in direct detection CPFSK transmission system	36
	3.1 PMD effect in direct detection CPFSK system	36
	3.2 System model	38
	3.3 Theoretical analysis	39
	3.3.1 Transfer function considering PMD and GVD effects	40
	3.3.2 Optical signal input to the MZI pair 1 and 2	41
	3.3.3 Transmittance of MZI	42
	3.3.4 Photodetector output current	43
	3.3.5 Noise power	45
	3.3.6 Conditional BER expression	46
	3.3.7 PDF of random output phase and average BER	47
	3.4 Results and discussion	50
	3.4.1 Conditional BER performance	50
	3.4.2 Average BER performance	52
	3.4.3 Average BER considering Maxwellian distribution	54

	3.5 Summary	55
Chapter 4	Effect of PMD in heterodyne optical CPFSK transmission system	57
	4.1 Introduction	57
	4.2 Delay demodulation receiver model	59
	4.3 Theoretical analysis	59
	4.3.1 Conditional bit error probability	64
	4.3.2 PDF of the random output phase and average BER	65
	4.4 Results and discussion	66
	4.5 Summary	71
Chapter 5	Single channel PMD compensation	72
	5.1 PMD compensation strategies	72
	5.1.1 Optical PMD compensation technique	74
	5.1.2 Electronic PMD compensation technique	75
	5.1.3 Passive PMD compensation technique	76
	5.2 Line codes (modulation formats) in PMD compensation	76
	5.2.1 Order 1 line coding: a multi-level optical line code	78
	5.2.2 CPFSK modulation with linecoding	81
	5.3 Results and discussion	83
	5.3.1 Comparison among different line codes	88
	5.4 Summary	90
Chapter 6	Effect of PMD in multichannel optical transmission system	91
	6.1 Interaction of cross phase modulation and PMD	91
	6.2 Pump probe configuration system model	94
	6.3 Theoretical analysis for pump-probe configuration (2-ch. WDM)	94

6.4	WDM multi-channel system model	98
6.5	Theoretical analysis for multi-channel WDM system	99
6.5.1	Determining the PDF of $\theta_j(z)$ and BER expression	105
6.6	Results and discussion	107
6.6.1	Performance of pump-probe configuration	107
6.6.2	Performance of 4-channel WDM system	111
6.6.3	OptSim software simulation	115
6.7	Summary	119
Chapter 7	Chirped fiber Bragg grating in PMD compensation	121
7.1	Fiber grating in dispersion compensation	121
7.2	LCFBG based PMD compensation system model	124
7.3.1	Characteristics of birefringent chirped grating	125
7.3.2	The effect of strain and temperature on LCFBG	127
7.3.3	Mathematical modeling of fiber Bragg grating	130
7.3.4	Analytical solution of coupled mode equations	131
7.3.5	Group delay and DGD of the reflected wavelength	134
7.4	Results and discussion	136
7.4.1	Performance of the LCFBG based PMD compensator	136
7.4.2	LCFBG based PMD compensator in a WDM/IM-DD system	144
7.5	Summary	148
Chapter 8	Conclusions and future work	150
8.1	Summary of major contribution	150
8.2	Suggestions for future research	155

Bibliography	158
Appendix A	177
Appendix B	181
Publications	190

List of Tables

Table 2.1	Different simulation parameters for single channel IM-DD transmission system	35
Table 5.1	Summary of the encoding criteria for novel optical codes	80
Table 5.2	The assumptions and parameter used in computing the BER performance results.	88
Table 6.1	Set of parameters and assumptions used in the analysis	111
Table 6.2	Comparison of results between 2- and 4-channel WDM system	115
Table 6.3	Different simulation parameters for a 4-channel WDM system	119
Table 7.1	Set of LCFBG parameters used in the computation	144
Table 7.2	Simulation parameters of Hi-Bi LCFBG based PMD-WDM compensation scheme	148

List of Figures

Fig. 1.1	Stresses and modes in a single mode fiber [7]	5
Fig. 1.2	(a) Intrinsic and (b) Extrinsic mechanism of fiber birefringence [7]	6
Fig. 1.3	A pulse launched with equal power on the two birefringence axes x and y (fast and slow axes) of a short fiber segment gets separated by the DGD ($\Delta\tau$) at the output [8].	6
Fig. 1.4	The measured probability density function of DGD and the Maxwellian fit (dotted line) [7]	10
Fig. 2.1	Bit error probabilities	22
Fig. 2.2	Bit error rate (BER) versus Q-factor	25
Fig. 2.3	Schematic configuration of an optical transmission system	26
Fig. 2.4	Plots of conditional BER versus received optical power, P_s for a 10 Gb/s system impaired by PMD	31
Fig. 2.5	Plots of unconditional BER versus received optical power for a 10 P_s Gb/s system impaired by PMD	31
Fig. 2.6	Simulation setup for a single channel IM-DD transmission system	32
Fig. 2.7	(a) Eye diagram at the input (back-to-back) (b) Eye diagrams for different values of seed (using Monte Carlo simulation)	33
Fig. 2.8	(a) BER vs input optical power, (b) Q-value vs input optical power	34
Fig. 2.9	Power penalty vs normalized mean DGD	34
Fig. 3.1	Block diagram of an optical CPFSK transmission system with MZI based direct detection	38
Fig. 3.2	Low pass equivalent direct detection CPFSK system model considering PMD and chromatic dispersion	39
Fig. 3.3	Plots of conditional BER versus received power, P_s for direct detection CPFSK system impaired by PMD	51

Fig.3.4	PMD-induced power penalty as a function of DGD/ bit duration ratio ($\langle \Delta\tau \rangle / T$) for NRZ- and RZ-OOK, NRZ-2DPSK and NRZ-CPFSK system	52
Fig. 3.5	Average BER versus received power, P_s for direct detection CPFSK system impaired by PMD (modulation index, $h=0.50$)	53
Fig.3.6	Average BER versus received power, P_s for direct detection CPFSK system impaired by PMD (modulation index, $h=1.0$)	53
Fig.3.7	PMD-induced power penalty as a function of DGD/ bit duration ratio ($\langle \Delta\tau \rangle / T$) for NRZ- and RZ-OOK, NRZ-2DPSK and NRZ-CPFSK system.	54
Fig. 3.8	Plots of average BER versus received power, P_s for direct detection CPFSK receiver impaired by PMD (modulation index $h = 0.50$)	54
Fig. 3.9	Plots of average BER versus received power, P_s for direct detection CPFSK receiver impaired by PMD (modulation index, $h = 1.0$)	55
Fig. 4.1	Block diagram of a heterodyne CPFSK delay demodulation receiver	59
Fig. 4.2	Plot of conditional BER versus received power, P_s for heterodyne CPFSK impaired by PMD at modulation index 0.50	67
Fig.4.3	Plot of conditional BER versus received power, P_s for heterodyne CPFSK impaired by PMD at modulation index 1.00	68
Fig. 4.4	Plot of average BER versus received power, P_s for heterodyne CPFSK receiver impaired by PMD at modulation index 0.50	69
Fig. 4.5	Plot of average BER versus received power, P_s for heterodyne CPFSK impaired by PMD at modulation index 1.00	69
Fig. 4.6	PMD-induced power penalty (considering average BER) as a function of DGD/bit duration ($\langle \Delta\tau \rangle / T$) for NRZ- and RZ-OOK, NRZ-DPSK and heterodyne NRZ-CPFSK system.	70
Fig. 5.1	Model of an optical linecoder generator	78
Fig. 5.2	Unipolar NRZ and AMI RZ linecoding	78

Fig. 5.3	(a) Elementary signals and (b) code state diagram of novel order 1 code	79
Fig. 5.4	Order 1 novel optical coded signal	80
Fig. 5.5	Plot of average BER versus received power, P_s at modulation index 0.50 with delay modulation linecoding	83
Fig. 5.6	Plot of average BER versus received power, P_s at modulation index 1.0 with delay modulation linecoding	84
Fig. 5.7	Plot of average BER versus received power, P_s at modulation index 0.50 with Alternate Mark Inversion (AMI) linecoding	84
Fig. 5.8	Plot of average BER versus received power, P_s at modulation index 1.0 with Alternate Mark Inversion (AMI) linecoding	85
Fig. 5.9	Plot of average BER versus received power, P_s at modulation index 0.50 with Order 1 linecoding	86
Fig. 5.10	Plot of average BER versus received power, P_s at modulation index 1.0 with Order 1 linecoding	86
Fig. 5.11	PMD-induced power penalty as a function of DGD/bit duration ($\langle \Delta\tau \rangle / T$) for NRZ, DM, AMI and Order 1 linecoding of a CPFSK system (modulation index =0.50)	87
Fig. 5.12	PMD-induced power penalty as a function of DGD/bit duration ($\langle \Delta\tau \rangle / T$) for NRZ, DM, AMI and Order 1 linecoding of a CPFSK system (modulation index = 1.00)	87
Fig. 6.1	Block diagram of a pump-probe configuration with EDFA in cascade	94
Fig. 6.2	Block diagram of a multi-channel/WDM system with EDFA in cascade	99
Fig. 6.3	Plots of pdf of $\theta(z)$ at different length of fiber link length with a channel separation 0.8 nm and PMD coefficient 0.5 ps/ $\sqrt{\text{km}}$	108
Fig. 6.4	Plots of pdf of $\theta(z)$ at different length of fiber link length with a channel separation 0.4 nm and PMD coefficient 0.2 ps/ $\sqrt{\text{km}}$	108
Fig. 6.5	Plots of variance of pump and probe polarization SOP vs fiber link length for different PMD parameters	109
Fig. 6.6	Plots of average BER vs pump power for different channel spacing	109

Fig. 6.7	Plots of average BER vs probe power for different pump power	110
Fig. 6.8	Plots of variance of pump and probe polarization SOP vs channel spacing for different link length.	111
Fig. 6.9	Plots of pdf of $\theta_j(z) = \hat{P}_j \cdot \hat{S}(z)$ at different length of fiber	112
Fig. 6.10	Plots of average BER vs pump power for different channel spacing	113
Fig. 6.11	Plots of average BER vs channel 2 power for different pump power	114
Fig. 6.12	Average amplitude transfer function vs fiber link length	114
Fig. 6.13	Setup of the system simulation model for a 4-channel WDM/IM-DD for PMD and XPM interaction	116
Fig. 6.14	(a) input optical spectrum, (b) output optical spectrum	116
Fig. 6.15	(a) Base line eye diagram (back-to-back), (b) Channel 1- 4 at the output for a PMD coefficient of 0.5 ps/ $\sqrt{\text{km}}$; (c) Channel 1- 4 at the output for a PMD coefficient of 1.5 ps/ $\sqrt{\text{km}}$	117
Fig. 6.16	(a) BER vs input pump power, (b) Q-value (in dB) vs input pump power (for chromatic dispersion coefficient, $D_c = 0 - 6$ ps/nm-km)	118
Fig. 6.17	(a) BER vs PMD coefficient, (b) Q-value vs PMD coefficient (for chromatic dispersion coefficient, $D_c = 3$ ps/nm-km)	119
Fig. 7.1	System model of the PMD compensation scheme. The incoming signal has polarization components along both the fast- (P_f) and slow (P_s) axis. The LCFBG generates the required DGD for the Bragg reflected signal (λ_r), while it does not affect the signal (λ_0) outside the grating bandwidth	125
Fig. 7.2	A typical chirped Bragg grating	126
Fig. 7.3	(a) Schematic diagram of the strain gradient cantilever structure, (b) Schematic structure of the Hi-Bi linearly chirped FBG. The reflected signal is introduced as a DGD between the 's' (along the slow axis) and 'f' (along the fast axis) polarization components.	130
Fig. 7.4	Schematic of the grating with boundary conditions	132

Fig. 7.5	The relationship between fiber grating bandwidth and grating length	137
Fig. 7.6	The relationship between fiber grating reflectivity and grating length	138
Fig. 7.7	Reflected relative time delay for the fast- and slow axis of polarization	139
Fig. 7.8	Reflection spectrum for the LCFBG under stretching and compression. Wavelength tuning shifts the passband to longer- or shorter wavelength regime without changing the shape of the spectrum	140
Fig. 7.9	Plots of DGD versus wavelength under stretched- and compressed condition of the LCFBG inputting from the fast wavelength port	141
Fig. 7.10	Variation of the DGD between two polarizations as the LCFBG stretched (the stretching ratio is the change in the length of the fiber grating divide by its original length ($\varepsilon = \Delta L/L$)).	142
Fig. 7.11	DGD as a function of wavelength tuning (as a result of the displacement Y) at a given signal wavelength $\lambda_s = 1550.5$ nm	143
Fig. 7.12	Fig. 7.12: DGD as function of grating length for short- and long wavelength ports	143
Fig. 7.13	Hi-Bi LCFBG based 4-channel PMD compensation fiber-optic WDM transmission system model	145
Fig. 7.14	Hi-Bi LCFBG based WDM-PMD compensation module	145
Fig. 7.15	Simulation diagram of a 4-channel WDM-PMD compensation scheme	146
Fig. 7.16	Eye diagram for a 4-channel (each channel at 10 Gbps, NRZ modulation) with and without WDM-PMD compensation. The output signal is received after 400 km transmission	146
Fig. 7.17	Eye opening penalty (EOP) at a probability of 10^{-3} in the dependence of the mean DGD for 4-channel and single transmission system	147

List of symbols

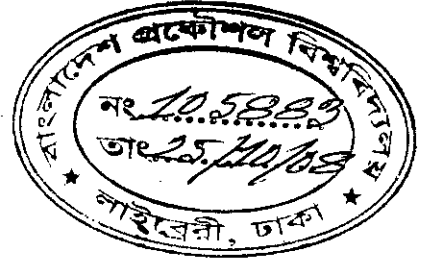
Δn_{eff}	Degree of birefringence
$\vec{\tau}$	Polarization mode dispersion vector
$\Delta\tau$	Differential group delay
\hat{p}	Direction of the PMD vector
β_s	Propagation constant along the slow axis
β_f	Propagation constant along the fast axis
n_s	Effective refractive index along the slow axis
n_f	Effective refractive index along the fast axis
$P_{\Delta\tau}(\Delta\tau)$	Maxwellian probability distribution function
f_{IF}	Intermediate frequency
$P(1/0)$	The probability of deciding 1 when 0 is received
$P(0/1)$	Probability of deciding 0 when 1 is received
σ_0^2	Noise variance for bit 0
σ_1^2	Noise variance for bit 1
T_0	Full width half maximum of the bit
T	Bit interval or bit period
i_m	Total output photo-detector current
ϕ_n	Phase noise of the transmitting laser
λ	Wavelength
R_b	Bit rate
$H_1(f)$	Fiber transfer function due to PMD and GVD along the slow PSP
$H_2(f)$	Fiber transfer function due PMD and GVD along the fast PSP
a_k	The random bit pattern of k th information
$\phi_s(t)$	The CPFSK modulating phase
$p(t)$	The elementary pulse shape
R_d	Responsivity of the photodetector
σ_m^2	Total noise power
ξ	Random output phase fluctuation due to ISI for random bit pattern
$\overline{\Delta\phi_s}$	Mean output phase error due to photodetector
f_c	Carrier frequency
P_T	The transmitted optical power
Δf	The peak frequency deviation

D	Chromatic dispersion L
L	Fiber length
h_{IF}	Impulse response of IF filter
$i_n(t)$	Total noise current
P_s	Output power at the fiber end
P_{Lo}	The local oscillator power
η	Phase distortion of the signal due to PMD and GVD
ρ	Intermediate frequency SNR
σ_k	Generic encoder state
ε	Small power penalty due to PMD
$ A_1\rangle$	Slow varying envelop of the pump (channel 1)
$ A_2\rangle$	Slow varying envelop of the probe (channel 2)
λ_1	Pump wavelength
λ_2	Low-power probe continuous wave
\hat{P}	Unit vector representing the SOP of the pump
\hat{S}	Unit vector representing the SOP of the probe
D_p	Polarization mode dispersion coefficient
$\theta(z)$	Random angle between the pump and probe SOP
S_0	The unperturbed probe power
P_0	The pump power
n_{eff}	Effective refractive index
$\delta n(z)$	Perturbation to the effective refractive index
v	Fringe visibility of the index change
Λ	Fiber grating period
λ_B	Bragg wavelength
κ	AC coupling coefficient
$\bar{\sigma}$	General dc (period averaged) self-coupling coefficient
$\Delta\lambda$	Grating bandwidth
τ_R	Time delay for light reflected of a grating
$R(\lambda)$	Reflectivity or power reflection coefficient
ρ_e	Photo-elastic coefficient
$B(\omega)$	Fiber birefringence
$\tilde{\chi}^{(3)}$	Instantaneous electronic response of the nonlinear medium
$P^{(3)}$	Third-order nonlinear polarization

List of abbreviations and acronyms

AMI	Alternate Mark Inversion
ASE	Amplified Spontaneous Emission
ASK	Amplitude Shift Keying
BER	Bit Error Rate
BPPM	Binary Pulse Position Modulation
CD	Chromatic Dispersion
CPFSK	Continuous Phase Shift Keying
CRZ	Chirped Return to Zero
DEMUX	Demultiplexer
DFE	Decision Feedback Equalizer
DGD	Differential Group Delay
DM	Delay Modulation
DMS	Dispersion Managed Solitons
DPSK	Differential Phase Shift Keying
DWDM	Dense Wavelength Division Multiplexing
EDFA	Erbium Doped Fiber Amplifier
FBG	Fiber Bragg Grating
FEC	Forward Error Correction
FSK	Frequency Shift Keying
FWM	Four Wave Mixing
GVD	Group Velocity Dispersion
Hi-Bi	High-Birefringence
IF	Intermediate Frequency
IID	Independent and Identically Distributed
IM-DD	Intensity Modulation – Direct Detection
ISI	Inter-symbol Interference
ITU	International Telecommunication Union

LCFBG	Linear Chirped Fiber Bragg Grating
LED	Light Emitting Diode
MLDS	Maximum Likelihood Detection Scheme
MUX	Multiplexer
MZI	Mach-Zehnder Interferometer
NRZ	Non-return to Zero
NPR	Nonlinear Polarization Rotation
OFD	Optical Frequency Discriminator
OOK	On-Off Keying
OSNR	Optical Signal-to-Noise Ratio
PBS	Polarization Beam Splitter
PDF	Probability Density Function
PDL	Polarization Dependent Loss
PMD	Polarization Mode Dispersion
PMF	Polarization Maintaining Fiber
PSD	Power Spectral Density
PSK	Phase Shift Keying
PSP	Principal State of Polarization
RZ	Return to Zero
SCNR	Signal to Crosstalk Noise Ratio
SMF	Single Mode Fiber
SNR	Signal-to-Noise Ratio
SOP	State of Polarization
SPM	Self Phase Modulation
TF	Transversal Filter
WDM	Wavelength Division Multiplexing
WWW	World Wide Web
XPM	Cross Phase Modulation



Chapter 1

INTRODUCTION

Due to the tremendous growth of Internet and World Wide Web (WWW), the data rate of current optical system has been pushed to 10 Gbit/s~ 40 Gbit/s and beyond. However, at these data rates polarization mode dispersion (PMD) constitutes one of the main limiting factors for reliable optical fiber communication system. In this chapter, at first we give an historical perspective of optical communication then provide some key concepts of PMD, literature review, motivation of the research work and its objectives, and finally an overview the thesis work.

1. 1 Historical perspective of fiber optic communication systems

Even though an optical communication system had been conceived in the late 18th century by a French Engineer Claude Chappe who constructed an optical telegraph, electrical communication systems became the first dominant modern communication method since the advent of telegraphy in the 1830s. Until the early 1980s, most of fixed (non-radio) signal transmission was carried by metallic cable (twisted wire pairs and coaxial cable) systems. However, large attenuation and limited bandwidth of coaxial cable limited its capacity upgrade.

The bit rate of most advanced coaxial systems which was put into service in the United States in 1975 was 274 Mbit/s. At around the same time, there was a need of conversion from analog to digital transmission to improve transmission quality, which requires further increase of transmission bandwidth. Many efforts were made to overcome drawbacks of coaxial cable during 1960s and 1970s. In 1966, Kao and Hockham [1] proposed the use of optical fiber as a guiding medium for optical signal. Four years later, a major breakthrough occurred when the fiber loss was reduced to about 20 dB/km from previous values of more than 1000 dB/km. Since that time, optical communication technology has developed rapidly to achieve larger transmission capacity and longer transmission distance. The capacity of transmission has been increased about 100 fold in every 10 years.

The first generation of optical communication was designed with multi-mode fibers and direct bandgap GaAs light emitting diodes (LEDs), which operate the 800 nm – 900 nm wavelength range. Compared to the typical repeater spacing of coaxial system (~ 1 km), the longer repeater spacing (~ 10 km) was a major motivation. Large modal dispersion of multi-mode fibers and high fiber loss at 850 nm (> 5 dB/km) limited both the transmission distance and bit rate. In the second generation, multi-mode fibers were replaced by single-mode fibers, and the center wavelength of light sources was shifted to 1300 nm, where optical fibers have minimum dispersion and lower loss of about 0.5 dB/km. However, there was still a strong demand to increase repeater spacing further, which could be achieved by operating at 1500 nm where optical fibers have an intrinsic minimum loss around 0.2 dB/km. Larger dispersion in 1550 nm window delayed moving to a new generation until dispersion shifted fiber became available. Dispersion shifted fibers reduce the large amount of dispersion in the 1550 nm window by modifying the index profile of the fiber while keeping the benefit of low loss at the 1500 nm window.

An important advancement was that an erbium-doped single mode fiber amplifier (EDFA) at 1550 nm was found to be ideally suited as an amplifying medium for modern fiber optic communication systems. Invention of EDFA had a profound impact especially on the design of long-haul undersea system, The EDFA band, or the range of wavelengths over which the EDFA can operate, proved to be an important factor in fixing the wavelength of operation of present day fiber optic systems. The EDFA band is wide enough to support many wavelengths simultaneously. This led to the development of wavelength division multiplexing (WDM) systems or the simultaneous propagation of several wavelengths of light through a fiber, where each wavelength can carry a different data stream.

In the late 1990s, the demand for bandwidth, especially with the huge growth of the Internet, fueled a rapid increase in the data rates. As the number of channels and data rates rose, certain phenomenon such as chromatic dispersion (CD) and nonlinearities began to show up as obstacles. CD being deterministic in nature could be effectively compensated for by using special fibers called dispersion compensating fibers and other novel devices. At high bit rates (≥ 10 Gb/s) PMD constitutes the ultimate impairment for the transmission of optical signals. Digital signals propagating through an optical fiber with PMD may be broadened during transmission and as a consequence spread beyond their allocated bit slot and interfere with neighboring bits. Researchers in late 1980s and early 1990s realized that PMD would have to be addressed because of its significant impact on the performance of multi-gigabit per second optical communication systems operating over the embedded optical fiber network [2]-[6].

1.2. Evolution of PMD and its characteristics

Polarization effects have historically played a minor role in the development of lightwave systems. The primary reason for this is that commercial optical

receivers detect optical power rather than the optical field and thus are insensitive to polarization. In recent years the importance of polarization in lightwave systems has dramatically grown as a result of two developments. First, due to the EDFA invention, optical path has dramatically increased and small effects as PMD accumulate in a span to the point where it becomes an important consideration for lightwave system developers. The second reason is that polarization effects have become important as the transmitter and receiver technologies pushed to Gb/s speed. The basic concepts of PMD and its cause are discussed in the following sections.

1.2.1 Definition of PMD, birefringence and PMD vector

A single-mode fiber is designed to support only one mode of propagation of light. The principal advantage of letting light propagate along only one mode is that inter-modal dispersion can be avoided. Inter-modal dispersion happens as a result of relative delay between the light propagating in the various modes in a multi-mode fiber. In single-mode fibers, as there is only one mode available for light propagation, inter-modal dispersion is non-existent. In reality, however, there are two degenerate modes of light even though a single-mode fiber which are orthogonally polarized. These degenerate modes will have the same mode index (n), only when the core of the fiber is perfectly cylindrical (*i.e.*, it has a uniform diameter). In spite of the measures taken to provide a symmetrical core cross-section, there is some asymmetry and the degeneracy is broken. The reasons for birefringence in single-mode fiber can be broadly classified as intrinsic and extrinsic. Intrinsic factors are those that are present in the fiber right from the manufacturing stage. It is not possible to produce a perfectly cylindrical glass fiber with no internal defect, although research on improving the manufacturing process has led to more pure and highly circular fiber cores and thus minimal asymmetry results. PMD levels are typically $< 0.1 \text{ ps}/\sqrt{\text{km}}$ for

such fibers. Extrinsic factors are those which induce birefringence in a fiber after its manufacture. Stress induced by cabling, micro or macro-bending (such as drum wrapping, kinking over sharp object), twisting, side pressure and temperature etc. are extrinsic factors. The extrinsic birefringence can occur due to environmental factors or during cabling process and the birefringence values produced by these effects are on the order of 10^{-5} - 10^{-7} , which is much smaller than core/cladding index difference ($\sim 10^{-3}$). Fig. 1.1 illustrates how stress can induce asymmetry in the fiber core and Fig.1.2 illustrates the intrinsic and extrinsic mechanism of fiber birefringence.

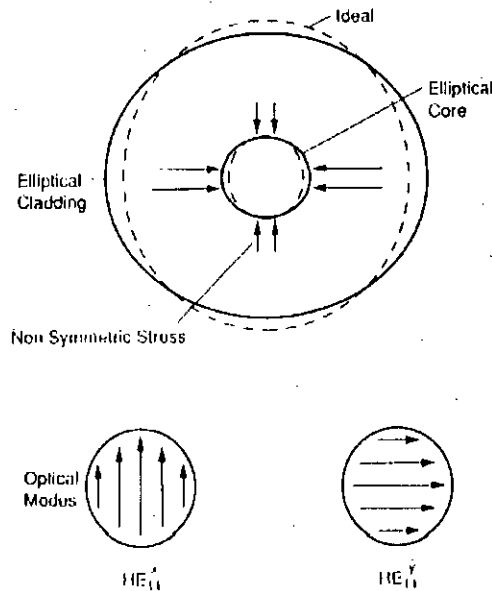


Fig. 1.1: Stresses and modes in a single mode fiber [7]

The consequence of this asymmetry of core cross-section is the existence of birefringence and two modes will experience a different mode index. The difference between these two indices is known as degree of birefringence, $\Delta n_{eff} = |n_f - n_s|$. As a result of birefringence, a signal launched into a fiber at a particular state of polarization, it is decomposed into two orthogonally polarized components that propagate with different propagation characteristics. The pulses

arrive at the output is differentially delayed. This difference between the delays is termed as the differential group delay (DGD). It is this DGD ($\Delta\tau$) that causes an input pulse to appear broadened at the output and this effect on the pulse is commonly called PMD. Although the PMD disturbances on the fiber are relatively small in magnitude, they tend to be random over the length of the fiber owing to their nature. Accumulation of these random little effects over the fiber is enough to cause system outages in high-speed optical data links. Fig. 1.3 illustrates the effect of birefringence on a pulse input into a short fiber segment.

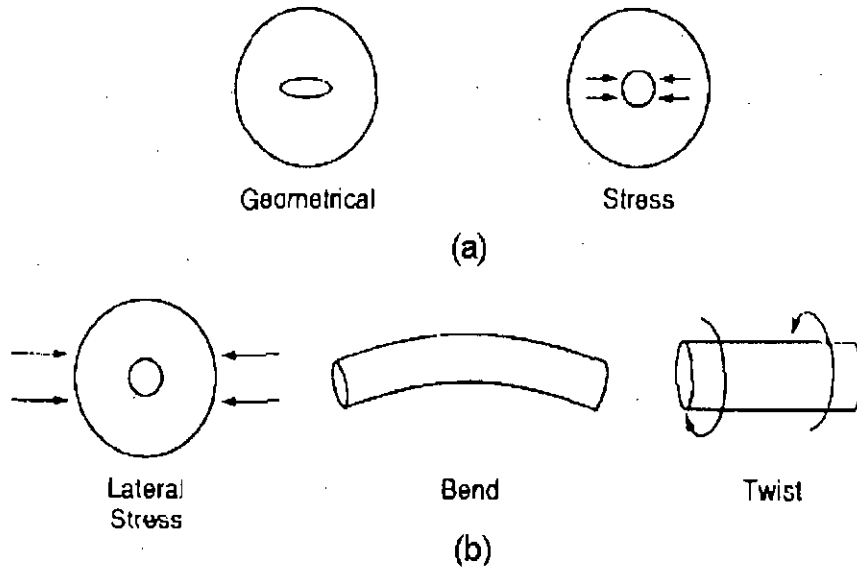


Fig. 1.2: (a) Intrinsic and (b) Extrinsic mechanism of fiber birefringence [7]

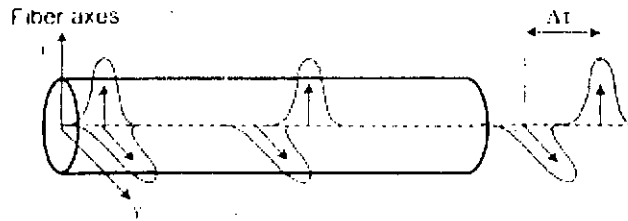


Fig. 1.3: A pulse launched with equal power on the two birefringence axes x and y (fast and slow axes) of a short fiber segment gets separated by the DGD at the output [8].

Fibers for which Δn_{eff} is large ($\sim 10^{-4}$) are called highly-birefringent (Hi-Bi) fibers. In general, the net effect of launching a signal with an arbitrary state of polarization into a piece of Hi-Bi fiber will give two replicas of the input signal, polarized at different orthogonal states of polarization and with a relative time shift between them. The input state of polarization which yields the lowest value of refractive index (n) is called the fast state of polarization and likewise the input state of polarization which yields the highest value of n is known as the slow input state of polarization.

In the absence of polarization dependent losses, the input (output) states of polarization are mutually orthogonal. These states are commonly referred as principal states of polarization (PSPs). The differential transmission time of the two undistorted signals polarized along mutually orthogonal states of polarization constitutes the first order effect of PMD. Both the PSPs and the DGD are assumed to be independent of frequency if only first order PMD effects are being considered. Using PSP concept, PMD can be characterized as a vector and represented as [8]:

$$\vec{\tau} = \Delta\tau \hat{p} \quad (1.1)$$

The PMD vector is a vector in 3- dimensional space (Stokes space). The length of the vector ($\Delta\tau$) is the DGD and the direction of the vector (\hat{p}) is along the axis that joins the two PSP points in Stokes space. Any input state of polarization (SOP) can be expressed as the vector sum of two components, each component being aligned with one of the PSPs. For a narrow band source (*i.e.*, considering only the first order PMD) the output electric field vector from a fiber can be given as [4],[7]:

$$\vec{E}_{\text{out}}(t) = c_+ \hat{p}_+ \vec{E}_m(t + \tau_+) + c_- \hat{p}_- \vec{E}_m(t + \tau_-) \quad (1.2)$$

where, $\vec{E}_{out}(t)$ and $\vec{E}_{in}(t)$ are output and input electric field vectors respectively. c_+ and c_- are complex coefficients required to indicate the field amplitude launched along the slow PSP and fast PSP respectively. The magnitudes $|c_+|$ and $|c_-|$, correspond to the power splitting ratio γ . \hat{p}_+ and \hat{p}_- are unit vectors specifying the output polarization states (referred as output PSPs) of the two components. The difference $(\tau_+ - \tau_-)$ is the DGD. This relation shows the amount of broadening of the output pulse due to PMD is dependent upon the values of the quantities $\Delta\tau$, c_+ and c_- .

1.2.2 PMD in short and long fibers

The effects of birefringence and PMD are considered differently for short and long single-mode fiber spans. All telecommunication fibers fall in the 'long' fiber category. Understanding the PMD mechanism in 'short' fibers would help explain the mechanism in the 'long' fibers. In short fiber segment, the stresses can be considered to be acting uniformly along the length. The single-mode fiber segment becomes bi-modal due to the birefringence induced by these stresses. The propagation constants along the two (propagation) modes are slightly different. Therefore, a differential delay develops in the fiber segment, which is capable of broadening the input pulse. Mathematically this can be explained as follows [7]:

If β_s and β_f are the propagation constants along the slow and fast propagation modes respectively and if n_f and n_s are their effective refractive indices, then:

$$\beta_s - \beta_f = \frac{\omega n_s - \omega n_f}{c} = \frac{\omega \Delta n}{c} \quad (1.3)$$

where, ω and c are angular frequency of the light signal and free space velocity of light respectively. The differential group delay, expresses as group delay per

unit length is obtained from equation (1.3) by taking the frequency derivative of the propagation constants.

$$\frac{\Delta\tau}{L} = \frac{d}{d\omega}(\beta_s - \beta_f) = \frac{\Delta n}{c} - \frac{\omega}{c} \frac{d(\Delta n)}{d\omega} \quad (1.4)$$

The group delay per unit length term $\Delta\tau/L$ is commonly known as the PMD coefficient of a fiber. Its unit is ps/km.

As mentioned earlier, since all telecommunication grade fibers fall in the 'long' fiber category, it is necessary to bring out their differences from the 'short' fibers. The relation between PMD induced delay and fiber length is no longer linear in the case of long fibers. This is because of the phenomenon called mode coupling that is taking place in all fibers longer than a certain statistical length called correlation length. The correlation length can vary between a few meters to more than kilometers depending on whether it is spooled or a cabled fiber. Telecommunication grade fibers will typically have a value of 100 m. Fibers that are longer than the correlation length is considered to belong to the 'long' fiber category. As a lightwave propagates down the long fiber, there is a constant sharing of energies between the two propagating modes. The random exchange of energies (also called mode coupling) is due to the varying stresses or perturbations that are experienced by the fiber along its length. The mode coupling process allows the DGD to grow proportionally to the square root of the length of the link rather than a linear dependence [5]. The DGD does not grow linearly with length in highly mode coupled fibers because the coupling between segments reduces the accumulated DGD, *i.e.*, when the slow PSP of one segment is very nearly aligned with the fast PSP of the next or previous segment the DGD of both segments will cancel each other out. However, in either case, PMD causes dispersion or broadening of the lightwave signal. Whereas this broadening is predictable in the case of 'short' length fibers, it is probabilistic for 'long' length fibers.

1.2.3 The statistical nature of PMD

The intersymbol interference (ISI) caused by pulse spreading due to PMD has a different origin from the ISI caused by the chromatic dispersion in the fiber. The latter one is deterministic, grows linearly with distance and can be compensated by using dispersion compensating fibers or any other commercially available dispersion compensation technique [9]. PMD however is a stochastic process [10]. The random configuration of birefringence which causes PMD depends on the stress induced by spooling, cabling, temperature changes and any other environmental factor that may cause the core of the fiber to deviate from being perfect cylindrical. The statistical properties of PMD theoretically and experimentally studied [11]-[14]. It was found that the evolution of DGD at particular frequency over time yield a Maxwellian probability density function given by equation (1.5). Fig. 1.4 illustrates how the plot of measured DGD closely matches that of Maxwellian function.

$$P_{\Delta\tau}(\Delta\tau) = \frac{32\Delta\tau^2}{\pi^2 \langle \Delta\tau \rangle^3} \exp\left(-\frac{4\Delta\tau^2}{\pi \langle \Delta\tau \rangle^2}\right) \quad \Delta\tau > 0 \quad (1.5)$$

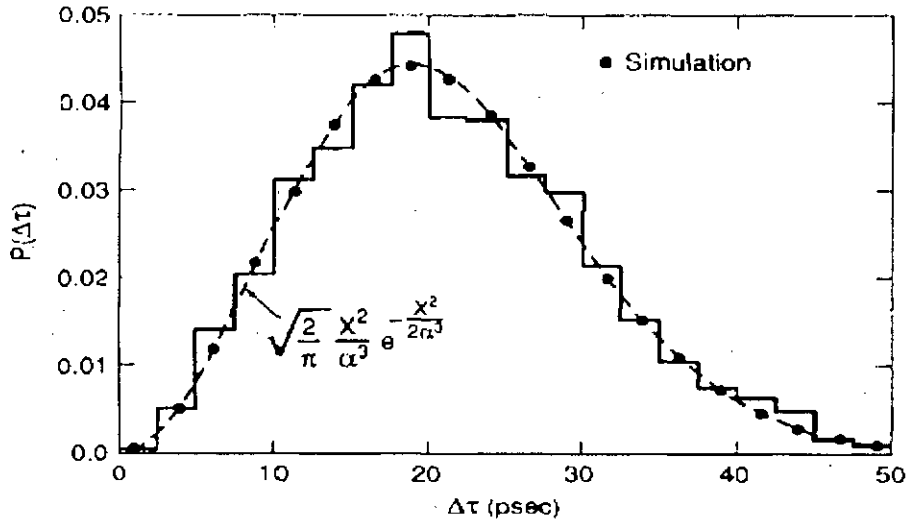


Fig.1.4: The measured probability density function of DGD and the Maxwellian fit (dotted line) [7]

Interestingly, as a result of the multiple factors which contribute to the randomly varying birefringence along the fiber, the statistics of PMD at a given frequency over time are the same as the statistics of PMD at a given time over a broad enough frequency range [10]. Even more interesting is the fact that the statistics of PMD over either time or frequency for a single fiber are the same as the statistics of PMD over an ensemble of fibers [12]. This makes PMD an ergodic process.

It is this highly statistical nature of PMD which makes it difficult to compensate. The PMD dependence on environmental factors introduces a time variation in the frequency response of the fiber, which in turn implies the need for an adaptive compensation technique. Not only does the frequency response of the fiber evolve with time but also with the input and output states of polarization. A successful PMD compensation scheme should therefore, be capable of tracking relatively fast variations in the frequency response of the fiber.

1.3 Literature review, motivation and research objectives

In the 21st century, we are seeing dramatic changes in the telecommunication industry that have far reaching implications for our lifestyles. There are many drivers for these changes. First and foremost is the continuing, relentless need for more data carrying capacity of the network. This demand is fueled by many factors. The tremendous growth of the Internet and WWW, both in terms of number of users as well as the amount of time and thus bandwidth taken by each user. To satiate the demand for greater network capacity, the data rate of current optical systems has been pushed to 10 Gbit/s ~ 40 Gbit/s. However, at these data rates, the most important transmission impairments associated with long-distance optical fiber communication systems include fiber CD, Kerr effect, PMD, noise accumulation from optical amplifiers and interaction between them.

In the early years of last decade the PMD was never a major concern as most of the optical network were not being used at high bit rates. Nevertheless with the modern high-speed (*i.e.* 10 Gbit/s ~ 40 Gbit/s) network PMD becomes a serious issue. Such high bandwidth requirements have pushed the network designers to include the PMD analysis before new high-speed link or network technology is purchased or installed. Thus, we have focused on the study of PMD effect and its compensation on the fiber optic communication systems in this thesis. PMD causes spectral broadening of the transmitted signal that leads to a reduced SNR, bit pattern corruption, higher bandwidth requirement and eventually contributes to bit error rate (BER) deterioration, performance variation or even system fading [8], [15]-[16].

The impact of PMD on optical transmission systems operating at Gb/s has been the subject of considerable research interest in the last few years. As analytical evaluation of the effect of PMD on the BER performance of an optical transmission system is not easily tractable, most of the previous research works have been focused on the evaluation of PMD effect by Monte-Carlo simulation to evaluate the eye penalty [17], Q-value analysis and evaluation by experiment [18]-[19] or by simulation [20], SNR degradation and determination of outage probability for an optical fiber communication system [21]-[22]. Several modulation schemes are also considered in different research works to find the robustness to the PMD effect [23]-[24].

S. J. Savory *et al* [15]; using Marcuse's perturbation method (conventional coupled mode equation) analyzed the propagation of pulses in optical fibers with PMD that disperse the pulse. They solved the equations perturbatively that gives the transfer function of the fiber and determine the impact of PMD on system parameter such as root mean square (rms) pulsewidth, eye penalty and outage probability.

H. Sunnerud *et al* [25], analytically investigated the PMD impairments as well as its compensation in terms of pulse width rms value and reported the benefits of using different passive techniques for mitigating the effects of PMD, including more advantageous data formats compared to conventional non-return to zero (NRZ) format, soliton transmission and forward error correction.

J. Wang *et al* [26], analyzed the impact of chromatic dispersion and PMD on systems using differential phase shift keying (DPSK) with NRZ and RZ formats and signals are received using optical pre-amplification, interferometric demodulation and direct detection. Results are presented in terms of BER and outage probability, and compute optical power penalties at fixed BER, and reported that either NRZ or RZ format is used; 2-DPSK exhibits lower power penalties than OOK in the presence of chromatic dispersion and PMD.

Using numerical simulation C. Xie *et al* [27], studied the PMD-induced degradation for on-off keying (OOK) and DPSK for long-haul optical transmission system for both compensated and uncompensated system at 40 Gb/s. They reported that DPSK systems have more tolerance than OOK for uncompensated and compensated system.

Due to the environmental variations, such as temperature changes, vibration and movement along the fiber, the DGD and the PSPs also drift randomly with time. This is the main reason why PMD is very complicated to compensate, since any compensation scheme has to dynamically adapt to these variations. A good number of research works have been carried out to mitigate the PMD effect using active devices in electronic and optical domain [28]-[30]. Meanwhile, there are several ways of passively mitigating the effect of PMD without employing active PMD compensators [31]-[34]. W. Kaiser *et al* [35], also

experimentally reported the reduced sensitivity of optical duobinary linecoding to the effects of PMD.

Due to the strong frequency dependence of PMD, the need for higher order PMD compensation grows as channel bit rate increases. S. Kim [36], analytically calculated the system performances in second- and third-order PMD compensation. They reported that the higher order PMD compensation based on counteracting the fiber PMD vector with compensation vector given by Taylor's expansion up to a certain order at a specific frequency does not work well and the deterioration of the system performance become more severe for large PMD values.

Recently, Hi-Bi grating has been introduced for PMD compensation, where a nonlinearly chirped grating written on a Hi-Bi fiber was used to provide a differential time delay for different states of polarization [37]- [38]. S. Lee *et al* [39], reported that a tunable nonlinearity-chirped FBG written into a high-birefringence fiber and used for compensating varying amounts of PMD. The high-birefringence fiber provides different time delay for SOPs and the nonlinear chirp of the grating provides the selectability of varying amounts of DGD when the FBG is stretched. This all fiber method showed good performance for a 10 Gb/s signal with 175 ps of adjustability.

Considering the above discussion, the analytical modeling to assess the impact of PMD in terms of BER for different modulation scheme and its compensation is very important and yet to be reported. Depending on specific application, various modulation and demodulation formats similar to those of traditional radio frequency communication are all also employed in intensity and coherent lightwave transmission system. These includes amplitude shift keying (ASK), phase shift keying (PSK), continuous phase shift keying (CPFSK), discontinuous

FSK, differential PSK, binary pulse position modulation (BPPM) etc. Each of these modulation schemes, such as ASK, PSK, FSK, DPSK etc. and combination thereof, with direct, homodyne and heterodyne or diversity receivers has its own merits and weaknesses. Optical CPFSK is an attractive modulation format as it allows generation of compact spectra, direct modulation of laser diode than amplitude shift keying (ASK) and PSK/DPSK system [40]. The FSK coherent lightwave system provides improved receiver sensitivity, allows transmission of multiple information channels and usher the prospect of tunability of receivers. The combination of these advantages allows maximum utilization of the enormous transmission capacity of single mode fibers. Therefore, it is necessary to develop analytical approaches for evaluating the impact of PMD in terms of conditional and average BER using different modulation schemes in single- and multi-channel fiber-optic transmission systems and to find appropriate compensation techniques and their performance results analytically.

The main objectives of this thesis are to study the fiber PMD effects and its compensation using different modulation formats on optical communication system. The whole research work is carried out to achieve the following specific goals:

- (i) To develop analytical models of fiber-optic transmission systems impaired by PMD with coherent and direct detection receivers.
- (ii) To carry out BER performance analysis based on the above analytical model for fiber-optic transmission systems using different modulation schemes, such as CPFSK, intensity modulation (IM) with coherent and direct detection receivers.

- (iii) To develop analytical models of different compensation techniques using linecoding as well as using fiber Bragg grating (FBG) to mitigate the impact of PMD on optical transmission system.
- (iv) To extend the analysis of PMD effect with different modulation and detection schemes along with and without their compensation schemes to multichannel optical transmission system, such as a wavelength division multiplexing (WDM) system.
- (v) To evaluate the performance results with and without compensation scheme for a single- and multi-channel fiber-optic transmission system and to find the optimum system design parameters.
- (vi) Finally, to compare the analytical results with the experimental and simulation results reported earlier to validate the analytical approximations.

1.4 Outline of the thesis

As mentioned in the title of this thesis, the key objective of this work is to study the PMD effects on fiber-optic transmission system. The thesis is organized as follows:

Chapter 2 gives the analytical method to evaluate the impact of PMD on IM-DD transmission system considering the effect of induced ISI among adjacent bits. The performance is determined in terms of average BER assuming Maxwellian distribution for the DGD at a bit rate of 10 Gbit/s. Simulation is carried out for a single channel transmission system in terms of eye diagram.

Chapter 3 starts with the motivation of modeling the direct detection CPFSK optical transmission system. A low pass equivalent system model is proposed. Following this low pass model, the expression for the output photocurrent of the direct detection receivers are derived considering PMD induced DGD and group velocity dispersion (GVD). Next, the expression of moments of the random phase noise process is derived from the knowledge of output phase fluctuation due to DGD. The probability density function (pdf) of the random phase fluctuation is then determined by inverse Fourier transform of its characteristic function which is found from moments of the phase noise process. Considering a given value of the random phase fluctuation conditional and average BER expression is derived and system performance is evaluated.

Chapter 4 provides theoretical approach for optical heterodyne CPFSK transmission system to evaluate the BER performance limitations due to PMD with delay-demodulation receiver. The method is based on the linear approximation of a linearly filtered angle-modulated signal such as CPFSK signal. For a given intermediate frequency (IF) SNR, the condition BER is conditioned on a given value of random phase fluctuation and DGD. Finally, the average BER performance is evaluated using the pdf, obtained by the method outline chapter 3.

Chapter 5 describes the analytical method to mitigate the impact of PMD on optical transmission for several linecoding, such as alternate mark inversion (AMI), delay modulation (DM) and order 1; in direct detection- and heterodyne detection CPFSK system. The linecoder is used as a linear time-invariant filter that acts on the input data signal and generate an output sequence. The relative effectiveness of the above linecodes is determined in overcoming the pulse dispersion performance degradation caused by PMD and compare the results.

Chapter 6 studies the interaction of PMD and cross-phase modulation (XPM) in a WDM transmission system. XPM is a nonlinear phenomena occurring in optical fibers when two or more optical fields are transmitted through a fiber simultaneously. Due to the presence of PMD, the angle between the SOP changes randomly and causes XPM modulation amplitude fluctuation random in the perturbed channel. The pdf of the random angle between the SOP of pump and probe is analytically determined and using the pdf, the impact of polarization mode dispersion on XPM is assessed in terms of BER, channel spacing etc. for pump-probe configuration and 4-channel WDM system.

Chapter 7 presents the mathematical formulations in detail for compensating the effect of PMD in a multi-channel environment using the Hi-Bi linear chirped fiber Bragg grating (LCFBG). A LCFBG based PMD compensation system model is proposed. PMD compensation is achieved by utilizing the effect of strain in LCFBG through a cantilever structure. With an optimal design of the grating and cantilever beam parameters, this PMD compensation device is well suited for WDM applications over a significant range of operating wavelength, where a number of channels can be compensated together. Using the proposed PMD compensator 4-channel WDM system is simulated.

The last chapter focuses on conclusions of the thesis, summarizes the achievements of the research and gives recommendations for future work. Due to the fast-developing technologies, one can never finish the exploration. Together in these eight chapters, I describe the work for my Ph. D thesis.

Chapter 2

BIT ERROR RATE AND EFFECT OF PMD IN IM-DD TRANSMISSION SYSTEM

In this chapter, first a brief introduction of direct- and coherent detection is given and then BER expression is derived to quantify the penalty of optical system. An analytical approach is used to evaluate the impact of PMD in an IM-DD optical transmission system in terms of average BER considering Maxwellian distribution for the DGD. Simulation is done for a single channel IM-DD system using the OptSim simulation software and a comparison is established between analytical and simulation results.

2.1 Intensity modulation and optical coherent system

The method of superimposing an information signal onto an optical carrier is called direct modulation. Modulation of laser diode can be accomplished by varying its driving current. This result in intensity modulation (IM), which is the most popular type of modulation, used in deployed fiber-optic communication systems. It can be represented as on-off keying (OOK) modulation with particularity that bit 0 and 1 do not have the same noise level. This is due to the predominance of the signal-amplified spontaneous emission (ASE) beat noise, which is larger for bit 1. At the receiver end, a photodetector converts the incoming optical stream into a stream of electrons. The electron stream (*i.e.*,

electrical current) is then amplified and passed through a threshold device. Whether a bit logical 0 or 1 is depends on whether the stream is above or below a certain threshold for bit duration and thus the receiver provides direct detection (DD). In short, the method is called IM-DD.

Coherent fiber-optic communication systems use a principle similar to heterodyne or homodyne detection in radio broadcasting. At the transmitter end, an information- carrying electrical signal modulates a microwave signal radiated by a local oscillator. This microwave signal, in turn, modulates a laser that presents modulated light for transmission. At the receiver end, the optical input signal mixes with light emitted by a local oscillator (laser) so that the information signal is detected at intermediate frequency (IF). A photodiode converts an optical signal into an electrical signal and information is extracted from the carrier at f_{IF} . If $f_{IF} = 0$ - that is the detected signal is at the original frequency of the information signal – the detection is called homodyne. If $f_{IF} \neq 0$ - that is, the detected signal at the IF – the detection is called heterodyne. A coherent system works effectively if – and only if – the polarization of an incoming optical signal coincides at the receiver end with the polarization of a local optical signal. This is why we need polarization-maintenance (PM) adapters at the transmitter and receiver ends. We also need a PM fiber for transmission or we have to use some other means to control the polarization state of the transmitting signal. This is one of the major drawbacks of a coherent system. The main motivation for developing a coherent system is to increase receiver sensitivity by 10 dB to 25 dB that is from 10 to 316 times [41]-[42].

In this work, we provide the BER to find expression and an analytical approach to evaluate conditional and unconditioned BER performance limitations of an optical IM-DD transmission system impaired by PMD. Since temporal behaviors of fiber PMD are of statistical nature as a result of the randomness of the birefringence variations along the fiber structure, therefore to determine more

accurately the optical transmission impairment due to PMD, we incorporate the PMD statistics. We determine the unconditional BER and power penalty analytically, considering the DGD to have a Maxwellian pdf.

2.2 Quantifying optical system penalty: BER expression

A very common approach to quantify the different optical transmission impairments, such as chromatic dispersion, PMD, nonlinearity etc., induced system penalty is to calculate the probability that the system reaches a certain unacceptable penalty level, which can be assessed by the eye closer, digital SNR, BER or optical SNR. This is very important from a practical point of view, because certain penalty level can be defined as an outage, *i.e.*, the system does not work beyond that penalty level.

Optical receivers convert incident optical power into electric current through a photodiode. Among a group of optical receivers, a receiver is said to be more sensitive if it achieves the same performance with less optical power incident on it. The communication system performance is characterized by a quality called BER which is defined as the average probability of incorrect bit identification of a bit by the decision circuit of the receiver [41]. For example, a BER of 2×10^{-6} would correspond to on average 2 errors per million bits. A commonly used criterion for digital optical receivers requires $BER \leq 1 \times 10^{-9}$. It is important for the signal to have minimum distortions in order to avoid a high BER at the receiver. This means that although the combined effects of PMD, GVD and nonlinear effect can not be eliminated, they need to be reduced so that a pulse can propagate with minimum distortions. In order to assess the system performance one needs to know how to calculate the BER of the system at the receiver end.

Fig. 2.1 shows schematically the fluctuating signal received by the decision circuit, which samples value I fluctuates from bit to bit around an average value I_1 or I_0 , depending on whether the bit corresponds to 1 to 0 in the bit stream. The decision circuit compares the sampled value with the threshold value I_D and calls it bit 1 if $I > I_D$ or $I < I_D$. An error occurs if $I < I_D$ for bit 1 or if $I > I_D$ for bit 0 due to noises that add into the signal in the system.

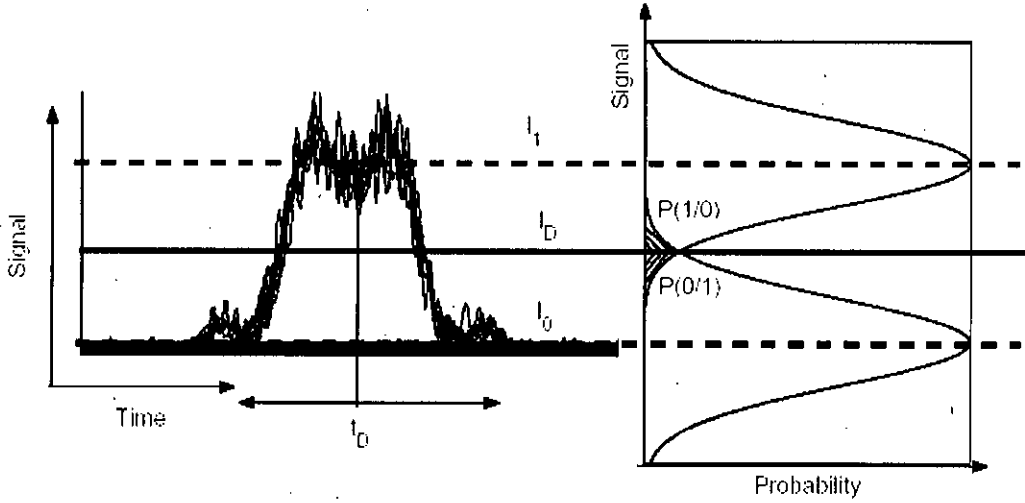


Fig. 2.1: Bit error probabilities

Both sources of errors can be included by defining the error probability as,

$$BER = p(1)P(1/0) + p(0)P(0/1) \quad (2.1)$$

where $p(1)$ and $p(0)$ are probabilities of receiving bits 1 and 0 respectively, $P(0/1)$ is the probability of deciding 0 when 1 is received, and $P(1/0)$ is the probability of deciding 1 when 0 is received. Since 1 and 0 bits are equally likely to occur, $p(1) = p(0) = 1/2$, and the BER becomes,

$$BER = \frac{1}{2} [P(1/0) + P(0/1)] \quad (2.2)$$

Fig. 2.1 shows how $P(0/1)$ and $P(1/0)$ depends on the probability density function $p(I)$ of the sampled value I . The functional form of $p(I)$ depends on

the statistics of noise sources responsible for current fluctuations. Assuming a Gaussian noise profile, one can write the functional form of $P(0/1)$ and $P(1/0)$ as,

$$P(0/1) = \frac{1}{\sigma_1 \sqrt{2\pi}} \int_{-\infty}^{I_D} \exp\left(-\frac{(I - I_1)^2}{2\sigma_1^2}\right) dI \quad (2.3)$$

$$P(1/0) = \frac{1}{\sigma_0 \sqrt{2\pi}} \int_{I_D}^{\infty} \exp\left(-\frac{(I - I_0)^2}{2\sigma_0^2}\right) dI \quad (2.4)$$

where σ_1^2 and σ_0^2 are the corresponding variances. From the definition of the complementary function we have,

$$\text{erfc}(x) = \frac{2}{\sqrt{\pi}} \int_x^{\infty} \exp(-x^2) dx \quad (2.5)$$

Using equation (2.5) in equation (2.3) we get,

$$P(0/1) = \frac{1}{2} \text{erfc}\left(\frac{I_1 - I_D}{\sqrt{2} \sigma_1}\right) \quad (2.6)$$

$$P(1/0) = \frac{1}{2} \text{erfc}\left(\frac{I_D - I_0}{\sqrt{2} \sigma_0}\right) \quad (2.7)$$

Using equation (2.6) in equation (2.2) we can write the BER as,

$$\text{BER} = \frac{1}{4} \left[\text{erfc}\left(\frac{I_1 - I_D}{\sqrt{2} \sigma_1}\right) + \text{erfc}\left(\frac{I_D - I_0}{\sqrt{2} \sigma_{01}}\right) \right] \quad (2.8)$$

Equation (2.8) shows that the BER depends on the decision threshold I_D .

2.2.1 Q-factor

In practice, I_D is optimized to minimize the BER. Hence we minimize BER with respect to I_D using,

$$\frac{d}{dx} \operatorname{erfc}[f(x)] = \frac{2}{\sqrt{\pi}} e^{-f^2} - \frac{df}{dx} \quad (2.9)$$

and obtain

$$\frac{(I_1 - I_D)^2}{\sigma_1^2} = \frac{(I_D - I_0)^2}{\sigma_0^2} + \ln\left(\frac{\sigma_1}{\sigma_0}\right) \quad (2.10)$$

For most practical cases, the last term is negligible and hence we get,

$$\frac{(I_1 - I_D)}{\sigma_1^2} = \frac{(I_D - I_0)}{\sigma_0^2} \quad (2.11)$$

Hence we find that the minimum occurs when,

$$I_D = \frac{\sigma_0 I_1 + \sigma_1 I_0}{\sigma_0 + \sigma_1} \quad (2.12)$$

when, $\sigma_1 = \sigma_0$, $I_D = (I_1 + I_0)/2$, which corresponds to setting the decision threshold in the middle. The BER is given by

$$BER = \frac{1}{2} \operatorname{erfc}\left(\frac{Q}{\sqrt{2}}\right) \quad (2.13)$$

where the factor Q is given by

$$Q = \frac{I_1 - I_0}{\sigma_1 + \sigma_0} \quad (2.14)$$

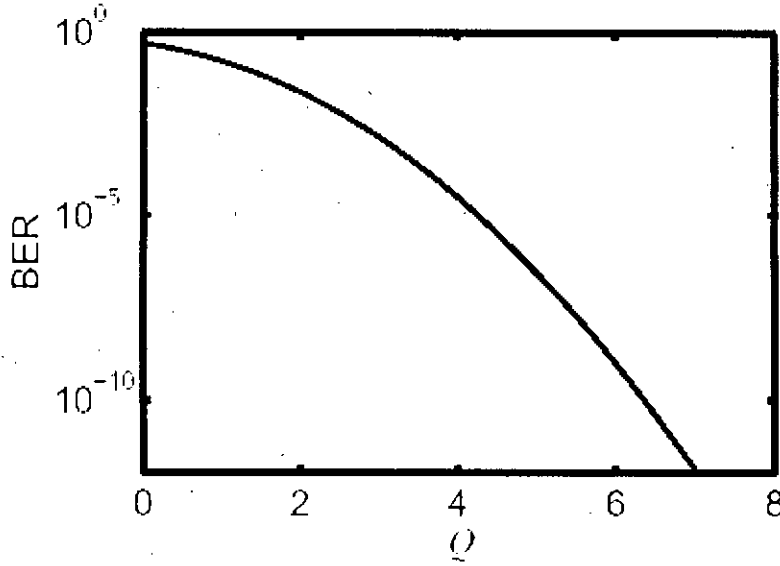


Fig. 2.2: Bit Error Rate (BER) versus Q factor

The Q factor is thus a dimensionless factor and is related to the BER as shown in Fig. 2.2. Figure 2.2 shows how BER varies with Q factor. The factor improves as Q increases and becomes lower than 10^{-12} for $Q=7$. Now the expression for Q is in terms of receiving current. Since the receiver current is directly a measure of optical power, P of the signal such that $I = RP$, where R is the responsivity of the photodetector, and the optical power is related to the energy of the signal pulse, we can write the Q factor in terms of pulse energy as,

$$Q = \frac{E^{(1)} - E^{(0)}}{\sigma_e^{(1)} + \sigma_e^{(0)}} \quad (2.15)$$

where $E^{(1)}$, $(\sigma_e^2)^{(1)}$ are the energy and variance in energy of the 1 bit and $E^{(0)}$, $(\sigma_e^2)^{(0)}$ are the energy and variance in the energy of the 0 bits. The variance in energy is defined as $\sigma_e^2 = \langle E^2 \rangle - \langle E \rangle^2$. Hence in order to evaluate the Q factor we need to calculate the variance in energies of 1 and 0 bits at the receiver end.

2.3 System model of IM-DD transmission system

The schematic configuration of an IM-DD optical transmission system model considered in the analysis is shown in Fig. 2.3. A DFB or DBR laser may be used at the transmitter. The pseudorandom data pattern at a rate of 10 Gb/s is used to intensity modulate the laser source and output fed to the SM fiber. A direct detection receiver with a PIN photodiode receives the optical signal. The output of the pre-amplifier is then filtered by a low-pass filter and fed to a sampler followed by a comparator. The threshold voltage of the comparator is set to zero value. If the output voltage is greater than zero a binary '1' is detected, otherwise a binary '0' is detected.

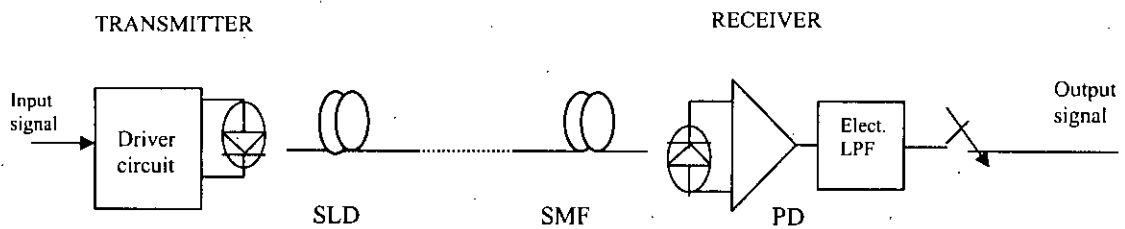


Fig.2.3: Schematic configuration of an optical transmission system model

2.4 Theoretical analysis

A very elegant way to study PMD is based on the model of the principal states of polarization (PSP). For a given fiber, at a fixed time and optical frequency, there always exist two polarization states, called PSP. When operating in a quasi-monochromatic regime, the output PSPs are the two orthogonal output states of polarization for which the output polarization does not depend on the optical frequency at first order. The corresponding orthogonal input polarization states are called the input PSPs.

The difference in arrival time $\Delta\tau$ between the PSPs is called DGD and it is the cause of pulse broadening at the output of a fiber when energy is split between the two PSPs at the input. If $\Delta\tau$ is the DGD between the PSP's, T is the bit interval, T_0 is the full width half maximum (FWHM) of the input pulse and 2θ is the angle between the Stokes vector representing the state of polarization of the input pulse and of the input PSP's, the output pulse width can be given by [43],

$$\sqrt{T^2 - T_0^2} = \frac{1}{2} \Delta\tau \sin(2\theta) \quad (2.16)$$

Generally for commercial SM fibers, PMD becomes the only serious consideration when an optical transmission system with a high bit rate distance product is operating in the wavelength where the fiber chromatic dispersion is negligible. Due to the more mature EDFA technology at the 1.55 μm wavelength window, PMD is relevant for system using dispersion-shifted fibers. Therefore, we assume dispersion-shifted fiber as a transmission medium. Fiber nonlinearities and optical amplifier related polarization sensitivities are also ignored in this work.

The optical field $E_i(t)$ coupled into the fiber can be modeled as

$$E_i(t) = \sqrt{P_i} \sum_{k=-\infty}^{\infty} b_k g(t-kT) (c_1 e_1 + c_2 e_2) \quad (2.17)$$

where P_i is the transmitted peak power, $b_k = 0, 1$ represents the transmitted bit, and $g(t)$ the transmitted pulse shape. The vectors represent the input PSP's are indicated with $e_i = (e_{ix} \ x + e_{iy} \ y)$ ($i = 1, 2$) and the complex coefficients c_1 and c_2 determine the SOP of the transmitted field ($|c_1|^2 + |c_2|^2 = 1$).

In deriving the output electric field we assume that the signal bandwidth is much smaller than the PSP's bandwidth. This constraint is fulfilled for all the practical values of the bit rate if a standard DFB or DBR laser is used at the transmitter.

Neglecting chromatic dispersion, in a reference frame solid to the output PSP's, the received field $E(t)$ is given by,

$$E(t) = \sqrt{P} \sum_{k=-\infty}^{\infty} b_k [\cos \theta g(t - kT) x + \sin \theta g(t - kT - \Delta\tau) e^{-i\phi} y] \quad (2.18)$$

where P is the received peak power, θ is the angle between the electric field representing the state of polarization (SOP) of the transmitted pulse and the direction of the input PSPs and ϕ is the fiber induced phase difference between the two waves. At the receiver, after detection by means of a photodiode and filtering by a baseband filter of pulse response $h(t)$, the photocurrent $j(t)$ taking into account the orthogonal property of the PSP's, the k th decision variable is given by [44],

$$j_k = R_p PM h [\cos^2 \theta \gamma(\Delta\tau \sin^2 \theta) + \sin^2 \theta \gamma(\Delta\tau \sin^2 \theta - \Delta\tau)] + R_p PM \sum_{h \neq k} b_h [\cos^2 \theta \gamma(t_k - hT) + \sin^2 \theta \gamma(t_k - hT - \Delta\tau)] + n(t_k) \quad (2.19)$$

where R_p represents the photodiode responsivity, M the photodiode average gain if an APD is used (if a PIN is used $M=1$), $t_k = (kT + \Delta\tau \sin^2 \theta)$, sampling instant $n(t_k)$ the noise sample and

$$\gamma(t) = \int_{-\infty}^{\infty} h(t - \xi) |g(\xi)|^2 d\xi \quad (2.20)$$

The noise power σ_k^2 , which depends on the received signal can be easily evaluated assuming the dark current noise is negligible and according to [45] it is expressed as $\sigma_k^2 = \sigma_T^2 + 2e \langle j_k \rangle BM^{2+\xi}$.

where σ_T^2 is the receiver thermal noise power in the signal bandwidth, ξ is a parameter typically of the adopted photodiode and $\langle * \rangle$ indicates the ensemble average for a fixed transmitted message, B is the bit rate.

From (2.19) it is evident that the main effect of polarization mode dispersion is to generate intersymbol interference (ISI). We represent this term by,

$$i_{isi} = R_p PM \sum_{h \neq k} b_k [\cos^2 \theta \gamma(t_k - hT) + \sin^2 \theta \gamma(t_k - hT - \Delta\tau)] + n(t_k) \quad (2.21)$$

The effect of ISI can be evaluated by approximating the (2.21) with terms $h = k-1, k-2, k-3, k-4$ and $h = k+1, k+2, k+3, k+4$, that is considering in a fourth approximation only the interference among the adjacent bits.

The probability that a '0' is received when a '1' is transmitted and the probability that '1' is transmitted when a '0' is transmitted can be given by

$$p(0/1) = 0.5 \operatorname{erfc} \left(\frac{(\langle j_k \rangle - \langle i_{isi} \rangle) - j_{th}}{\sqrt{2} \sigma_i} \right) \quad (2.22)$$

$$p(1/0) = 0.5 \operatorname{erfc} \left(\frac{\langle i_{isi} \rangle - j_{th}}{\sqrt{2} \sigma_i} \right) \quad (2.23)$$

where j_{th} is the optimum threshold value and σ_i the noise sample standard deviation corresponding to the considered pattern. Of course the value of j_{th} depends on different conditions as pulse shape, noise, filter shape and so on. We can express the BER conditioned on a given value of $\Delta\tau$ as,

$$BER(\Delta\tau) = 0.25 \left(\operatorname{erfc} \left(\frac{(\langle j_k \rangle - \langle i_{isi} \rangle) - j_{th}}{\sqrt{2} \sigma_i} \right) + \operatorname{erfc} \left(\frac{\langle i_{isi} \rangle - j_{th}}{\sqrt{2} \sigma_i} \right) \right) \quad (2.24)$$

Equation (2.22) - (2.24) allow the system conditional BER to be evaluated if the system parameters, as the transmitted pulse shape, the transmitted SOP are known.

The temporal behavior of the PMD is stochastic due to relatively fast changes in the environment such as ambient temperature and local vibration, or slow change such as aging. Even if the fiber is perfectly circular, external mechanical or thermal stresses cause small asymmetric to the fiber core. Thus DGD changes with time due to external stress and as a result beyond the birefringence correlation length, the polarization axes of the fiber are uncorrelated. It is shown that if the fiber length is much longer than the correlation length of the

disturbances that cause the changes of symmetry in fiber geometry and stress, the DGD $\Delta\tau$ between the two PSP's follows a Maxwellian probability density function.

Thus, the average bit error probability can now be evaluated as,

$$BER = \int_{-\infty}^{\infty} BER(\Delta\tau) P_{\Delta\tau}(\Delta\tau) d(\Delta\tau) \quad (2.25)$$

2.5.1 Analytical results and discussion

Following the analytical approach, the BER performance results for conditional case where the input power is equally divided among the PSPs according to (2.18), are evaluated at a bit rate of 10 Gb/s with several values of instantaneous DGD. The evaluation is performed assuming $\xi = 1$ and $M=1$ for the PIN photodiode and supposing that the electrical pulse has a Gaussian shape.

The plots for conditional BER versus received optical power P_s are shown in Fig. 2.4 for the DGD of 0, 40 ps, 60 ps, 80 ps, 100 ps, 120 ps, 140 ps and 160 ps respectively. The results show that the BER is highly degraded when the DGD is higher for a given fiber length and the system suffers a significant amount of power penalty due to the effect of PMD. It is observed that the penalty at given BER is increasing with increasing value of the DGD. Penalty is found to be approximately 0.30 dB, 0.55 dB, 1.0 dB, 2.05 dB, 3.90 dB and 7.75 dB for DGD of 40 ps, 80 ps, 100 ps, 120 ps, 140 ps and 160 ps respectively.

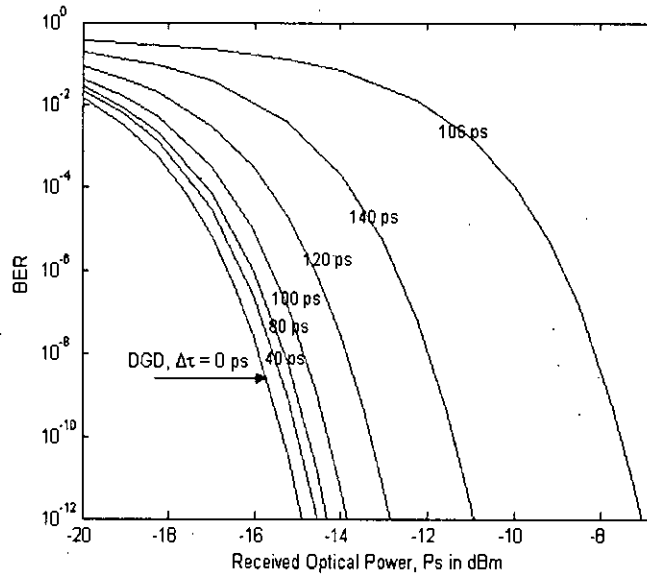


Fig. 2.4: Plots of conditional BER versus received optical power, P_s , for a 10 Gb/s system impaired by PMD

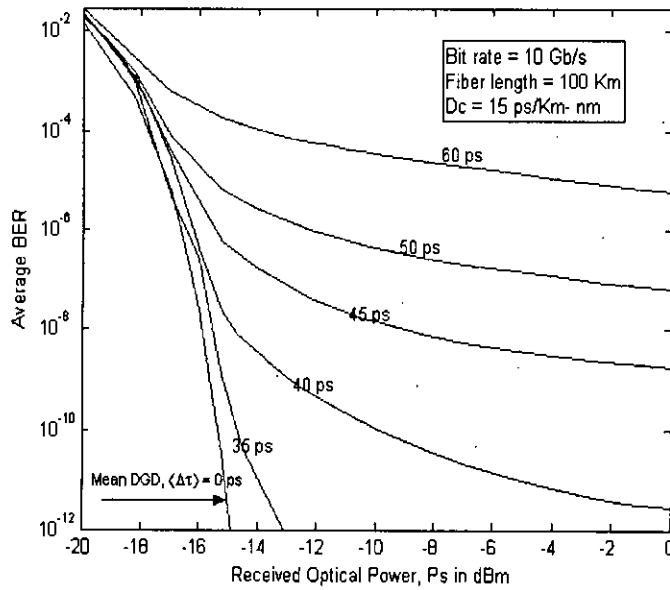


Fig. 2.5: Plots of unconditional BER versus received optical power for a 10 Gb/s system impaired by PMD

The plots for average BER versus received optical power P_s are shown in Fig. 2.5 for 10 Gb/s and different values of mean DGD. The results show that the BER is highly degraded when the mean DGD is higher for a given fiber length and the system suffers a significant amount of power penalty due to the effect of PMD. It is observed that the penalty at $BER=10^{-9}$ is increasing with increasing value of the mean DGD. Penalty is found to be approximately 0.27dB, 0.38 dB, 0.45 dB and 2.4 dB for mean DGD 20 ps, 30ps, 35 ps and 40 ps respectively. Further increase of DGD leads to a BER floor above 10^{-9} .

2.5.2 Simulation results and discussion

We have carried out simulation to assess the impact of PMD in a single channel IM-DD transmission system. The simulation setup is shown in Fig. 2.6. The different parameter used in the simulation is shown in Table 2.1

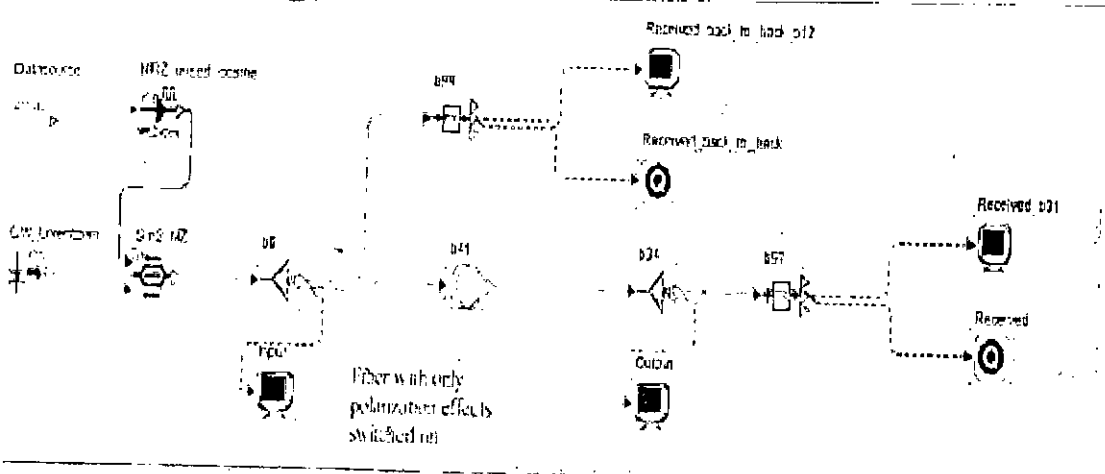
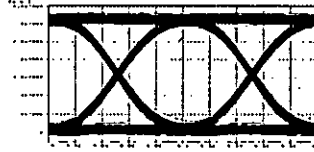


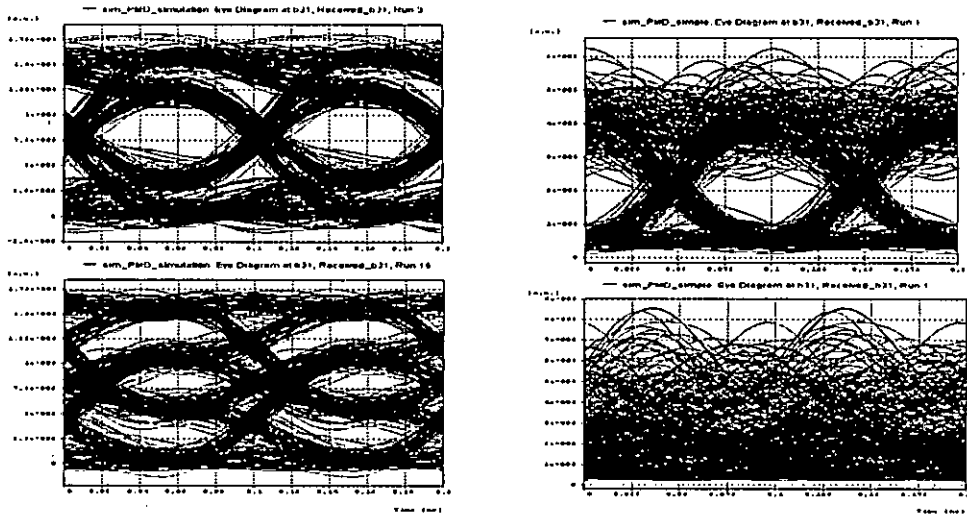
Fig. 2.6: Simulation setup for a single channel IM-DD transmission system

As the PMD effect is random in nature, we use Monte Carlo simulation using different seeds. We monitor the optical spectrum, electrical spectrum and eye diagram at the input and output of the transmission link. Fig. 2.7 shows the eye diagram at the input and output (for different seeds). From the figure, we found the effect of PMD on the signal as the eye opening become less or even closed.

Fig. 8 shows the BER vs input optical power and Q-value vs input optical power for different fiber link length



(a)



(b)

Fig. 2.7: (a) Eye diagram at the input (back-to-back) (b) Eye diagrams for different values of secd (using Monte Carlo simulation)

Finally we calculate the average eye-opening penalty (EOP) due to PMD for this single channel transmission system. Here, we define the parameter of the eye-opening penalty (EOP) as,

$$EOP = -10 \log \left(\frac{a}{b} \right)^2 \quad (2.26)$$

$$\Delta\tau = D_{PMD} \sqrt{L} \quad (2.27)$$

Now we plotted the power penalty curve from the analytical results and simulation results and it is depicted in Fig. 2.9.

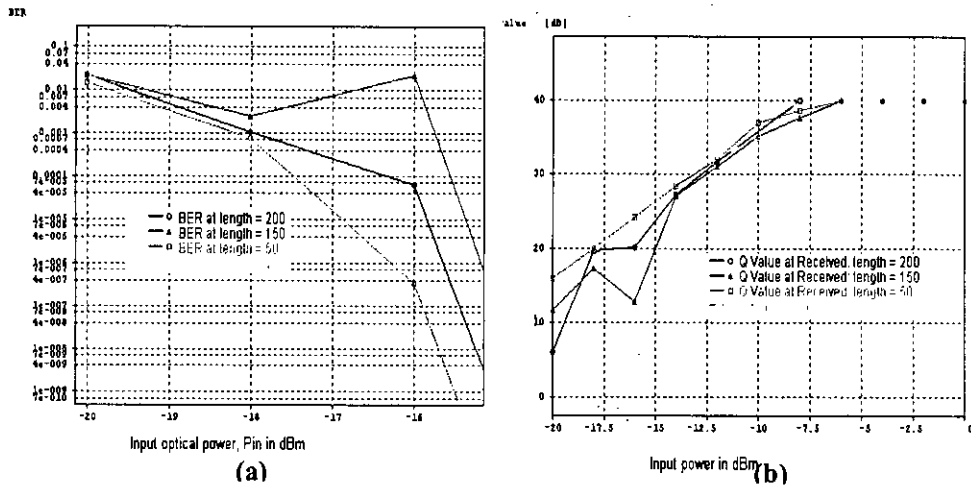


Fig.2.8: (a) BER vs input optical power, (b) Q-value vs input optical power

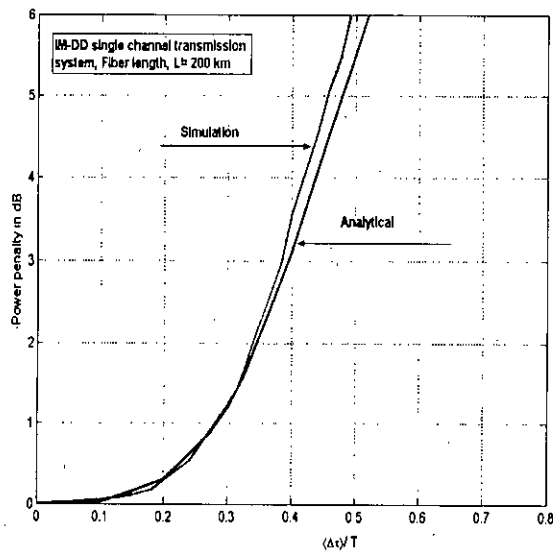


Fig. 2.9: Power penalty vs normalized mean DGD

From the Fig.: 2.9, we found that analytical and simulation results the same power penalty up to 35 ps DGD and the simulation gives little bit better result than that of analytical approach at DGD >35 ps.

Sl no.	Parameters (unit)	Value
1	Fiber length (km)	200
2	Input power (dBm)	15
3	PMD coefficient (ps/ $\sqrt{\text{km}}$)	2
4	Bit rate (Gbit/s)	10
5	Receiver sensitivity (dBm at 10^{-9})	24
6		

Table 2.1: Different simulation parameters for single channel IM-DD transmission system

2.6 Summary

In the first part of this chapter, we describe the basic working principle of IM-DD, optical heterodyne transmission system and the BER expression for quantifying the optical system performance degradation is derived.

In the second part, an analytical method is presented to evaluate the impact of PMD on the BER performance of an IM-DD system. BER performance results are evaluated for a range of instantaneous and mean values of DGD. The results show that the performance of an IM-DD system suffers power penalty of 0.27 dB, 0.45 dB and 2.4 dB corresponding to mean DGD of 20 ps, 35 ps and 40 ps respectively at a BER of 10^{-9} operating at a bit rate of 10 Gb/s. Furthermore, at increased values of the mean DGD there occur BER floors above 10^{-9} which can not be lowered by further increasing the signal power. It is noticed that BER floors occur at about 2×10^{-9} , 10^{-7} and 10^{-5} corresponding to mean DGD of 45 ps, 50 ps and 60 ps respectively at 10 Gbit/s. The effect of PMD is found to be more detrimental at higher bit rates. For conditional BER performance based on the instantaneous DGD and the amount of power penalty is about 7.75 dB for a corresponding DGD of 160 ps. The results also show that the power penalty due to PMD suffered by an IM-DD system is significant at higher mean DGD between the two polarization modes. Simulation is done for a single channel optical transmission in terms of eye diagram and a comparison is established between the analytical and simulation results.

Chapter 3

EFFECT OF PMD IN DIRECT DETECTION CPFSK TRANSMISSION SYSTEM

In this chapter we propose a low pass equivalent direct detection continuous system considering the effect of PMD and chromatic dispersion. Based on this model analytical approach is presented to determine the impact of signal phase distortion due to PMD in a single mode fiber on the BER performance of an optical continuous phase frequency shift keying (CPFSK) transmission system with MZI based direct detection receiver. The pdf of the random phase fluctuation due to PMD and group velocity dispersion (GVD) at the output of the receiver is also determined analytically. On the basis of developed pdf, the random phase fluctuation the BER performance results are evaluated at a bit rate of 10 Gbit/s fiber for different values of the mean DGD.

3.1 PMD effect in direct detection CPFSK system

Optical CPFSK is an attractive modulation format as it allows generation of compact spectra that allows for receiver envelopes detection by properly selecting the modulation index [46]. However, the effect of PMD constitutes one of the main limiting factor for reliable optical fiber system performance at gigabits transmission rates. As the two polarization fields move at different group

velocities with a DGD, there is a fluctuation in signal phase between the two principal states of polarization which causes a random phase fluctuation of the signal itself resulting in spectral broadening of the transmitted signal that leads to bit pattern corruption and higher bandwidth requirement, and eventually contributes to BER deterioration, performance variation or system fading even at moderate bit rate [3], [47]-[49].

The effect of PMD has been the subject of considerable research interests during the past few years and the developed ideas are briefly described in a series of publication [50]-[56]. The effect for PMD on the error probability is theoretically assessed at a bit rate of 2.5 Gb/s for an IM-DD system and the BER in a IM/DD has been shown to strongly depend on the state of polarization and DGD [50]. Some studies treated PMD as deterministic term in numerical solution or are based on simple analytical approach of determining the conditional bit error probability [51]. The simulation results on the effects of PMD on an amplified IM-DD system is reported in [52] as a function of the DGD. The effect of PMD on the bit error rate performance of heterodyne FSK system is also reported [57]. Recently, the performance of optical DPSK system with direct detection receiver is reported in presence of PMD [26]. Several attempts have been reported to compensate the effect of PMD in electronic as well as in optical domain [58]-[60]. Although there are many approaches reported to minimize the effect of PMD, there is no analytical development to evaluate the impact of PMD on the BER performance of an optical transmission system.

In this work, we provide an analytical approach to evaluate the BER performance limitations of an optical direct detection CPFSK system impaired by PMD. The method is based on the linear approximation of the output phase of a linearly filtered angle-modulated signal such as the CPFSK signal. The expression for the overall degradation in signal phase is derived following an analytical approach by using an equivalent transfer function of a single mode fiber (SMF) which includes the effects of PMD in presence of GVD. The conditional BER is then determined using the pdf's of the random phase

fluctuation due to PMD and GVD at the receiver output in the presence of receiver noise for different values of mean DGD. Power penalty suffered by the system due to PMD is evaluated at a bit rate of 10 Gb/s.

3.2 System model

The block diagram of an optical CPFSK transmission system with direct detection model is shown in Fig. 3.1. Fig. 3.2 shows the low pass equivalent CPFSK system model considering PMD and chromatic dispersion. The signal components in the two output PSPs propagate independently through the entire system from the modulator to the balanced receiver. In the transmitter, non-return to zero (NRZ) data at 10 Gb/s is used to directly modulate a laser to generate the CPFSK signal that is transmitted through a single mode fiber. At the receiving end, MZI based direct detection receiver detects the received optical signal. The fields corresponding to the two PSPs are separately detected and the resulting photocurrents are summed. We decompose the entire system into a pair of subsystems, each corresponding to one PSP. We sum the outputs of the two subsystems to obtain sampled decision variables $i_m(t) = i_{m1}(t) + i_{m2}(t)$. The output photocurrent is filtered by a low pass filter and fed to a sampler followed by a comparator. The threshold voltage of the comparator is set to zero value. If the output voltage is greater than zero a binary '1' is detected, otherwise a binary '0' is detected.

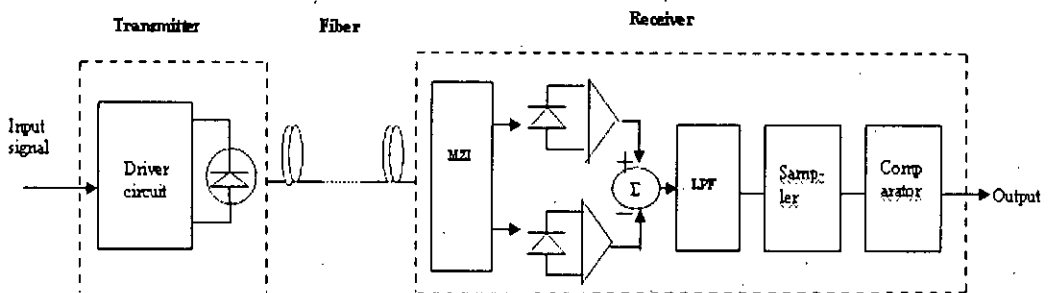


Fig.3.1: Block diagram of an optical CPFSK transmission system with MZI based direct detection receiver

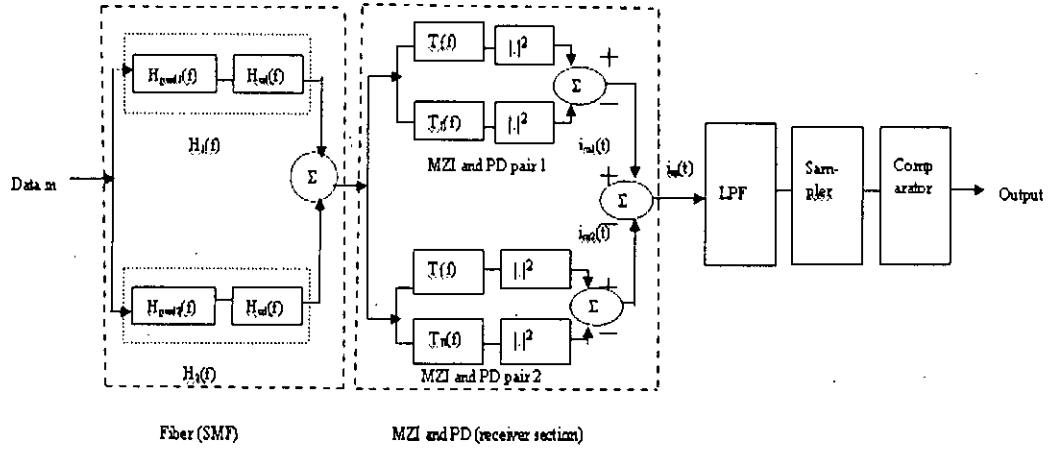


Fig.3.2: Low pass equivalent direct detection CPFSK system model considering PMD and chromatic dispersion

3.3 Theoretical analysis

The complex envelope of the electric field at the output of CPFSK transmitter and input envelope of the fiber is represented as,

$$E_m(t) = \sqrt{2P_T} \exp[j\{2\pi f t + \phi_s(t) + \phi_n(t)\}] \quad (3.1)$$

$\phi_n = 2\pi \int_0^t \mu(t_1) dt_1$; where $\mu(t)$ represents the laser instantaneous frequency

fluctuation which is gaussian distribution with zero mean and having a white power spectral density of magnitude $\Delta\nu/2\pi$ of the transmitting laser. For NRZ format the signal phase,

$$\phi_s(t) = 2\pi \Delta f \int_{-\infty}^t I(t) dt \quad (3.2)$$

$$\text{and } I(t) = \sum_{k=-\infty}^{\infty} a_k p(t - kT) \quad (3.3)$$

where, $a_k = \pm 1$ is the random bit pattern of the k th information bit, $\phi_s(t)$ is the CPFSK modulating phase, $p(t)$ represents the elementary pulse shape of

duration T seconds (bit rate $B = 1/T$).

3.3.1 Transfer function considering PMD and GVD effects

We now consider the first-order PMD effects. We also assume that there is negligible polarization dependent loss. In this situation we can use the principal state of polarization (PSP) concept to model PMD. The input field can be projected onto two inputs PSPs. Accordingly the input field can be expressed as

$$E_{in}(t) = \sqrt{\alpha} E_a(t) \hat{\varepsilon}_{a+} + \sqrt{1-\alpha} E_a(t) \hat{\varepsilon}_{a-} \quad (3.4)$$

where α = PMD power splitting ratio

If electric field experienced a total DGD, $\Delta\tau$ in the fiber; then the electric field at the output of the fiber,

$$E_o(t, \Delta\tau) = \sqrt{\alpha} E_a(t - \frac{\Delta\tau}{2}) \hat{\varepsilon}_{b+} + \sqrt{1-\alpha} E_a(t + \frac{\Delta\tau}{2}) \hat{\varepsilon}_{b-} \quad (3.5)$$

The transfer function of the fiber due to PMD corresponding to two PSPs are given by,

$$H_{pmd1}(f) = \exp[j2\pi f(-\frac{\Delta\tau}{2})] \quad (3.6a)$$

$$H_{pmd2}(f) = \exp[j2\pi f(\frac{\Delta\tau}{2})] \quad (3.6b)$$

$$\text{and } H_{pmd}(f) = H_{pmd1}(f) + H_{pmd2}(f) \quad (3.6c)$$

So the output electric field due to PMD expressed as,

$$E_o(t, \Delta\tau) = E_{in}(t) \otimes h_{pmd}(t, \Delta\tau) \quad (3.6d)$$

where

$$h_{pmd}(t, \Delta\tau) = F^{-1}[H_{pmd1}(f) + H_{pmd2}(f)] \quad (3.6e)$$

If we assume that SMF is lossless and consider only that chromatic dispersion (CD) is present, then the SMF transfer function due to GVD is given by,

$$H_{cd}(f) = \exp(-j\gamma(\pi f T)^2); \text{ where, } \gamma = \text{chromatic dispersion index} = \frac{\lambda^2}{\pi c} D_c R_b L;$$

where, T is the pulse duration, λ is the wavelength, D_c is the chromatic

dispersion coefficient, R_b is the bit rate and L is the fiber length.

Now taking into accounts both of the GVD and first order PMD and combining into a single transfer function for two independent PSPs, and the implicit expression for $H_1(f)$ and $H_2(f)$ are given by

$$H_1(f) = \sqrt{\alpha} \exp[j2\pi f(-\frac{\Delta\tau}{2}) - j\gamma(\pi f T)^2] \quad (3.7a)$$

$$H_2(f) = \sqrt{1-\alpha} \exp[j2\pi f(\frac{\Delta\tau}{2}) - j\gamma(\pi f T)^2] \quad (3.7b)$$

where,

$$h_1(t) = h_{pmd1}(t) \otimes h_{cd}(t) \quad (3.7c)$$

$$h_2(t) = h_{pmd2}(t) \otimes h_{cd}(t) \quad (3.7d)$$

$h_{cd}(t) = F^{-1}[H_{cd}(f)]$; Fiber impulse response due to chromatic dispersion

$h_{pmd}(t) = F^{-1}[H_{pmd}(f)]$; Fiber impulse response due to PMD

3.3.2 Optical signal input to the MZI pair 1 and 2

The optical input to the first pair of the Mach-Zehnder interferometers can be expressed as

$$E_{s1}(t) = \sqrt{2P_s} \exp[j\{2\pi f t + \phi_{s1}(t)\}] \quad (3.8)$$

where $\phi_{s1}(t)$ = output phase

$$\phi_{s1}(t) = \text{Re}[\exp(j\phi_s(t)) \otimes h_1(t)] \quad (3.9a)$$

$$= \text{Re}[\int_{-\infty}^t h_1(t') \exp(j\phi_s(t-t')) dt'] \quad (3.9b)$$

$$\text{again, } \phi_s(t-t') = \phi'_s(t-t') + \phi_{n1}(t-t') \quad (3.9c)$$

Thus, for linear phase approximation, we can write,

$$\begin{aligned} \phi_{s1}(t-t') &= \text{Re}[\int_{-\infty}^t h_1(\tau) \phi'_s(t-\tau) d\tau] + \text{Re}[\int_{-\infty}^t h_1(\tau) \phi_{n1}(t-\tau) d\tau] \\ &= \theta'_{s1}(t) + \theta'_{n1}(t) \end{aligned} \quad (3.10a)$$

where, $\theta'_{s1}(t)$, the filtered output signal phase of the 1st pair MZI,

$\theta'_{n1}(t)$, Laser phase noise and

$$\begin{aligned}
 \theta'_{s1}(t) &= \text{Re} \left[\int_{-\infty}^t h_1(\tau) \phi'_s(t-\tau) d\tau \right] \\
 &= \phi'_s(t) \otimes h_1(t) \\
 &= 2\pi \Delta f \int_{-\infty}^t I(t) dt \otimes h_1(t) \\
 &= 2\pi \Delta f \int_{-\infty}^t \sum_k a_k p(t-kT) \otimes h_1(t) dt
 \end{aligned} \tag{3.10b}$$

$$\theta'_{s1}(t) = 2\pi \Delta f \int_{-\infty}^t \sum_k a_k g_1(t-kT) dt; \tag{3.10c}$$

$$\text{where } g_1(t) = \text{Re}[p(t) \otimes h_1(t)] \tag{3.10d}$$

The detailed derivation of the $g_1(t)$ is given in the *Appendix A*

Similarly, the filtered output signal phase of the 2nd pair MZI is given by,

$$\theta'_{s2}(t) = 2\pi \Delta f \int_{-\infty}^t \sum_k a_k g_2(t-kT) dt \tag{3.11a}$$

$$\text{where } g_2(t) = \text{Re}[p(t) \otimes h_2(t)] \tag{3.11b}$$

3.3.3 Transmittance of MZI

In the FSK direct detection receiver with Mach-Zehnder interferometers (MZI), the MZIs are act as optical filter and differentially detect the 'mark' and 'space' of the received FSK signal, which are then directly fed to a pair of photo-detectors. $T_1(f)$ and $T_2(f)$ represent the transfer function of the Mach-Zehnder interferometer from its input port to its sum and difference ports respectively. Suppose, one branch of MZI has a delay equal to τ sec. Thus the transmittances of the two branches are:

$$T_1(f) = \frac{1}{2} [\cos^2(\pi f \tau)] \tag{3.12a}$$

$$T_2(f) = \frac{1}{2} [\sin^2(\pi f \tau)] \tag{3.12b}$$

where, τ is the time delay between the two branches of the MZI.

$\tau = \frac{1}{4 \Delta f}$ and $\Delta f = \frac{f_c}{2n+1}$, f_c is the carrier frequency of the FSK signal

and n is an integer. The 'mark' and 'space' of the FSK signals are represented by

f_1 and f_2 respectively, where $f_1 = f_c + \Delta f$ and $f_2 = f_c - \Delta f$. Therefore, when 'mark' is transmitted, $T_1(f)=1$ and $T_2(f)=0$. Similarly, for transmission of 'space', $T_1(f)=0$ and $T_2(f)=1$. Thus, two different signals f_1 and f_2 can be extracted from two output ports of the MZI. Here, the MZI is used in our analysis only as an optical frequency discriminator (OFD) as our analysis is based on single channel operation.

3.3.4 Photodetector output current (1st and 2nd balanced detector)

For a mark transmission, the current at the output of the first balanced photodetector is given by,

$$i_{m1}(t) = R_d P_s \cos[2\pi f_c \tau + \Delta\theta_{s1}(t, \tau) + \Delta\theta_{n1}(t, \tau)] \quad (3.13)$$

where,

$$\begin{aligned} \Delta\theta_{s1}(t, \tau) &= \theta'_{s1}(t) - \theta'_{s1}(t - \tau) \\ &= 2\pi \Delta f \int_{-\infty}^t \sum_k a_k g_1(t - kT) dt - 2\pi \Delta f \int_{-\infty}^{t-\tau} \sum_k a_k g_1(t - kT) dt \\ &= 2\pi \Delta f \int_{t-\tau}^t \sum_k a_k g_1(t - kT) dt \end{aligned} \quad (3.14)$$

τ is the time delay between the two branches of the MZI and

$$\Delta\theta_{n1}(t, \tau) = \theta_n(t) - \theta_n(t - \tau) \quad (3.15)$$

$$i_{m1}(t) = R_d P_s \cos[2\pi f_c \tau + 2\pi \Delta f \int_{t-\tau}^t \sum_k a_k g_1(t - kT) dt + \Delta\theta_{n1}(t, \tau)] \quad (3.16a)$$

$$\begin{aligned} &= R_d P_s \cos[2\pi f_c \tau + 2\pi \Delta f \int_{t-\tau}^t a_0 g_1(t - kT) dt + \\ &2\pi \Delta f \int_{t-\tau, k \neq 0}^t \sum_k a_k g_1(t - kT) dt + \Delta\theta_{n1}(t, \tau)] \end{aligned} \quad (3.16b)$$

For mark transmission, $a_0 = 1$ and ideal CPFSK demodulation condition (assuming NRZ data), we have, $2\pi f_c \tau = (2n + 1)\pi/2$, where n is an integer. For $n = 0$; $2\pi \Delta f \tau = \pi/2$; Also for optimum demodulation, $\tau = T/2h$ and $h (= 2\Delta f T)$ is the modulation index. Now applying the condition of ideal (optimum) CPFSK demodulation, in the above equation,

$$i_{m1}(t) = R_d P_s \cos[2\pi f_c \tau + 2\pi \tau \Delta f q_1(t) + 2\pi \tau \Delta f \sum_{k \neq 0} a_k q_1(t - kT) + \Delta\theta_{n1}(t, \tau)] \quad (3.17a)$$

$$= R_d P_s \cos[2\pi f_c \tau + \frac{\pi}{2} - \frac{\pi}{2} + \frac{\pi}{2} q_1(t) + \frac{\pi}{2} \sum_{k \neq 0} a_k q_1(t - kT) + \Delta\theta_{n1}(t, \tau)] \quad (3.17b)$$

$$\text{where, } q_1(t) = \frac{1}{\tau} \int_{t-\tau}^t g_1(t) dt ; \quad g_1(t) = \text{Re}[p(t) \otimes h_1(t)]$$

$$\Delta\theta_{n1}(t, \tau) = \theta_{n1}(t) - \theta_{n1}(t - \tau) \quad (3.18)$$

where $\Delta\theta_{n1}(t, \tau) = \int_{t-\tau}^t \mu(t_1) dt_1$, Phase distortion due to laser phase noise and

$$2\pi f_c \tau + \frac{\pi}{2}, \text{ Expected phase change for 'mark'}$$

In equation (3.17b) the first two terms in the argument of the cosine function provides the expected phase change for the 'mark' received in an 'ideal' case, the next three terms represent the phase distortion of the signal. So, the phase distortion or output phase noise due to PMD and GVD given by,

$$\Delta\theta_{pmd,cd1}(t, \tau) = -\frac{\pi}{2} + \frac{\pi}{2} q_1(t) + \frac{\pi}{2} \sum_{k \neq 0} a_k q_1(t - kT) \quad (3.19a)$$

$$= \Delta\varphi_{s1}(t, \tau) + \frac{\pi}{2} \sum_{k \neq 0} a_k q_1(t - kT) \quad (3.19b)$$

$$= \Delta\varphi_{s1}(t, \tau) + \xi_1 \quad (3.19c)$$

where, $\Delta\varphi_{s1}(t, \tau)$, Mean output phase error due the first pair of photodetector, and

ξ_1 , Random output phase fluctuation due to ISI for random bit pattern caused by PMD and GVD in the 1st pair of MZI.

For a mark transmission, the current at the output of the second balanced photodetector is given by,

$$i_{m2}(t) = R_d P_s \cos[2\pi f_c \tau + 2\pi \tau \Delta f q_2(t) + 2\pi \tau \Delta f \sum_{k \neq 0} a_k q_2(t - kT) + \Delta\theta_{n2}(t, \tau)] \quad (3.20a)$$

$$= R_d P_s \cos[2\pi f_c \tau + \frac{\pi}{2} - \frac{\pi}{2} + \frac{\pi}{2} q_2(t) + \frac{\pi}{2} \sum_{k \neq 0} a_k q_2(t - kT) + \Delta\theta_{n2}(t, \tau)] \quad (3.20b)$$

where, $q_2(t) = \frac{1}{\tau} \int_{t-\tau}^t g_2(t) dt$; $g_2(t) = \text{Re}[p(t) \otimes h_2(t)]$ and

$$\Delta\theta_{pmd,cd2}(t, \tau) = \Delta\varphi_{s2}(t, \tau) + \xi_2 \quad (3.21)$$

where, $\Delta\varphi_{s2}(t, \tau)$, Mean output phase error of the second pair of photodetector, and

ξ_2 , Random output phase fluctuation due to ISI for random bit pattern caused by PMD and GVD in the 2nd pair MZI.

3.3.5 Noise power

The output noise contributed by the photodetector quantum shot noise, the receiver thermal noise, the interferometric noise due to input intensity fluctuation.

The different spectral densities are:

$$S_{pd}(f) = 2R_d P_s = 2e\langle i \rangle BW \quad (3.22a)$$

$$S_{th}(f) = i_{th}^2 = \frac{4KT BW}{R_L} \quad (3.22b)$$

$$S_{pdi}(f) = 0.5R_d^2 P_s^2 [S_x(f) - \bar{x}^2 \delta(f)] \quad (3.22c)$$

where $S_x(f)$ and \bar{x} represent the PSD and the mean value of $x(t)$ respectively and $\delta(f)$ is a delta function in frequency. Denoting the total noise power spectral density by,

$$S_n(f) = S_{pd}(f) + S_{th}(f) + S_{pdi}(f) \quad (3.23)$$

The total noise power at the receiver output can be obtained as,

$$\sigma_m^2 = \sigma_s^2 = \int_{-\infty}^{\infty} S_n(f) |H_R(f)|^2 df \quad (3.24)$$

where, $H_R(f)$ is the transfer function of a Gaussian low-pass filter in the receiver of 3-dB bandwidth equal to 0.75 B.

3.3.6 Conditional BER expression

The total output signal currents corresponding to a 'mark' and 'space' are given by,

$$\begin{aligned} i_m(t) &= i_{m1}(t) + i_{m2}(t) \\ &= R_d P_s x_1(t) + R_d P_s x_2(t) \end{aligned} \quad (3.25)$$

and

$$\begin{aligned} i_s(t) &= -[i_{s1}(t) + i_{s2}(t)] \\ &= -[R_d P_s x_1(t) + R_d P_s x_2(t)] \end{aligned} \quad (3.26)$$

where, $x_1(t)$ and $x_2(t)$ describe the phase noise induced by the interferometer intensity due to random phase fluctuation and can be expressed as,

$$x_1(t) = \cos[\Delta\varphi_1(t)] \quad (3.27a)$$

$$\text{and } x_2(t) = \cos[\Delta\varphi_2(t)] \quad (3.27b)$$

again, $\Delta\varphi_1(t)$ and $\Delta\varphi_2(t)$ are given by.

$$\Delta\varphi_1(t) = \Delta\theta_{pmd,cd1}(t) + \Delta\varphi_n(t) \quad (3.27c)$$

$$\Delta\varphi_2(t) = \Delta\theta_{pmd,cd2}(t) + \Delta\varphi_n(t) \quad (3.27d)$$

$\Delta\varphi_n(t)$ is the low pass filtering effect.

Now, ignoring the low pass filtering effect on the phase noise dependent signal term and if we consider the mean phase error only then, the low-pass filter output for 'mark' transmitted, at a sampling time t is,

$$i_m(t) = R_d P_s [\cos(\Delta\varphi_{s1}(t, \tau)) + \cos(\Delta\varphi_{s1}(t, \tau))] + n(t) \quad (3.28a)$$

$$i_s(t) = -2 R_d P_s [\cos(\delta\varphi) \cos(\Delta\varphi)] + n(t) \quad (3.28b)$$

where, $\delta\varphi = \frac{\Delta\varphi_{s1}(t, \tau) - \Delta\varphi_{s2}(t, \tau)}{2}$, $\Delta\varphi = \frac{\Delta\varphi_{s1}(t, \tau) + \Delta\varphi_{s2}(t, \tau)}{2}$ and $n(t)$ is

the sample function of the filtered output noise contributed by the photodetector quantum shot noise, receiver thermal noise and the interferometric noise due to input intensity fluctuation.

$$\text{Let } Q = \frac{i_m(t) - i_s(t)}{\sigma_m + \sigma_s} \quad (3.29a)$$

$$Q = \frac{4R_d P_s [\cos(\bar{\delta\varphi}) \cos(\bar{\Delta\varphi})]}{\sigma_m + \sigma_s} \quad (3.29b)$$

Then, the conditional bit error rate can be expressed as,

$$P(e | \bar{\delta\varphi}, \bar{\Delta\varphi}) = \frac{1}{2} \operatorname{erfc}\left(\frac{Q}{\sqrt{2}}\right) \quad (3.30)$$

For a given value of mean DGD, $\Delta\tau$, the conditional BER can be expressed as:

$$\text{BER}(\Delta\tau) = \int_{-\infty}^{\infty} \int_{-\infty}^{\infty} P(e | \bar{\delta\varphi}, \bar{\Delta\varphi}) P_{\delta\varphi}(\delta\varphi) P_{\Delta\varphi}(\Delta\varphi) d(\delta\varphi) d(\Delta\varphi) \quad (3.31)$$

3.3.7 PDF of random output phase and average BER

Considering the effect of random output phase fluctuation caused by PMD and GVD, the output current for 'mark' is given by,

$$i_m(t) = R_d P_s [\cos(\Delta\varphi_{s1}(t, \tau) + \xi_1) + \cos(\Delta\varphi_{s1}(t, \tau) + \xi_2)] + n(t) \quad (3.32)$$

The contribution of the term (random phase fluctuation) ξ_1 and ξ_2 can be evaluated by finding the pdf. Assuming $\{a_k\}$ are independent and identically distributed (iid) random variables, the characteristic function of ξ_1 and ξ_2 is given by [61],

$$\Phi_{\Delta\theta_{s1}}(j\xi_1) = \prod_{i=1}^{\infty} \cos[\xi_1 q_{1i}(t)] = \sum_{i=1}^{\infty} \frac{(j\xi_1)^{2i}}{(2i)!} M'_{2i} \quad (3.33a)$$

$$\Phi_{\Delta\theta_{s2}}(j\xi_2) = \prod_{i=1}^{\infty} \cos[\xi_2 q_{2i}(t)] = \sum_{i=1}^{\infty} \frac{(j\xi_2)^{2i}}{(2i)!} M''_{2i} \quad (3.33b)$$

where, $q_{1i}(t) = |q_1(t - iT)|$, $q_{2i}(t) = |q_2(t - iT)|$, M'_{2i} and M''_{2i} are the even order moments of the characteristic function of random variable ξ_1 and ξ_2 respectively;

which can be evaluated by using the following recursive relations [62].

$$M'_{2r} = Y'_{2r}(N) \quad (3.34a)$$

$$M''_{2r} = Y''_{2r}(N) \quad (3.34b)$$

$$Y'_{2r}(i) = \sum_{j=0}^r {}^{2r}C_{2j} Y'_{2j}(i-1) q_{1i}^{2r-2j} \quad (3.34c)$$

$$Y''_{2r}(i) = \sum_{j=0}^r {}^{2r}C_{2j} Y''_{2j}(i-1) q_{2i}^{2r-2j} \quad (3.34d)$$

where, ${}^{2r}C_{2j}$ is the binominal coefficient and N is the actual number of terms.

The pdf of ξ_1 and ξ_2 random variable over an interval T' can be obtained as,

$$P_{\xi_1} = F^{-1}[\Phi_{\Delta\theta_1}(j\xi_1)] \quad (3.35a)$$

$$P_{\xi_2} = F^{-1}[\Phi_{\Delta\theta_2}(j\xi_2)] \quad (3.35b)$$

where, F^{-1} denotes the inverse Fourier transformation.

$$i_m(t) = 2R_d P_s \cos\left[\frac{\Delta\theta_{pmd,cd1}(t) - \Delta\theta_{pmd,cd2}(t)}{2}\right] \cos\left[\frac{\Delta\theta_{pmd,cd1}(t) + \Delta\theta_{pmd,cd2}(t)}{2}\right] + n(t) \quad (3.36a)$$

$$\text{Let, } \delta\varphi = \frac{\Delta\theta_{pmd,cd1}(t) - \Delta\theta_{pmd,cd2}(t)}{2} \quad (3.36b)$$

$$\text{and } \Delta\varphi = \frac{\Delta\theta_{pmd,cd1}(t) + \Delta\theta_{pmd,cd2}(t)}{2} \quad (3.36c)$$

$$\text{So, } i_m(t) = 2R_d P_s [\cos(\delta\varphi) \cos(\Delta\varphi)] + n(t) \quad (3.36d)$$

Similarly, for 'space' the current is,

$$i_s(t) = -2R_d P_s [\cos(\delta\varphi) \cos(\Delta\varphi)] + n(t) \quad (3.37)$$

Now according to the equation (3.36b) and (3.36c) equations, the ultimate

characteristic functions of $\delta\varphi$ and $\Delta\varphi$ are,

$$\Phi_{\delta\varphi}(j\xi) = \Phi_{\Delta\theta_1}(j\xi_1) \Phi_{\Delta\theta_2}^*(j\xi_2) \quad (3.38a)$$

$\Phi_{\Delta\theta_2}^*(j\xi_2)$ is the complex conjugate of $\Phi_{\Delta\theta_2}(j\xi_2)$ pdf

$$\Phi_{\Delta\varphi}(j\xi) = \Phi_{\Delta\theta_1}(j\xi_1) \Phi_{\Delta\theta_2}(j\xi_2) \quad (3.38b)$$

The pdf of $\delta\varphi$ and $\Delta\varphi$ can given by,

$$P_{\delta\varphi}(\delta\varphi) = F^{-1}[\Phi_{\delta\varphi}(j\xi)] \quad (3.39a)$$

$$P_{\Delta\varphi}(\Delta\varphi) = F^{-1}[\Phi_{\Delta\varphi}(j\xi)] \quad (3.39b)$$

The joint pdf of $\delta\varphi$ and $\Delta\varphi$ can expressed as,

$$P_{\delta\varphi, \Delta\varphi}(\delta\varphi, \Delta\varphi) = P_{\delta\varphi}(\delta\varphi) \otimes P_{\Delta\varphi}(\Delta\varphi) \quad (3.39c)$$

The average bit error rate of a direct detection CPFSK system is then,

$$BER(\Delta\tau) = \int_{-\infty}^{\infty} \int_{-\infty}^{\infty} P(e | \delta\varphi, \Delta\varphi) P_{\delta\varphi, \Delta\varphi}(\delta\varphi, \Delta\varphi) d(\delta\varphi) d(\Delta\varphi) \quad (3.40)$$

where, $P_{\delta\varphi}(\delta\varphi)$ and $P_{\Delta\varphi}(\Delta\varphi)$ are the probability density function of $\delta\varphi$ and $\Delta\varphi$ respectively.

Till now we assume that the DGD increases linearly along the length of fiber link. But in real fiber the DGD does not increase linearly due to coupling of two propagating modes. The amount of coupling between the modes is strongly dependent on the length of the fiber. It is shown that if the fiber length is much longer than the correlation length of the disturbances that cause the changes of symmetry in fiber geometry and stress, the DGD $\Delta\tau$ between the two PSPs follows a Maxwellian probability density function [11].

Using equation (1.5), the average error probability for mean DGD can be evaluated as

$$BER(\langle\Delta\tau\rangle) = \int_{-\infty}^{\infty} BER(\Delta\tau)P_{\Delta\tau}(\Delta\tau)d(\Delta\tau) \quad (3.41)$$

where, $P_{\Delta\tau}(\Delta\tau)$ is the PDF of $\Delta\tau$ which has Maxwellian distribution with $\Delta\tau_m$ as quadratic mean of $\Delta\tau$.

3.4 Results and discussion

Following the analytical approach, the bit error rate performance results for direct detection CPFSK receiver with post detection low pass filter are evaluated at a bit rate of 10 Gb/s with several values of mean DGD and fiber lengths for the following cases:

- (i) Conditional BER performance
- (ii) Average BER performance
- (iii) Average BER performance considering Maxwellian distribution for mean DGD.

3.4.1 Conditional BER performance

Based on equation (3.31) the plots of conditional BER versus received power P_s are shown in Fig. 3.3 for mean DGD of 10 ps, 20 ps, 30 ps, 40 ps, 50ps and 60 ps with fiber length of 100 km and modulation index of 0.50 and 1.0. The results show that the BER is highly degraded when the mean DGD is higher for a given fiber length and the system suffers a significant amount power penalty at $BER = 10^{-9}$ which is increasing with increasing value of the mean DGD.

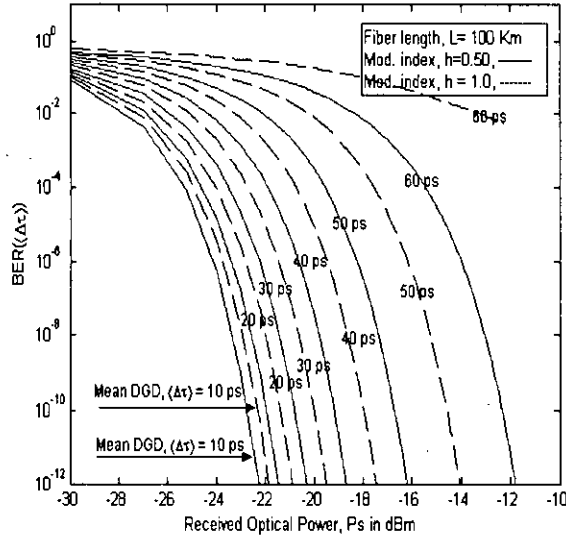


Fig. 3.3 : Plots of conditional BER versus received power, P_s for direct detection CPFSK system impaired by PMD

The amount of power penalty is found to be approximately 0.50 dB, 1.45 dB, 2.70 dB and 4.50 dB for mean DGD of 10 ps, 20 ps, 30 ps and 40 ps respectively when the modulation index is 0.50. It is further observed that the penalty is much higher at higher modulation index such as $h=1$ compared to $h=0.50$ i.e., the penalty is approximately 5.25 dB when mean DGD is 40 ps and $h=1.0$. The penalty due to PMD suffered by the direct detection CPFSK system without post detection low pass filter at $BER 10^{-9}$ is plotted in Fig. 3.4 as a function of DGD normalized by bit rate. The plots of penalty due to other modulation scheme as reported in [26] are also shown for comparison. It is found that penalty suffered by direct detection CPFSK is higher than that of OOK and DPSK system. For example, the penalty is 1.50 dB and 2.75. dB corresponding to DGD/bit duration ratio ($\Delta\tau/T$) are 0.20 and 0.30 respectively for direct detection CPFSK system.

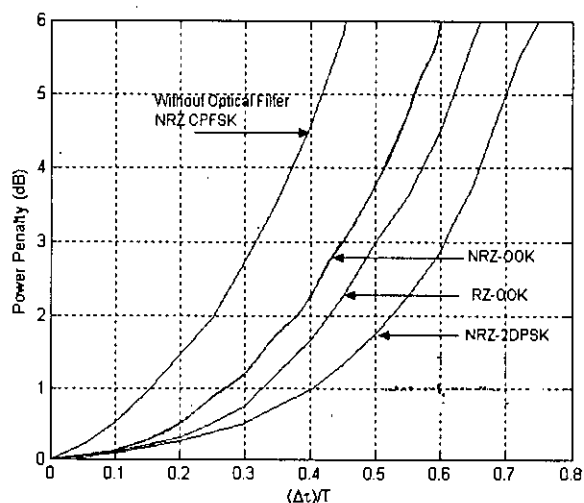


Fig. 3.4: PMD-induced power penalty as a function of DGD/ bit duration ratio ($\langle \Delta\tau \rangle / T$) for NRZ- and RZ-OOK, NRZ-2DPSK and NRZ-CPFSK system.

3.4.2 Average BER performance

We derive equation (3.40) based on the pdf of the random output phase fluctuation due the PMD and GVD. The plots of average BER versus received optical power P_s are shown in Fig. 3.5 for mean DGD of 10 ps, 20 ps, 30 ps, 40 ps, 50ps and 60 ps with fiber length of 100 km and modulation index of 0.50 and plots for modulation index 1.0 are shown in Fig.3.6. The results show that the BER is highly degraded when the mean DGD is higher for a given fiber length and the system suffers a significant amount power penalty at $BER = 10^{-9}$ which is found to increase with increasing value of the mean DGD.

The penalty due to PMD suffered by the direct detection CPFSK system with post detection low pass filter at $BER = 10^{-9}$ is plotted in Fig. 3.7 as a function of DGD normalized by bit rate. The plots of penalty due to other modulation scheme as reported in [26] are also shown for comparison. The amount of power penalty is found to be approximately 0.50 dB, 1.10 dB, 2.10 dB and 3.50 dB for mean DGD of 20 ps, 30 ps, 40 ps and 50 ps respectively when the modulation index is 0.50. It is further observed that the penalty is much higher at higher

modulation index such as $h=1$ compared to $h=0.50$ i.e., the penalty is approximately 4.10 dB when mean DGD is 40 ps and $h=1.0$. It is further noticed that penalty suffered by direct detection CPFSK is lower than that of NRZ-OOK system. But at higher modulation index penalty suffered by CPFSK with 0.50 is higher than that of OOK and DPSK system.

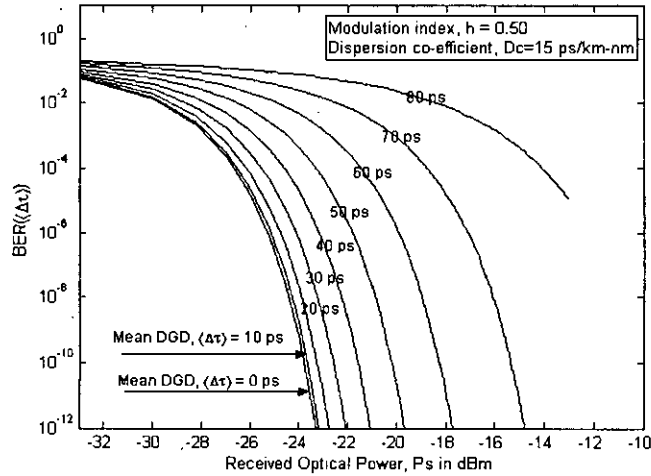


Fig.3.5: Average BER versus received power, P_s for direct detection CPFSK system impaired by PMD (modulation index, $h=0.50$)

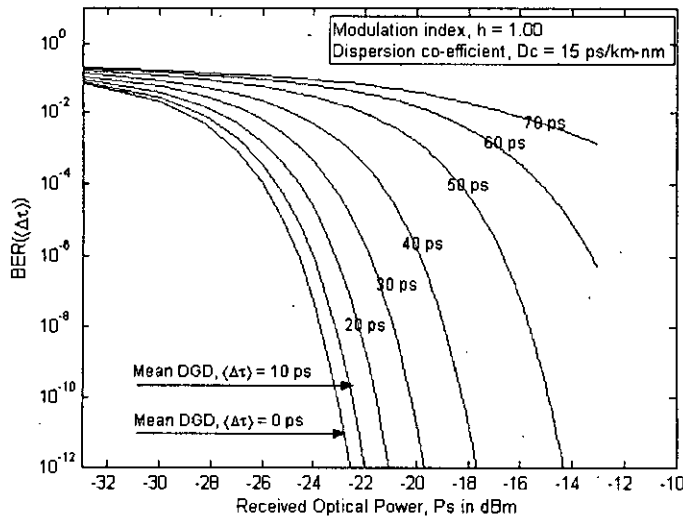


Fig.3.6: Average BER versus received power, P_s for direct detection CPFSK system impaired by PMD (modulation index, $h=1.0$)

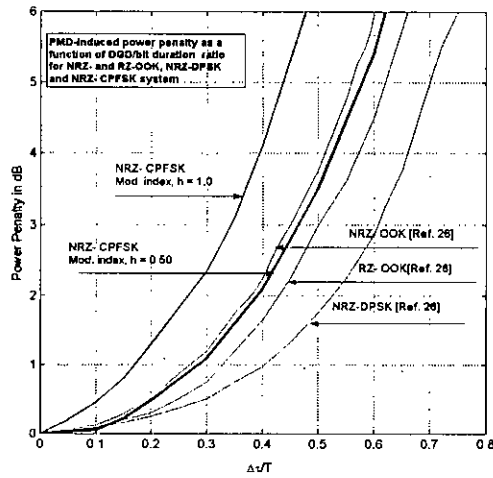


Fig.3.7: PMD-induced power penalty as a function of DGD/ bit duration ratio ($\Delta\tau > /T$) for NRZ- and RZ-OOK, NRZ-2DPSK and NRZ-CPFSK system.

3.4.3 Average BER considering Maxwellian distribution of DGD

Considering the fiber-optic link length is much larger than the correlation length, where the coupling between the propagating modes is strong and DGD follows a Maxwellian distribution. Based on the above assumption we derive equation (3.42) and hence the BER performance of direct detection CPFSK is obtained.

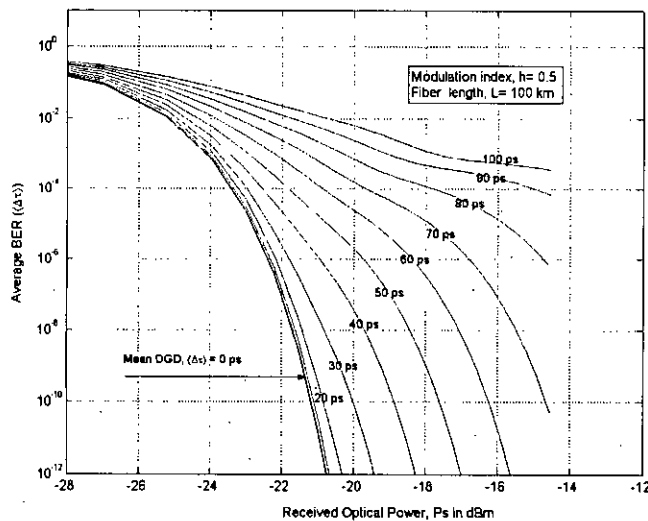


Fig. 3.8 : Plots of average BER versus received power, P_s for direct detection CPFSK receiver impaired by PMD (modulation index $h = 0.50$)

The plots of average BER versus received power, P_s are shown in Fig. 3.8 and Fig.3.9 at modulation index of 0.50 and 1.0 respectively for different values of mean DGD at a bit rate of 10 Gb/s. The results show that the BER performance is more affected at higher values of mean DGD and at higher modulation index.

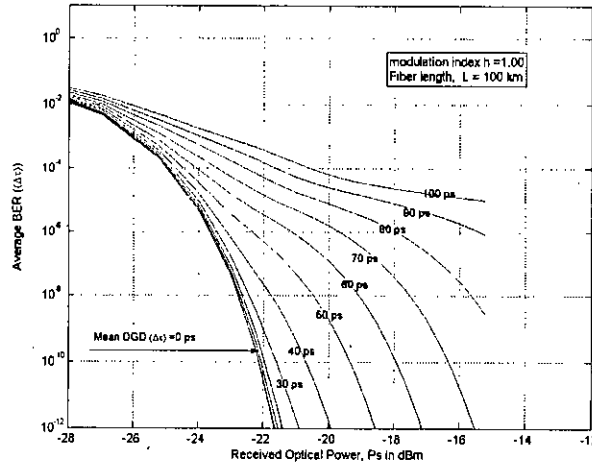


Fig. 3.9: Plots of average BER versus received power, P_s for direct detection CPFSK receiver impaired by PMD (modulation index, $h = 1.0$)

The penalty due to PMD suffered by the direct detection CPFSK system at BER 10^{-9} is plotted in Fig.3.10 as a function of DGD normalized by bit duration. It is observed from Fig.3.8 that the penalty at BER = 10^{-9} is increasing with increasing values of the mean DGD. The amount of penalty is found to be approximately 0.15 dB, 1.0 dB, 3.40 dB and 6.40 dB corresponding to mean DGD of 20 ps, 40 ps, 60 ps and 80 ps respectively. Further increase of DGD leads to a BER floor above 10^{-9} which can not be lowered by further increasing the signal power. It is observed from Fig. 3.8 and Fig.3.9 that BER floors occur at about 10^{-4} and 10^{-8} for modulation index of 0.50 and 1.0 respectively to a corresponding mean DGD of 90 ps.

3.5 Summary

An analytical approach is presented to evaluate the impact of PMD on the bit error rate performance of direct detection CPFSK system. The results show that

the penalty due to PMD suffered by the CPFSK system is significant at higher modulation index and higher value of the DGD between two-polarization modes. The results show that the penalty due to PMD suffered by the direct detection CPFSK system is 4.0 dB corresponding to a mean DGD of 60 ps at modulation index of 1.0. Thus the amount of power penalty is higher at higher values of modulation index and higher values of the differential group delay between the two polarization axes. Also a direct-detection CPFSK system with modulation index of 0.50 suffers slightly higher amount of power penalty than a direct detection NRZ-DPSK system

Chapter 4

EFFECT OF PMD IN HETERODYNE OPTICAL CPFSK TRANSMISSION SYSTEM

Recently, there has been considerable activity in the lightwave community aimed at comparing the performance similarities and differences between preamplified direct – detection lightwave systems and heterodyne lightwave systems. Coherent optical transmission systems using heterodyne or homodyne detection are attractive due to their improved receiver sensitivity compared with direct detection. In this chapter, a theoretical analysis is developed to evaluate the BER performance degradation of an optical heterodyne CPFSK system caused by signal phase distortion due to PMD in a single mode fiber. The conditional and unconditional BER performance results are evaluated at a bit rate of 10 Gb/s considering Maxwellian distribution for the DGD.

4.1 Introduction

Optical heterodyne CPFSK may be an attractive modulation format for future multi-channel optical system, because of the tolerance of CPFSK receivers to laser phase noise and modulation can be easily performed using direct laser diode. In particular, CPFSK modulation with a frequency deviation equal to half

the bit rate has a more compact spectrum than the PSK signal and is therefore suitable for high speed transmission system. Heterodyne lightwave system offers the possibility of frequency selectivity, which allows the transmission of multiple information channels by closely spaced frequency division multiplexing and the use of cascades of optical amplifiers. In homodyne or heterodyne optical communication system, the receiver sensitivity deteriorates significantly due to the fluctuation of state of polarization (SOP). The requirement and automatic polarization control methods for coherent optical communication are described in detail in [63]-[65]. The impact of PMD to coherent optical signal was reported in [66] and the effects of PMD to DPSK signal was studied [26]-[27],[68]. B. Hu *et al* [69], demonstrated a novel chromatic and PMD monitoring method based on coherent heterodyne detection and RF signal processing. The effect of PMD on the conditional bit error rate performance of heterodyne FSK system is presented in [57].

The contribution of this work is to assess the BER performance limitations analytically of an optical heterodyne CPFSK with delay-demodulation system impaired by PMD. The temporal behaviors of the fiber PMD are of statistical in nature due to randomness of the birefringence variations along the fiber structure. Therefore to assess accurately the optical transmission impairment due to PMD, we analytically determine pdf of the random phase fluctuation due to PMD and GVD at the output of the receiver. Using the pdf we evaluate the average BER and power penalty for different mean values of DGD in the correlation length regime and considering Maxwellian probability density function for the DGD beyond the correlation length, at the receiver output in the presence of receiver noise. The bit error rate performance and power penalty suffered by the system due to PMD at a BER of 10^{-9} are evaluated at a bit rate of 10 Gb/s.

4.2 Delay demodulation receiver model

The received optical signal is combined with the optical signal output from the local oscillator and the two signals are detected by photo-detector. The output of the photodetector which is an intermediate frequency (IF) signal is amplified by the receiver pre-amplifier and then filtered by a Gaussian filter with center frequency set to the IF. The bandwidth of the IF is kept twice the bit rate for optimum demodulation. The output of the filter is then demodulated using a delay line discriminator. The output of the discriminator is then filtered by a low-pass filter and fed to a sampler followed by a comparator. The threshold voltage of the comparator is set to zero value. If the output voltage is greater than zero than a binary '1' is detected, otherwise a binary '0' is detected. The block diagram of a CPFSK delay demodulation receiver is shown in Fig. 4.1.

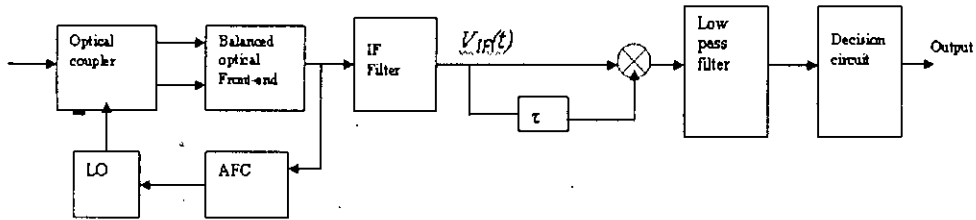


Fig. 4.1: Block diagram of a heterodyne CPFSK delay demodulation receiver

4.3 Theoretical analysis

The complex electric field at the output of the continuous phase FSK (CPFSK) transmitter and input to the fiber is represented as

$$E_1(t) = \sqrt{2P_T} \exp[j2\pi f_c t + j\phi_s(t)][c_1.e_1] \quad (4.1)$$

$$E_2(t) = \sqrt{2P_T} \exp[j2\pi f_c t + j\phi_s(t)][c_2.e_2] \quad (4.2)$$

where, f_c is the carrier frequency, P_T is the transmitted optical power and the CPFSK modulating phase $\phi_s(t)$ is given by

$$\phi_s(t) = 2\pi \Delta f \int_{-\infty}^t I(t) dt + \phi_n(t) \quad (4.3)$$

$$I(t) = \sum_{k=-\infty}^{\infty} a_k p(t - kT) \quad (4.4)$$

where $a_k = \pm 1$ is the random NRZ bit pattern of the k th information, Δf is the peak frequency deviation, $p(t)$ is the elementary pulse shape of duration T seconds and $\phi_n(t)$ is the phase noise of the transmitting laser. Here, c_1, c_2 represent unit vectors and e_1, e_2 represent the two principal states of polarization (PSPs) respectively.

The electric field output of the fiber is then given by

$$E_{01}(t) = \sqrt{2P_T} \exp[j2\pi f_c t + j\phi_s(t)] [c_1 \cdot e_1] \otimes h_1(t) \quad (4.5)$$

$$E_{02}(t) = \sqrt{2P_T} \exp[j2\pi f_c t + j\phi_s(t)] [c_2 \cdot e_2] \otimes h_2(t) \quad (4.6)$$

where $h_1(t)$ and $h_2(t)$ are the inverse Fourier transform of the fiber low pass transfer function of a non-dispersion shifted lossless fiber $H_1(f)$ and $H_2(f)$ respectively, which include the effect of PMD and group velocity dispersion and \otimes denotes convolution. Here, we assume that there is a negligible amount of polarization dependent loss. Thus the input electric field is projected onto two PSPs. The implicit expression for $H_1(f)$ and $H_2(f)$ are given by,

$$H_1(f) = \sqrt{\alpha} \exp[j2\pi f (-\frac{\Delta\tau}{2}) - j\gamma(\pi f T)^2] \quad (4.7)$$

$$H_2(f) = \sqrt{1-\alpha} \exp[j2\pi f (\frac{\Delta\tau}{2}) - j\gamma(\pi f T)^2] \quad (4.8)$$

where α is the PMD power splitting ratio, $\Delta\tau$ represents the DGD between the two PSPs and

$$\gamma = \text{Chromatic dispersion index} = \frac{\lambda^2}{\pi c} DR_b L;$$

T = pulse duration, λ = wavelength, D = Chromatic dispersion, R_b = Bit rate

and L = fiber length

Now, assuming linear phase approximation, the output electric fields for two polarization states can be given as,

$$E_{01}(t) = \sqrt{2P_s} \exp[j2\pi f_c t + j\phi_{01}(t)] [c_1 \cdot e_1] \quad (4.9)$$

$$E_{02}(t) = \sqrt{2P_s} \exp[j2\pi f_c t + j\phi_{02}(t)] [c_2 \cdot e_2] \quad (4.10)$$

where,

$$\phi_{01}(t) = \text{Re}[\phi_s(t) \otimes h_1(t)] \quad (4.11a)$$

$$= 2\pi \Delta f \int_{-\infty}^t \sum_k a_k \text{Re}[p(t-kT) \otimes h_1(t)] dt \quad (4.11b)$$

and

$$\phi_{02}(t) = \text{Re}[\phi_s(t) \otimes h_2(t)] \quad (4.12a)$$

$$= 2\pi \Delta f \int_{-\infty}^t \sum_k a_k \text{Re}[p(t-kT) \otimes h_2(t)] dt \quad (4.12b)$$

The signal at the output of the IF filter is given by,

$$i_0(t) = R_d \sqrt{P_s P_{Lo}} \{ \exp[j2\pi f_{IF} t + j\phi'_{01}(t)] + \exp[j2\pi f_{IF} t + j\phi'_{02}(t)] \} + i_n(t) \quad (4.13)$$

now considering the real part only

$$i_0(t) = R_d \sqrt{P_s P_{Lo}} \{ \cos[2\pi f_{IF} t + \phi'_{01}(t)] + \cos[2\pi f_{IF} t + \phi'_{02}(t)] \} + i_n(t) \quad (4.14)$$

where $i_n(t)$ represents the total noise current consisting of shot noise and receiver thermal noise, R_d is the responsivity of the photodetector, P_s is the output power at the fiber end, P_{Lo} is the local oscillator power, f_{IF} is the IF frequency.

The phases $\phi'_{01}(t)$ and $\phi'_{02}(t)$ are given by

$$\phi_{01}(t) = \text{Re}[\phi_s(t) \otimes h_1(t) \otimes h_{IF}(t)] \quad (4.15a)$$

$$\phi'_{01}(t) = 2\pi \Delta f \int_{-\infty}^t \sum_k a_k g_1(t - kT) dt \quad (4.15b)$$

$$\text{where, } g_1(t) = \text{Re}[p(t) \otimes h_1(t) \otimes h_{IF}(t)] \quad (4.15c)$$

$$\text{and } \phi_{02}(t) = \text{Re}[\phi_s(t) \otimes h_2(t) \otimes h_{IF}(t)] \quad (4.16a)$$

$$\phi'_{02}(t) = 2\pi \Delta f \int_{-\infty}^t \sum_k a_k g_2(t - kT) dt \quad (4.16b)$$

$$\text{where, } g_2(t) = \text{Re}[p(t) \otimes h_2(t) \otimes h_{IF}(t)] \quad (4.16c)$$

where $h_{IF}(t)$ is the impulse response of the IF filter. The IF signal current is then given by [using (14)],

$$i_0 = 2R_d \sqrt{P_s P_{Lo}} \cos\{2\pi f_{IF} t + [\frac{\phi'_{01} + \phi'_{02}}{2}]\} \cos[\frac{\phi'_{01} - \phi'_{02}}{2}] + i_n(t) \quad (4.17)$$

$$\text{Let } \phi'_0(t) = \frac{\phi'_{01} + \phi'_{02}}{2} \quad \text{and} \quad \phi''_0(t) = \frac{\phi'_{01} - \phi'_{02}}{2}$$

$$\text{So, } i_0(t) = 2R_d \sqrt{P_s P_{Lo}} \cos \phi''_0(t) \cos[2\pi f_{IF} t + \phi'_0(t)] + i_n(t) \quad (4.18)$$

The output of the IF filter can be expressed as,

$$v_0(t) = 2R_d \sqrt{P_s P_{Lo}} a(t) \cos[2\pi f_{IF} t + \phi'_0(t)] + n(t) \quad (4.19)$$

Assuming, $a(t) = \cos \phi''_0(t)$ is the amplitude due to PMD and GVD

$n(t)$ is the receiver noise due to photodetection with one sided spectral density and variance, $N_0 = 2eR_d P_{Lo} B_{IF}$, e representing the charge and B_{IF} is the bandwidth of the bandpass filter. It is convenient to assume that $H(f)$ is an ideal bandpass filter about f_{IF} of bandwidth $2B$, where B is the baseband bandwidth of the transmitted digital signal.

Following the delay demodulation (delay time τ) and low pass filtering (wide enough to pass the signal undistorted), the low pass filter (LPF) output is given by,

$$v_{out}(t) = V_0 a(t) \cos[\Delta\phi_0(t, \tau)] \quad (4.20a)$$

$$v_{out}(t) = A(t) \cos[\Delta\phi_0(t, \tau)] \quad (4.20b)$$

where,

$$\begin{aligned} A(t) &= V_0 a(t) \\ &= 2R_d \sqrt{P_s P_{Lo}} \cos\phi_0''(t) \end{aligned}$$

$A(t)$ is the amplitude and the differential output phase of $v_{out}(t)$ of the LPF can be expressed as,

$$\Delta\phi_0(t, \tau) = 2\pi f_{IF} \tau + \Delta\phi_0'(t, \tau) + \Delta\theta_n(t, \tau) \quad (4.21)$$

$$\text{where, } \Delta\phi_0'(t, \tau) = \phi_0'(t) - \phi_0'(t, \tau) \quad (4.22a)$$

$$= 2\pi \Delta f \int_{-\infty}^t \sum_k a_k g_0(t - kT) dt - 2\pi \Delta f \int_{-\infty}^{t-\tau} \sum_k a_k g_0(t - kT) dt \quad (4.22b)$$

$$= 2\pi \Delta f \int_{t-\tau}^t \sum_k a_k g_0(t - kT) dt \quad (4.22c)$$

$$= 2\pi \Delta f \int_{t-\tau}^t \sum_k a_0 g_0(t - kT) dt + 2\pi \Delta f \int_{t-\tau}^t \sum_{k \neq 0} a_k g_0(t - kT) dt \quad (4.22d)$$

Say, a 'mark' is transmitted, thus $a_0 = 1$

$$\Delta\phi_0'(t, \tau) = 2\pi \tau \Delta f q(t) + 2\pi \tau \Delta f \sum_{k \neq 0} a_k q(t - kT) \quad (4.22e)$$

$$\Delta\phi_0'(t, \tau) = \Delta\phi_0(t, \tau) + \xi \quad (4.22f)$$

$$\text{where } q(t) = \frac{1}{\tau} \int_{t-\tau}^t g_0(t) dt \quad \text{and} \quad g_0(t) = \frac{1}{2} [g_1(t) + g_2(t)]$$

using the notation,

$$\Delta\theta_n(t, \tau) = 2\pi \int_{t-\tau}^t \theta_n(t_1) dt_1 \quad (4.23)$$

$$\text{and } \theta_n(t) = \arctan \left[\frac{n_s(t)}{A(t) + n_c(t)} \right] \quad (4.24)$$

105883

$n_c(t)$ and $n_s(t)$ are the in-phase and quadrature components of noise $n(t)$ respectively, with zero mean and variance σ_n^2 . It is assumed that the IF filter is a finite band-pass integrator which is symmetric around f_{IF} with bandwidth $B_{IF} = 2/T$ and demodulation time $\tau = T/2h$, $h \leq 1$ (narrowband CPFSK) and for the IF filter chosen, the correlation between $\theta_n(t)$ and $\theta_n(t-\tau)$ is zero. For other types such as a gaussian or second order Butterworth, the noise correlation is negligibly small for $B_{IF} \geq 2$ and $h \leq 1$ (for NRZ data).

4.3.1 Conditional bit error probability

In delay demodulation receiver the data decisions are based on the polarity of $v_{out}(t)$. Assuming a 'mark' is transmitted (say $a_0 = 1$) and under ideal CPFSK demodulation condition, $2\pi f_{IF} \tau = (2n+1)\pi/2$; n is an integer and $2\pi \Delta f \tau = \pi/2$ for NRZ data. Now, applying the above conditions, the phase of $v_{out}(t)$ at the sampling instant t_0 can be written as [using (4.21) and (4.22e)],

$$\Delta\phi_0(t_0, \tau) = 2\pi f_{IF} \tau + 2\pi \Delta f \tau q(t_0) + 2\pi \tau \Delta f \sum_{k \neq 0} a_k q(t_0 - kT) + \Delta\theta_n(t_0, \tau) \quad (4.25a)$$

$$\Delta\phi_0(t_0, \tau) = 2\pi f_{IF} \tau + \frac{\pi}{2} - \frac{\pi}{2} + \frac{\pi}{2} q(t_0) + \frac{\pi}{2} \sum_{k \neq 0} q(t_0 - kT) + \Delta\theta_n(t_0, \tau) \quad (4.25b)$$

Note that the first two terms in (4.25b) provide the expected phase change during the demodulation interval τ corresponding to the ideal situation, the next three terms, in fact, represent the undesired contribution to the phase due to PMD and GVD and the last term, $\Delta\theta_n(t_0, \tau)$ represents the phase distortion due to receiver noise.

Denoting the phase distortion of the signal only due to PMD and GVD as η

$$\eta = -\frac{\pi}{2} + \frac{\pi}{2} q(t_0) + \frac{\pi}{2} \sum_{k \neq 0} a_k q(t_0 - kT) \quad (4.26a)$$

$$= \bar{\Delta}\alpha_0(t, \tau) + \xi \quad (4.26b)$$

where, $\bar{\Delta\alpha}_0(t, \tau)$ is mean output phase error and

ξ , the random output phase fluctuation due to ISI for random bit pattern caused by PMD and GVD.

For a given IF SNR, the conditional bit error probability $P(e|\xi)$, conditioned on a given value of ξ given by [70],

$$P(e|\xi) = P(-\pi \leq \Delta\phi_0(t) \bmod 2\pi \leq 0 | \xi)$$

$$= \frac{1}{2} - \frac{1}{2} \rho e^{-\rho} \sum_n \frac{(-1)^n}{2n+1} \left[I_n\left(\frac{\rho}{2}\right) + I_{n+1}\left(\frac{\rho}{2}\right) \right]^2 \times \quad (4.27a)$$

$$\exp[-(2n+1)^2 \pi \Delta\nu \tau] \times \cos[(2n+1)(\bar{\Delta\alpha}_0(t, \tau) + \xi)]$$

$$= \frac{1}{2} - F(\bar{\Delta\alpha}_0(t, \tau), \xi) \quad (4.27b)$$

where, $\rho = \frac{V_0^2}{2\sigma_n^2}$ is the IF SNR, $I_\alpha(x)$ is the modified Bessel function of first kind and order α , σ_n^2 is the variance of $n(t)$. The second term in (4.26b) implicitly defines $F(\bar{\Delta\alpha}_0, \xi)$ in (4.27b).

4.3.2 Pdf of the random output phase and average BER

The probability density function (pdf) of ξ , $P_\xi(\xi)$ can be obtained by inverting the characteristic function of ξ . The characteristic function of random output phase, ξ can be expressed as,

$$F_\xi(j\xi) = \prod_{i=1}^{\infty} \cos[\xi q_i(t)] = \sum_{i=1}^{\infty} \frac{(j\xi)^{2i}}{(2i)!} M_{2i} \quad (4.28)$$

where $q_i(t) = |q(t - iT)|$, M_{2i} are the even order moments of the characteristic function of random output phase ξ . Moments M_{2i} can be evaluated by using the following recursive relations,

$$M_{2r} = Y_{2r}(N) \quad (4.29a)$$

$$Y_{2r}(i) = \sum_{j=0}^r {}^{2r}C_{2j} Y_{2j}(i-1) q_i^{2r-2j} \quad (4.29b)$$

where ${}^{2r}C_{2j}$ is the binominal coefficient and N is the actual number of terms

The pdf of the random output phase, ξ can be written as,

$$P_{\xi}(\xi) = F^{-1}[F_{\xi}(j\xi)] \quad (4.29c)$$

So for a given value of mean differential group delay (DGD), $\Delta\tau$ the unconditional BER can be expressed as,

$$BER(\Delta\tau) = \int_{-\infty}^{\infty} P(e|\xi) P_{\xi}(\xi) d\xi \quad (4.30)$$

The above integration can be carried out by Gauss-quadrature rule.

The unconditional BER expression of equation (4.30) is based on the assumption that DGD in the short-length regime is deterministic because the birefringence is inherently additive. In reality the fiber length in today's terrestrial and submarine transmission systems are 100's or 1000's of km, and the birefringence along the fiber length, causing polarization mode coupling wherein the fast and slow polarization modes from one segment each decomposes into both the fast and slow modes of the next segment. Due to mode coupling, the birefringence of each section may either add to or subtract from the total birefringence, and therefore the DGD does not accumulate linearly with the fiber length. In fact it has shown that in long fiber spans DGD on average increases with the square root of distance.

Thus, the average error probability can be evaluated as,

$$BER(\langle\Delta\tau\rangle) = \int_{-\infty}^{\infty} BER(\Delta\tau) P_{\Delta\tau}(\Delta\tau) d(\Delta\tau) \quad (4.31)$$

4.4 Results and discussion

Following the analytical approach outlined above, we evaluated the conditional and average BER performance results of an optical heterodyne CPFSK

transmission system with delay demodulation for several values mean DGD at a bit rate of 10 Gb/s. The plot for conditional BER versus received optical power, P_s are shown in Fig. 4.2 and Fig. 4.3 for different values of DGD at a modulation index of 0.5 and 1.0 respectively

The results from Fig. 4.2 and Fig. 4.3 show that the BER is degraded when the instantaneous DGD is higher for given fiber length and the system suffers a significant amount of power penalty due to the effect of PMD. At BER 10^{-9} the penalty is found to be approximately 0.70 dB, 1.75 dB, 3.50 dB and 5.75 dB corresponding to instantaneous DGD of 20 ps, 40 ps, 60 ps and 80 ps respectively at modulation index 0.50. It is further observed that the penalty is much higher at higher modulation index such as $h = 1$ compared to $h = 0.5$, e.g. the penalty is approximately 5.25 dB when instantaneous DGD is 70 ps and $h = 1.0$.

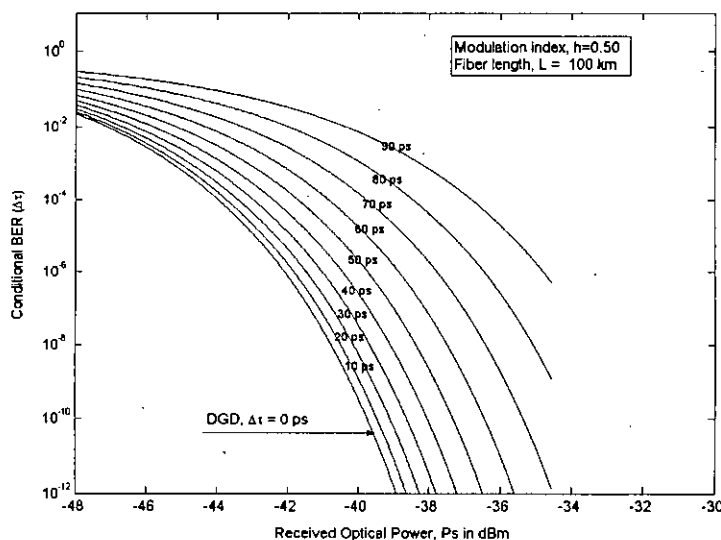


Fig. 4.2: Plot of conditional BER versus received power, P_s for heterodyne CPFSK impaired by PMD at modulation index 0.50

Figure 4.4 and Fig. 4.5 shows the plot of average BER versus received power, P_s are shown at modulation index of 0.50 and 1.0 respectively at a bit rate 10

Gb/s for different values of mean DGD. The results show that the BER performance is more affected at higher values of mean DGD and at higher modulation index.

The penalty due to PMD suffered by the heterodyne CPFSK system at BER 10^{-9} is plotted in Fig. 4.6 as a function of DGD normalized by bit duration. It is observed from Fig.4.3 that the penalty at BER = 10^{-9} is increasing with increasing values of the mean DGD. It is observed that the amount of power penalty is approximately 0.75 dB, 2.00 dB, 3.50 dB and 5.70 dB corresponding to mean DGD of 20 ps, 30 ps, 40 ps and 50 ps respectively at a modulation index of 0.50. Further increase of DGD leads to a BER floor above 10^{-9} which can not be lowered by further increasing the signal power

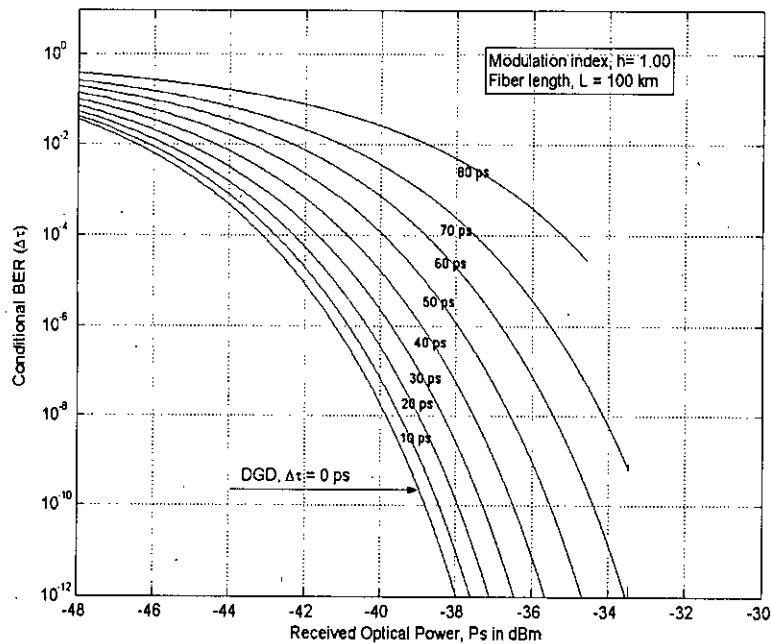


Fig. 4.3: Plot of conditional BER versus received power, P_s for heterodyne CPFSK impaired by PMD at modulation index 1.00

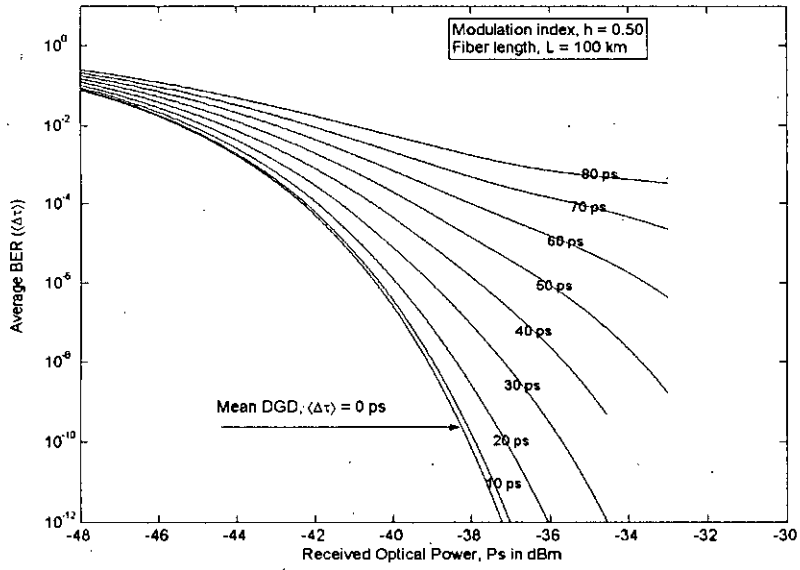


Fig. 4.4: Plot of average BER versus received power, P_s for heterodyne CPFSK receiver impaired by PMD at modulation index 0.50

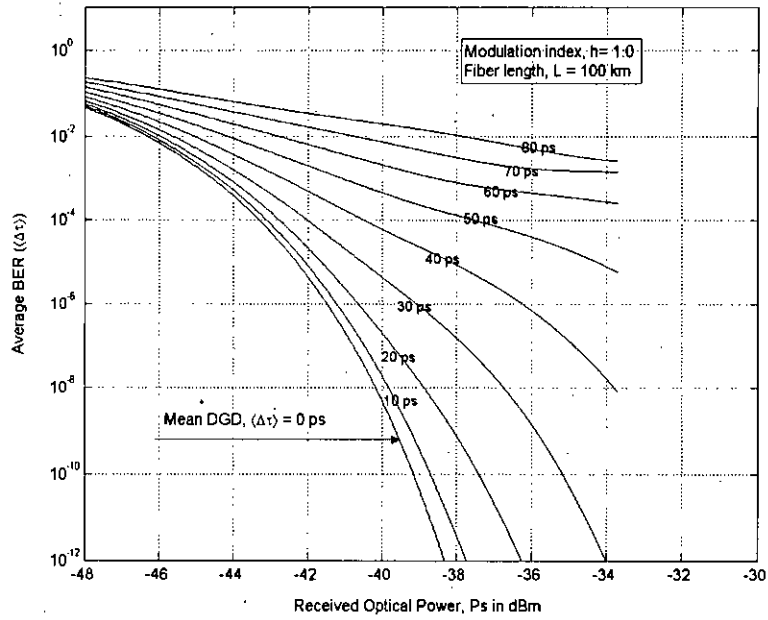


Fig. 4.5: Plot of average BER versus received power, P_s for heterodyne CPFSK impaired by PMD at modulation index 1.00

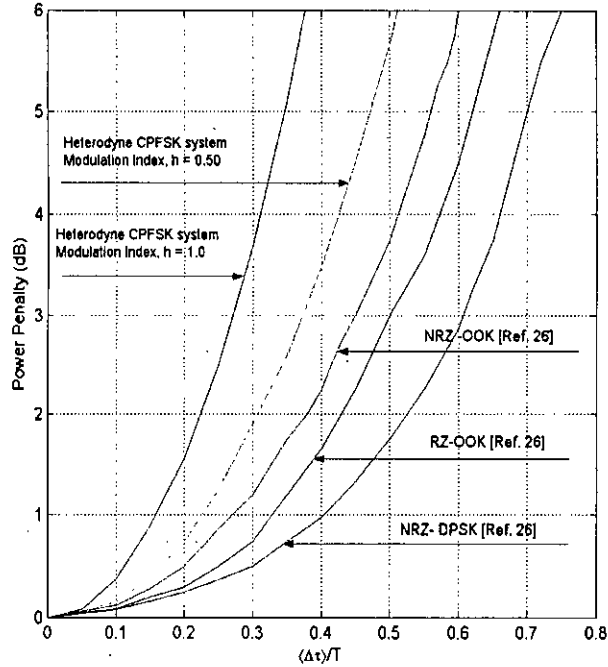


Fig. 4.6: PMD-induced power penalty (considering average BER) as a function of DGD/bit duration ($(\Delta\tau)/T$) for NRZ- and RZ-OOK, NRZ-DPSK and heterodyne NRZ-CPFSK system.

It is noticed that BER floors occur at about 2×10^{-8} , 10^{-5} and 2.5×10^{-4} corresponding to mean DGD of 60 ps, 70 ps and 80 ps respectively at 10 Gb/s and modulation index of 0.50. The amount of penalty is approximately 6.80 dB when mean DGD is 40 ps at modulation index 1.0. The plots of power penalty due to other modulation schemes as reported in [26] are also shown in Fig.4.6 for comparison. It is further noticed that penalty suffered by heterodyne detection CPFSK with modulation index 0.50 is higher than that of NRZ-OOK system. But at higher modulation index, penalty suffered by heterodyne CPFSK is also higher than that of OOK and DPSK system.

4.5 Summary

An analytical approach is presented to evaluate the impact of polarization mode dispersion on the BER performance of heterodyne CPFSK system. The results show that how PMD induces sensible penalty degradation in such a system when the fiber link presents a mean DGD equal to 80 ps. Our analysis allows us to conclude that PMD generally induces a relevant degradation in the heterodyne CPFSK long haul transmission link and controls have to be made in order to avoid the presence of either fibers or optical components with higher value of PMD.

successfully in research. The application of these channel rates is limited for many installed fiber by their PMD. Designers have ensure that the probability of an eye opening penalty or BER penalty due to PMD beyond some value occur only a very fraction of the time. For example, a designer might require that a penalty larger than 1 dB occurs with probability 10^{-7} or less. With the evolution of specialized manufacturing methods, PMD in present day telecommunication grade fibers is kept low (<0.1 ps/ $\sqrt{\text{km}}$). Still, no matter how good the fiber may be, at some bit-rate-length product, PMD will be an issue. Hence, there is need to investigate strategies for PMD mitigation. Over the years, much effort has been spent on understanding PMD impairments and developing PMD mitigation techniques. Due to the scholastic nature of PMD in fibers and the fact that all the orders of PMD are bound together, it is not trivial to evaluate PMD penalties and compensate for PMD impairments. PMD can be mitigated in three ways, *i.e.*, optical compensation, electrical compensation and by use of passive techniques.

Optical PMD compensators typically comprise of a polarization controlling device, an optical delay element (fixed or variable) and allied electronics which provides control signals to the optical components based on feed-back information about the link's PMD [58].

Electronic compensation technique consists of equalization using digital filters, which reduces ISI. When applied to digital fiber-optic communication system, such methods are adopted after the receiver, to reduce the ISI due to impairments [58], [71]. Since they are used in the post detection stages, the phase of the optical signal will not be available.

In passive PMD mitigation approach, there is no active component. This can be achieved in many ways, such as adopting advanced manufacturing technique [72]-[73], incorporating forward error correction (FEC) [74] and using PMD tolerant linecoding [75]-[76]. Modern fiber manufacturing process improvements ensure better fiber geometry, reduce the asymmetry stress level and introduce controlled polarization coupling by fiber spinning.

5.1.1 Optical PMD compensation technique

For optical PMD compensation different setups have been reported in the literature [77]-[79]. The performance of these compensators was characterized by applying first order PMD or higher order PMD, too. An accurate assessment of compensators is performed by using common feedback signals, by applying a realistic adaptation control and tracking scheme implemented in the PMD compensation control logic, and by using the high PMD values occurring with the system relevant low probability.

Optical PMD compensators are classified as half-order, first-order and second-order compensator. A half-order compensator comprises of a polarization controller and a fixed optical delay element. A first-order compensator has a variable delay element and feedback mechanism provides control signals for adjusting both the polarization controller and delay element. The first-order compensator can be employed to counter different amount of PMD values. The second-order compensator uses two pieces of highly birefringent fiber and two polarization controllers. The compensator's PSPs are made to vary linearly with frequency so as to compensate for PMD over a large bandwidth. Given the increasing data rates and the expanding bandwidth, importance has been attached to second-order PMD.

Since PMD is a randomly changing entity, adaptive techniques are necessary to continually track the changing DGD and PSPs and perform effective PMD compensation. It is also necessary to provide reliable estimates of the DGD and PSPs to the PMD compensator. The control signals to the variable delay element and polarization controller can be generated using different PMD monitoring techniques.

Despite the obvious advantages of compensating an optical phenomenon with optical components, optical compensation has several disadvantages. First, optical scheme require expensive and relatively bulky optical components. Also, because of the dynamic nature of PMD, compensators must be adaptive.

Adaptation is not easily achieved in the optical domain because of the relative lack of flexibility in optical components and because of the difficulty in extracting an appropriate error signal to control the adaptation.

5.1.2 Electronic PMD compensation technique

Electronic PMD compensation using digital filters is an attractive method for reducing ISI. Such electronic PMD equalizers can be integrated into the receiver, thus saving installation costs. The goal of electronic equalizers is minimization of ISI at the receiving end (regardless of the phenomenon that is causing it, be it PMD or chromatic dispersion or any other).

Some of the electronic filters used for ISI reduction are the transversal filter (TF), decision feedback equalizer (DFE) and the maximum likelihood sequence detection scheme (MLSD). The TF divides the signal into two copies, delays the copies by constant delay stages, ΔT , and superimposes the differentially delayed signals at the output port. The tap weights are adjusted to minimize ISI in the received signal. The DFE is a non-linear filter. Non-linear filters are advantageous in the sense that they can improve signal quality even if the received eye-diagram is poor (severe ISI condition), unlike TF which requires an "open" eye-diagram [8]. However, DFE requires high-speed signal processors. The MLD scheme is based on the correlation between an undistorted signal sequence and an estimate of the received signal sequence, over many bits. The selection of the sequence and the maximization of the correlation are the factors based on which the decision for each individual bit is made. A theoretical study comparing the performance of the above three schemes yielded the result in [80]. It has been reported that a concatenation of the TF and DFE would yield better performance than either the TF or the DFE. However, the MLSD scheme provided the best possible performance.

Electronic compensation methods can be integrated into the receiver, thus saving installation costs. As the data rate rise beyond 10 Gb/s, it will be a challenging task to perform electronic equalization because of the difficulty in finding electronic delay stages and filters that can operate at such high speeds.

5.1.3 Passive PMD compensation technique

Passive PMD mitigation techniques do not require any dynamically adjusted components. It includes fiber manufacturing process improvement to make low PMD fiber and use of more PMD robust line coded signal and soliton transmission, allocating more margins to PMD distortions, FEC coding, channel switching and polarization scrambling. FEC can help increases the tolerance of a system to effects of noise, CD and PMD. Some experiments uses, Reed-Solomon error-correcting codes along with first-order PMD compensator to effectively increase the PMD tolerance of a 10 Gb/s system [74]-[76]. For DWDM systems, Sarkimukka *et al* [81], proposed a system by moving traffic off of PMD-impaired channels onto spare channels that are not experiencing PMD degradation. They showed that with this approach five times as much as PMD can be tolerated compared to the suggested ITU limit (G.691). A novel family of optical line codes were also used to counteract the fiber chromatic dispersion and it is reported that a relative improvement of 2 dB at BER 10^{-12} for distances greater than about 140 km at 10 Gb/s over standard fibers [76].

5.2 Line codes (modulation formats) in PMD compensation

The most widely adopted signaling format in contemporary fiber-optic communication systems is the non return-to-zero (NRZ). However, in recent years, novel modulation formats and their resistance to signal degrading phenomena, such as PMD have also been studied widely. Return-to-zero (RZ) signals are considered more resistant to penalties caused by broadening than NRZ. The signal energy is more confined to the center of each bit and is the

reason for the increased resistance of RZ modulation [8]. As DGD increases, the power in isolated zeros rises only slowly, whereas in the case of NRZ, the power rises in isolated zeros quickly and combines with the ones to cause greater penalty. In addition to RZ, there are the chirped RZ (CRZ), classical solitons and dispersion-managed solitons (DMS), which are known to be more resistant to PMD effects. A comparison of the penalties incurred by NRZ, RZ, CRZ and DMS signals in the presence of high PMD has been made using computer simulation in a 10-Gb/s terrestrial system, [82]. The results showed that RZ, DMS and CRZ signals performed better than NRZ for spans of up to about 600 km.

The linecoder may be viewed as a linear time invariant filter that acts on the input data signal and generate an output sequence as shown in Fig. 5.1. A theoretical analysis for evaluating the performance of a linecoded CPFSK optical transmission system for direct detection and heterodyne system is presented. It accounts for the combined effects of signal phase distortion due to PMD and GVD in a single mode fiber. The analysis is carried out for three different linecoding schemes, i.e., alternate mark inversion (AMI) or bipolar, order-1 and delay modulation coding, to investigate the efficacy of the linecoding in counteracting the effect of PMD in CPFSK optical transmission system. Fig. 5.2 shows the conventional NRZ- and AMI linecoding. In AMI, '0' is encoded by no pulse and '1' is encoded by a pulse $p(t)$ or $-p(t)$ depending whether the previous '1' is encoded by $-p(t)$ or $p(t)$. One of the advantages of this code is that if an error made in the detecting pulses, the received pulse sequence will violate the bipolar rule and the error is immediately detected. The delay modulation (DM) is also known as Miller coding. In DM, a '1' is represented by a transition at the midpoint of the bit interval. A '0' is represented by no transition, unless it is followed by another zero. In this case, a transition is placed at the end of the bit interval of the first zero. The average BER performance results are evaluated with the above line codes and compared with NRZ-CPFSK system at a bit rate of 10 Gb/s considering Maxwellian probability distribution for the DGD due to PMD.

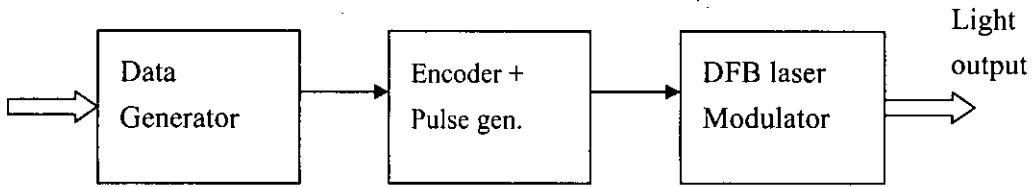


Fig. 5.1: Model of an optical linecode generator

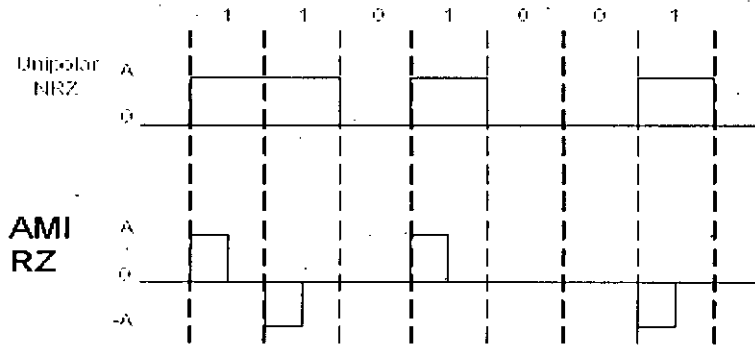


Fig. 5.2: Unipolar NRZ and AMI RZ linecoding

5.2.1 Order 1 line coding: a multi-level novel optical line code

Novel optical line coding is similar to conventional Miller coding with the difference being that two of them are scaled by a factor $\alpha < 1$ and transmitted in sequence according to the duobinary logic. Novel optical codes are ranging from order 1, 2, ..., n and in our case we have used order 1 code. The first order code uses four wave forms $s_i(t)$, and the state diagram is shown in the Fig. 5.3, where \sum_1 and \sum_2 are the code status and the elementary signals $s_i(t)$, where $i = 1, 2, 3, 4$ are depicted. Elementary signals form two pairs with $s_1(t) = -s_4(t)$ and $s_2(t) = -s_3(t)$. In addition two of the elementary signals $s_2(t)$ and $s_3(t)$ are scaled by α . In our case, α is chosen as 0.5 to produce best spectral shape.

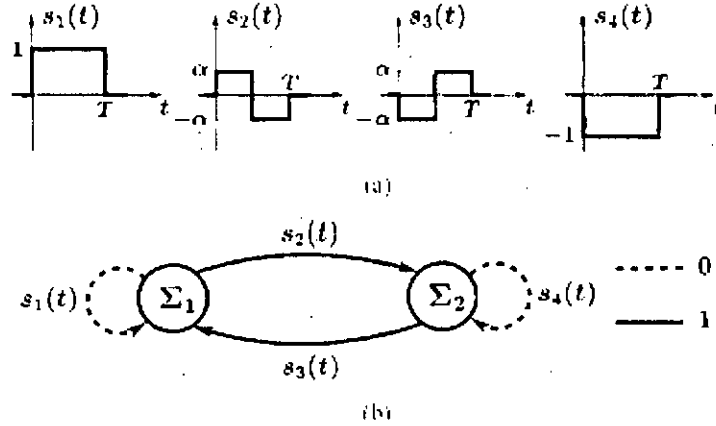


Fig. 5.3: (a) Elementary signals and (b) code state diagram of novel order 1 code

The information (data) sequence $\{u_k\}$ is encoded to form the coded signal,

$$x(t) = \sum_{k=-\infty}^{\infty} g_k(\sigma_k) s_e(t - kT; u_k) \quad (5.1)$$

where σ_k denotes the generic encoder state and $g_k(\sigma_k)$ is a coefficient defined by the following rule

$$g_1(t, u_k) = \begin{cases} 1, \dots, s_1(t) & \text{if } \sigma_k = \sum_1 \\ -1, \dots, s_2(t) & \text{if } \sigma_k = \sum_2 \end{cases} \quad (5.2)$$

where, \sum_1 and \sum_2 indicates the states allowed to the encoder, and $s_e(t; u_k)$ is one of the two elementary signals $s_1(t)$ and $s_2(t)$ selected in accordance with the following rule:

$$\sigma_k + 1 = g_2(u_k, \sigma_k) \quad (5.3)$$

The above encoding rules are summarized in table 5.1 and an example of a waveform generated by the order 1 code with $\alpha=0.5$ is shown in Fig. 5.4.

Information sequence (u_k)	Generic encoder state (σ_k)	Sequence of the state of the encoder (g_2)	Encoded signal $x_e(t)$
0	Σ_1	Σ_1	$s_1(t)$
0	Σ_2	Σ_2	$-s_1(t) = s_4(t)$
1	Σ_1	Σ_2	$s_2(t)$
1	Σ_2	Σ_1	$-s_2(t) = s_3(t)$

Table 5.1: Summary of the encoding criteria for novel optical code

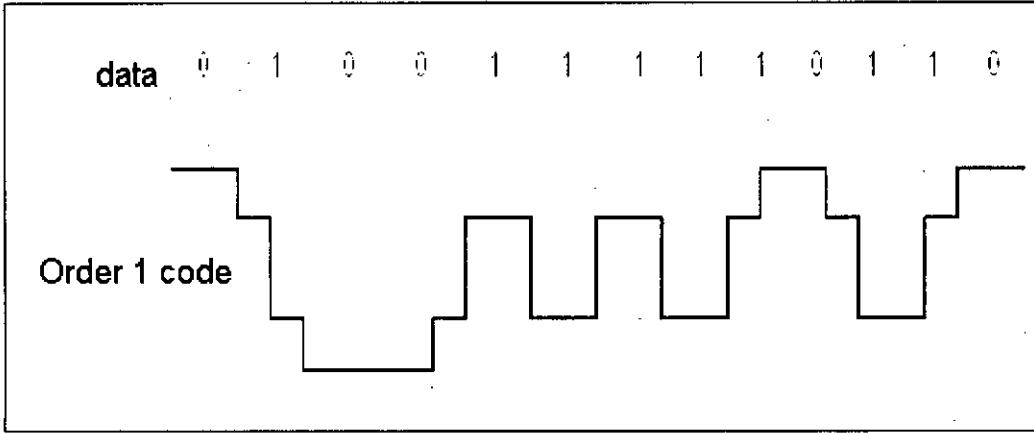


Fig. 5.4: Order 1 novel optical coded signal

Additional insight into the structure and characteristics of the order-1 code can be gained by expressing the four elementary signals in Fig.5.3 as linear combinations of rectangular pulses of duration $T/2$.

$$c(t) = \begin{cases} 1; & 0 < t < T/2 \\ 0 & \text{elsewhere} \end{cases} \quad (5.4)$$

Now, the elementary signals $s_i(t)$ for $i=1,2,3,4$ in terms of $c(t)$ is given by,

$$s_1(t) = c(t) + c(t - T/2) \quad (5.5a)$$

$$s_2(t) = \alpha [c(t) - c(t - T/2)] \quad (5.5b)$$

$$s_3(t) = -s_2(t) \quad (5.5c)$$

$$s_4(t) = -s_1(t) \quad (5.5d)$$

5.2.2 CPFSK modulation with linecoding

As mentioned earlier, appropriate linecoding of the DBF laser driving signal can overcome the adverse effects of PMD. Three linecoding schemes are considered, *i.e.*, DM, AMI and order 1. The main objective is to study the relative effectiveness of the above linecodes in overcoming the pulse dispersion performance degradation caused by PMD. The linecoder shown in Fig. 5.1 can be viewed as a linear time-invariant filter that acts on the input data signal of equation (3.3) or (4.4) to generate an output sequence of data given ,

$$r'(t) = \sum_{k=-\infty}^{\infty} b_k r(t - kT) \quad (5.6)$$

where, b_k 's are independent and identically distributed (iid) random variable taking values ± 1 and $r(t) = p(t) \otimes c(t)$. The Fourier transform of $r(t)$ is given by,

$$R(f) = C(f).P(f) \quad (5.7)$$

where,

$$C(f) = \sum_{k=0}^{K-1} c_k \exp(-j2\pi k f T) \quad (5.8)$$

is the transfer function of the encoder and where $c(t) = F^{-1}[G(f)]$ is pulse shaping due to linecoding. The sequence of symbols $\{b_k\}$ is generated to avoid error propagation by a precoder defined by

$$a_k = \sum_{i=0}^{K-1} c_i b_{k-i} \text{ mod}(2) \quad (5.9)$$

The K code coefficients $c_0, c_1, c_2, \dots, c_{K-1}$ are usually integers and can be

properly chosen to generate a specific linecoding scheme.

It is therefore possible to apply the same procedure for average BER evaluation of CPFSK with NRZ data in Section A to the present situation with linecoded data by merely replacing $g_1(t)$ and $g_2(t)$ in the previous case

$$g_1(t) = \text{Re}[p(t) \otimes c(t) \otimes h_1(t) \otimes h_{IF}(t)] \quad (5.10)$$

$$g_2(t) = \text{Re}[p(t) \otimes c(t) \otimes h_2(t) \otimes h_{IF}(t)] \quad (5.11)$$

For the linecoded signal, the pulse shaping function $c(t)$ can be obtained from the following $C(f)$ for:

Alternate mark inversion (AMI):

$$C(f) = 0.5[1 - \exp(-j2\pi fT)] \quad (5.12)$$

Delay modulation (DM):

$$C(f) = \frac{[3 + 2\cos(\pi fT) + \cos(2\pi fT) - \cos(3\pi fT)] + j[6\sin(2\pi fT) + \sin(\pi fT) + 3\sin(3\pi fT) + 4\sin(4\pi fT)]}{9 + 12\cos(2\pi fT) + 4\cos(4\pi fT)} \quad (5.13)$$

Order 1 :

$$C(f) = \frac{1}{T} \left[(1 + \alpha) \cos\left(\frac{\pi fT}{2}\right) + (1 - \alpha) \cos\left(\frac{3\pi fT}{2}\right) \right]^2 \quad (5.14)$$

where α is the scaling factor

Now following the derivation of CPFSK direct detection or CPFSK heterodyne detection the average BER can be found for AMI, DM and order 1 linecoding using the following expression,

$$BER = \int_{-\infty}^{\infty} BER(\Delta\tau) P_{\Delta\tau}(\Delta\tau) d(\Delta\tau) \quad (5.15)$$

5.3.1 Results and discussion

In this section, we present the theoretical performance results of an optical heterodyne CPFSK transmission system with delay demodulation receiver for several values of mean DGD with and without linecoding at a bit rate of 10 Gb/s. The assumptions used in computing the BER performance results are shown in Table 5.2.

The plots of average BER versus received power, P_s are shown in Fig. 5.5 and Fig.5.6 at modulation index of 0.50 and 1.00 respectively for different values of mean DGD. The results show that the BER performance is more affected at higher values of mean DGD and at higher modulation index. It is noticed that BER floors occur at about 2×10^{-8} , 10^{-5} and 2.5×10^{-4} corresponding to mean DGD of 60 ps, 70 ps and 80 ps respectively at modulation index of 0.50, which means that at these mean DGD's BER can not be lowered by further increasing the signal power. The amount of penalty is approximately 6.80 dB when the mean DGD is 40 ps at modulation index 1.0.

The BER performance for delay modulation with linecoding is shown Fig. 5.5, Fig.5.6 and for modulation index of 0.5 and 1.00 respectively. For the purpose of comparison, the previous work without linecoding results reported in [83].

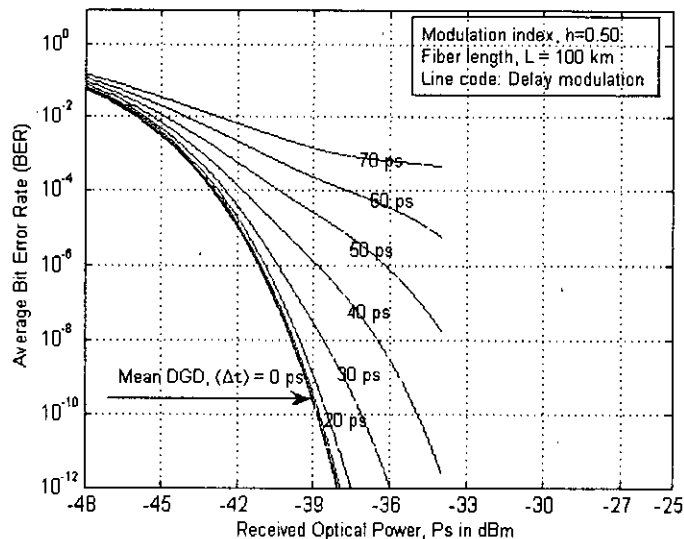


Fig. 5.5: Plot of average BER versus received power, P_s at modulation index 0.50 with delay modulation linecoding

It is found from all Figures (Fig. 5.5 to Fig. 5.10) that the amount of power penalty due to PMD suffered by CPFSK transmission system up to 30 ps mean DGD is relatively small. It is approximately 0.85dB and 0.30 dB for AMI- and order-1-CPFSK respectively at BER 10^{-9} . For delay demodulation (Fig.4) linecoding, it is about 1.5 dB at the same BER and for a mean DGD of 30 ps.

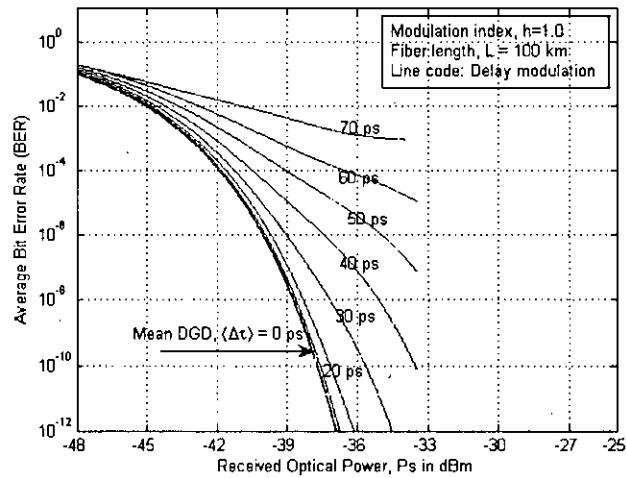


Fig. 5.6: Plot of average BER versus received power, Ps at modulation index 1.0 with delay modulation linecoding

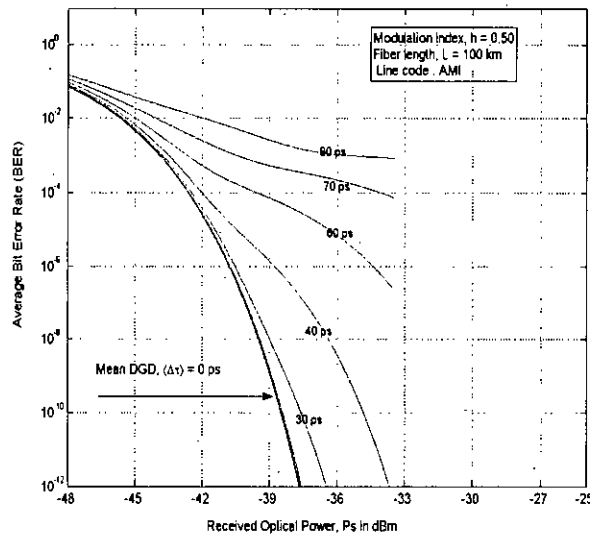


Fig. 5.7: Plot of average BER versus received power, Ps at modulation index 0.50 with Alternate Mark Inversion (AMI) linecoding

For small power penalties PMD follows the following expression [7],

$$\varepsilon \text{ (in dB)} = A \left(\frac{\langle \Delta \tau \rangle}{MT} \right)^2 \alpha(1-\alpha) \quad (5.16)$$

where, MT is the symbol duration A is a dimensionless parameter determined by the pulse shape. In our case, $M=1$ and the value of A is about 39, 22, 19 and 16 corresponding to NRZ, DM, AMI and order-1 codes respectively.

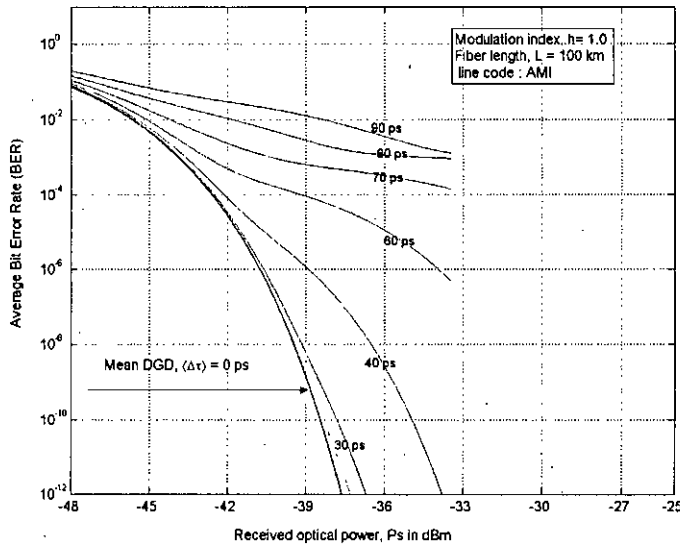


Fig. 5.8: Plot of average BER versus received power, P_s at modulation index 1.0 with Alternate Mark Inversion (AMI) linecoding

It is noticed that BER floors occur at about 10^{-4} (at DGD 70 ps), 3.5×10^{-5} (at DGD 60 ps) and 5×10^{-5} (at DGD 60 ps) for AMI, order-1 and delay modulation linecoding respectively. Above these values of mean DGD, the BER can not be lowered by further increasing the signal power

Single Channel PMD Compensation

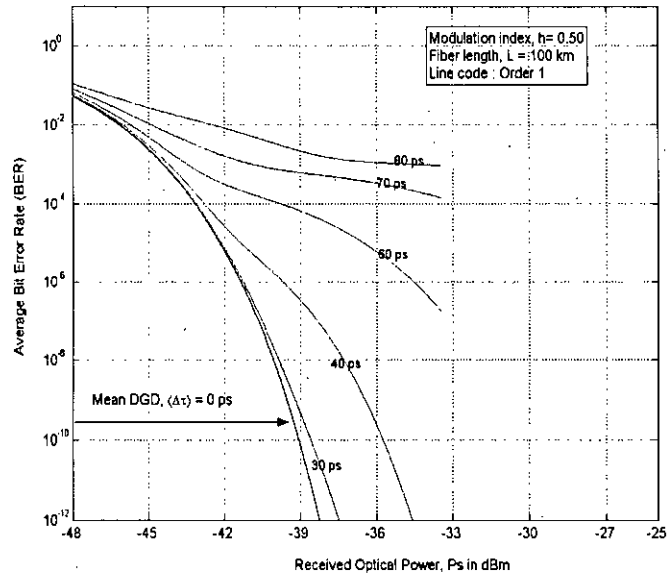


Fig. 5.9: Plot of average BER versus received power, P_s at modulation index 0.50 with Order 1 linecoding

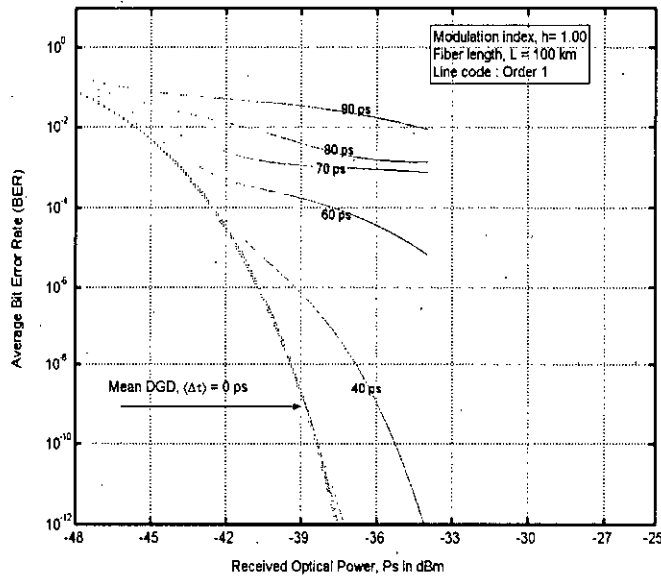


Fig. 5.10: Plot of average BER versus received power, P_s at modulation index 1.00 with Order 1 linecoding

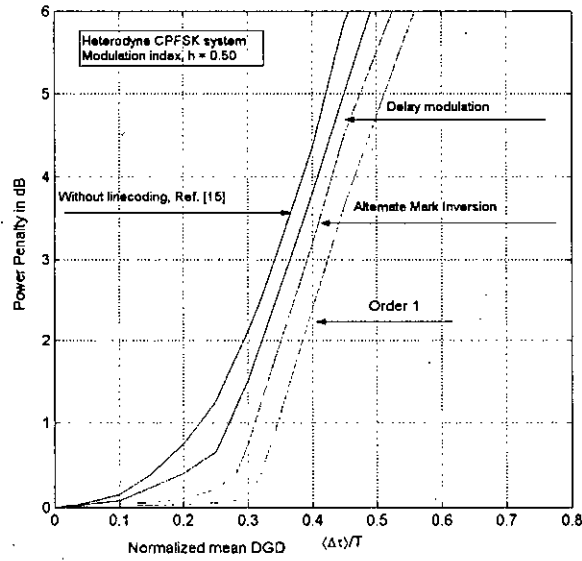


Fig. 5.11: PMD-induced power penalty as a function of DGD/bit duration ($\langle \Delta\tau \rangle / T$) for NRZ, DM, AMI and Order 1 linecoding of a CPFSK system (modulation index =0.50)

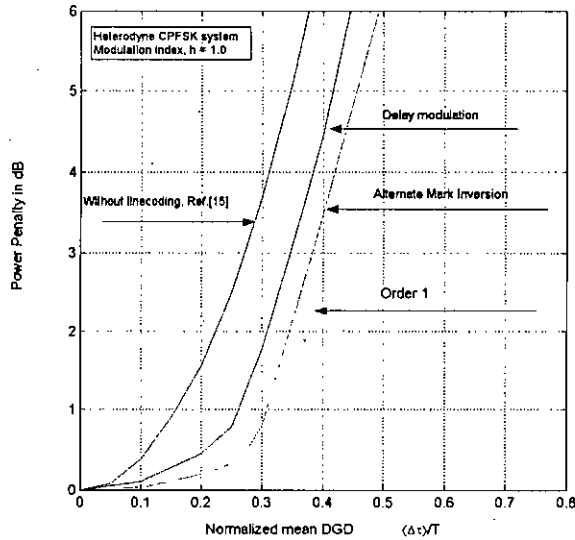


Fig. 5.12: PMD-induced power penalty as a function of DGD/bit duration ($\langle \Delta\tau \rangle / T$) for NRZ, DM, AMI and Order 1 linecoding of a CPFSK system (modulation index = 1.00)

Parameter	Values	unit
Temperature (T)	300	K
Bandwidth (B)	10	GHz
Receiver load (R_L)	50	Ohm
Receiver responsivity (R_d)	1	A/W
Wavelength (λ)	1550	nm
Operating frequency (f)	1.93355×10^{14}	Hz
Scaling factor (β)	0.50	Unitless
Dispersion index (γ)	15	ps/nm-km
Power splitting ratio (α)	0.50	Unitless

Table: 5.2: The assumptions used in computing the BER performance results

Fig. 5.11 shows the 10^{-9} BER power penalty of NRZ-, AMI-, order-1- and DM-CPFSK, versus the ratio of mean DGD to bit duration $\langle \Delta\tau \rangle / T$ at a modulation index of 0.50. The performance limitations of an optical heterodyne NRZ-CPFSK transmission system affected by PMD are reported in [83]. As seen in Fig.5, for weak PMD the effect of linecoding more pronounced and order-1 linecoding is more superior to AMI and DM. For example, the power penalty improvements are about 0.5 dB, 1.15 dB and 1.95 dB corresponding to DM, AMI and order-1 respectively at mean DGD of 30 ps with respect to NRZ-CPFSK. From Fig.5.11, it is also observed that the power penalty improvements above 30 ps mean DGD is almost constant for all linecodes and the amounts are about 0.30 dB, 0.80 dB and 1.65 dB corresponding to DM, AMI and order-1 respectively. This is to be expected, because in NRZ, the symbol duration is twice as long as for three linecoding schemes. As these linecodes use shorter pulse duration and exhibit much greater PMD tolerance than their NRZ counterparts. It is also observed that order-1 linecoding gives nearly twice the maximum allowable value of $\langle \Delta\tau \rangle / T$ than NRZ data

5.3.2 Comparison among different linecodes in PMD mitigation

Passive PMD mitigation techniques do not require any dynamically adjusted

components. It includes use of more PMD robust line coded signal and soliton transmission, allocating more margin to PMD distortions, forward error correction (FEC) coding, channel switching and polarization scrambling. FEC can help increases the tolerance of a system to effects of noise, CD and PMD. Some experiments uses, Reed-Solomon error-correcting codes along with first-order PMD compensator to effectively increase the PMD tolerance of a 10 Gbit/s system.

Linecoding	Observation method	Amount of compensation (per 100 km)	Reference
Delay modulation (DM)	BER vs received optical power	0.30 dB for DGD >30 ps	Our work
Alternate Mark Inversion (AMI)	BER vs received optical power	0.80 dB for DGD >30 ps	Our work
Order 1	BER vs received optical power	1.65 dB for DGD>30 ps	Our work
Duo binary	Eye diagram	1.20 dB for DGD>35 ps	Ref.[118]
Modified duo binary	Eye diagram	1.35 dB for DGD>35 ps	Ref.[118]
Low-density parity-check (LDPC)-coded	BER vs electrical SNR E_b/N_0	1.30 dB for DGD > 30 ps	Ref [119]
A novel chirped intra-bit polarization diversity modulation (C-IPDM)	Q-factor	1.45 dB for DGD>40 ps and compensates second order PMD	Ref. [120]

Table 5.1: PMD mitigation with different optical linecoding

The linecoder may be viewed as a linear time invariant filter that acts on the input data signal and generate an output sequence. The effectiveness of all Linecoding techniques lies substantially in the fact that the linecoded signal

spectrum is shifted away from the highly nonuniform region of the FM characteristics to lower frequency.

In our research work, we have studied three linecodes (DM, AMI & order 1) to find their tolerance in first order PMD. We compare our research work other contemporary works in Table 5.1. From the table we found that order 1 line code is most effective and it can mitigate about 1,65 dB for mean DGD > 30 ps

5.4 Summary

In this research work, an analytical technique without and with linecoding is provided for the performance evaluation of a heterodyne CPFSK system impaired by PMD in presence of chromatic dispersion. The effectiveness of several linecoding schemes, *i.e.*, AMI, order-1 and DM, in alleviating the performance degradation due to the PMD is quantitatively assessed. We found that for lower values of PMD the compensation effect of linecoding is more pronounced than higher values of DGD. The power penalty improvements above 30 ps mean DGD is almost constant for all linecodes and the amounts are about 0.30 dB, 0.80 dB and 1.65 dB corresponding to DM, AMI and order-1 respectively. Among the three linecodes order-1 linecoding is superior to AMI and DM. From the analytical results, we observed that order-1 is the best, AMI is better than DM linecoding. For example, at 30 ps mean DGD, order-1 effects is 0.80 dB and 1.40 dB higher than AMI and DM respectively. This happens due to the compact spectrum of order 1 linecoding.

Chapter 6

EFFECT OF PMD IN MULTICHANNEL OPTICAL TRANSMISSION SYSTEM

In this chapter, we propose system models for treating PMD in two channel (pump-probe) as well as N-channel WDM transmission system and deduce the pdf of random amplitude fluctuation due to PMD in a channel pump-probe configuration and also the combined pdf for a birefringence fiber. Based on these models, optical signal propagation behaviors in two and multi-channel WDM system with PMD are analytically analyzed and assessed. Simulation is also carried out using OptSim simulation software for a 4-channel WDM transmission system in terms of eye diagram.

6.1 Interaction of cross phase modulation and PMD

Transmission in optical fiber communication systems is impaired and ultimately limited by the four 'horsemen' of optical fiber communication systems - chromatic dispersion, amplified spontaneous emission noise from amplifier, polarization effects and fiber nonlinearity [84]. Cross-phase modulation (XPM) is a nonlinear phenomena occurring in optical fibers when two or more optical fields are transmitted through a fiber simultaneously. XPM has an important impact on the performance of high-speed WDM in optical fiber communication

systems. Physically, each intense optical wave changes the refractive index of fiber through the Kerr effect and induces a nonlinear phase shift on other co-propagating waves. If this wave is in the form of an optical pulse, the XPM-induced nonlinear phase shift becomes time dependent and leads to spectral broadening of the co-propagating waves. The self phase modulation (SPM) and XPM phenomenon in optical fibers has been studied extensively over the last two decades [85]-[91]. The nonlinear phase modulation induced through XPM depends on the bit pattern of the inducing channel and is transferred as intensity fluctuation to neighboring channel through GVD that result the inter-channel crosstalk.

One important feature of nonlinear fiber effects is that the strength of interaction depends on light polarization of the propagating waves. Both absolute (linear, circular, elliptical) and relative light polarization of co-propagating waves (*i.e.* identical or orthogonal polarizations) strongly affect the nonlinear coupling strength. In the last few years, many research works have been carried out on the interaction among nonlinearity, polarization variation and polarization mode dispersion [92]-[107]. Physically, PMD has its origin in the birefringence that is present in any optical fiber. Just like signal distortion due to chromatic dispersion and nonlinearity accumulate along the length of the communication link, so does the polarization and PMD. Polarization fluctuation and PMD has become increasingly important as the per-channel data rates have increased and now arguably the most important of the polarization effects. PMD results in system degradation due to PMD-induced pulse broadening, and also leads to fading in both coherent and direct detection systems, induce signal distortion and significant fluctuations of the BER, particularly in WDM systems. PMD of the fiber installed in the past is usually high so the influence of PMD must be considered.

The interaction between PMD and non-linearity can be particularly complex. Q. Lin *et al* [92], developed a vector theory of XPM in optical fiber and used to investigate the effect of PMD on XPM crosstalk in a WDM system in terms of amplitude of probe fluctuation induced by a co-propagating pump channel and the results show that PMD reduces the difference in the average crosstalk level between cases of copolarized and orthogonally polarized channels. G. Zhang *et al* [94], experimentally reported that SPM can suppress PMD penalty and XPM-induced polarization scattering in dense WDM transmission systems can reduce the PMD impairment. C. R. Menyuk *et al* [95], analyzed the interaction of PMD and Kerr nonlinearity and derive the Manakov-PMD equation using multiple-length scale techniques and gave the transparent physical meaning of all its terms with appropriate examples for single- and multichannel transmission systems. Sometimes, in combination with chirp, a system with both PMD and nonlinearity is less impaired than a system with the same amount of nonlinearity and no PMD [97]-[98]. More often, the combination of PMD and nonlinearity can be harmful. R. Khosravani *et al* [100], by numerically and experimentally reported that nonlinear polarization rotation can alter the polarization states of the bits, so that they vary from one bit to the next in a way that is difficult to predict and in such cases, conventional PMD compensation becomes impossible.

PMD-induced fluctuations in the relative orientation between the pump and probe SOP cause the XPM modulation amplitude to be random. In this contribution, we analytically determined the pdf of the random angle $\theta(z)$ between the pump and probe SOP fluctuation that produce intensity dependent pulse distortion on a propagating signal. Using the pdf we analyzed the impact of PMD on XPM in terms of average BER for an IM-DD WDM system at a bit rate of 10 Gb/s. we also find the variance of the SOP between pump and probe with respect to fiber link and channel spacing. To best of our knowledge the influence of PMD on XPM in terms of BER is yet to be reported.

6.2. Pump - probe optical configuration system model

The block diagram of a pump-probe configuration WDM system with EDFA in cascade used for theoretical analysis is shown in Fig.6.1. The pump and probe are multiplexed by WDM MUX and the composite signal is transmitted through a SMF. To describe the effect of PMD on XPM, we assume that the pump, $|A_1\rangle$ act as channel 1, which modulates the transmitted (f_1) data from the laser diode at wavelength, λ_1 and the probe, $|A_2\rangle$ act as channel 2, which is a low-power continuous wave (cw) at wavelength, λ_2 . The in-line EDFA's are used in cascade to compensate the fiber losses. Finally, the composite signal is demultiplexed at WDM DEMUX and from the modulated carrier, λ_2 original signal f_1 is recovered through IM-DD method.

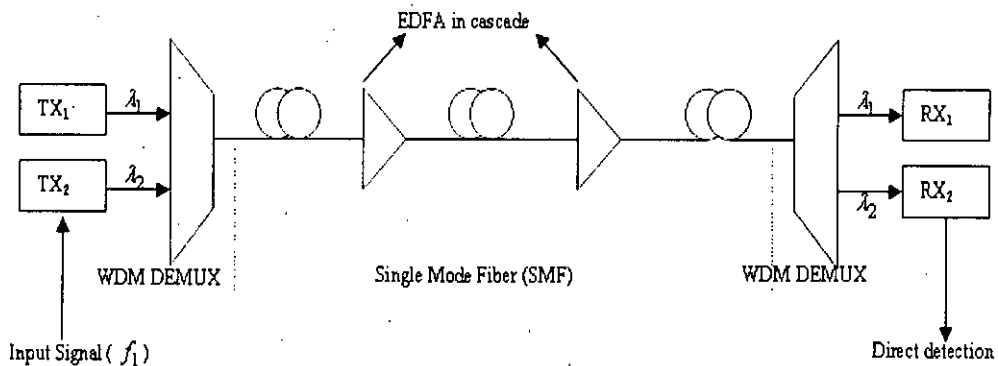


Fig. 6.1: Block diagram of a pump-probe configuration with EDFA in cascade

6.3 Theoretical analysis for pump-probe configuration (2-ch. WDM)

The probe is assumed to be weak enough that the SPM, XPM and intrachannel PMD induced by it can be neglected. Although these effects broadens pulse in each channel, they barely affect the interchannel XPM interaction because the channel spacing typically is much larger than channel bandwidth and the

evolution of SOP of the channels is mainly governed by the birefringence. The XPM induces a time dependent phase shift as well as nonlinear polarization rotation on the probe channel that cause the XPM induced modulation amplitude to be random. The cw probe field is modulated by the pump field by the combination of XPM and PMD. To study the temporal modulation of cw probe field as a consequence of pump field, let us linearize the probe field $|A_2\rangle$ by assuming unperturbed, $|A_{20}\rangle$ and perturbed, $|A_{21}\rangle$ probe fields respectively. With these simplifications (as shown in Appendix B), we can write the following equations for pump and probe field evolutions as,

$$\frac{\partial |A_1\rangle}{\partial z} = -\delta\beta_1 \frac{\partial |A_1\rangle}{\partial \tau} - \frac{i\beta_{21}}{2} \frac{\partial^2 |A_1\rangle}{\partial \tau^2} - \frac{\alpha_1}{2} |A_1\rangle - i\varepsilon_1 P_0 |A_1\rangle \quad (6.1)$$

$$\frac{\partial |A_{20}\rangle}{\partial z} = -\frac{\alpha_2}{2} |A_{20}\rangle - \frac{i}{2} \Omega b \cdot \sigma |A_{20}\rangle \quad (6.2)$$

$$\frac{\partial \langle A_{20} | A_{21} \rangle}{\partial z} = -\frac{i\beta_{22}}{2} \frac{\partial^2 \langle A_{20} | A_{21} \rangle}{\partial \tau^2} - \alpha_2 \langle A_{20} | A_{21} \rangle + \frac{i\varepsilon_2}{2} P_0 S_0 [3 + \cos\theta(z)] \quad (6.3)$$

where, $P_0 = \langle A_1 | A_1 \rangle$ and $S_0 = \langle A_{20} | A_{20} \rangle$ are the pump and unperturbed probe power; $\hat{P} = \langle A_1 | \sigma | A_1 \rangle / P_0$ and $\hat{S} = \langle A_{20} | \sigma | A_{20} \rangle / S_0$ are the unit vector representing the SOP of the pump and unperturbed probe on the Poincare sphere; $\Omega = (\omega_2 - \omega_1)$ is the channel spacing, $\varepsilon_1 = 8/9 \gamma_1$ and $\varepsilon_2 = 8/9 \gamma_2$ are the effective nonlinear parameters, $\theta(z) = \hat{P} \cdot \hat{S}(z)$ is the random angle between the pump and probe SOP, $\delta\beta_1 = (\beta_{11} - \beta_{12})$ is the group velocity mismatch between the two channels and $\tau = (t - \beta_{12}z)$ is the reduced temporal variable.

From (6.1) we see that the pump polarization \hat{P} remain fixed in the rotating frame. However, PMD changes the relative orientation between the pump and probe stokes vectors at a rate dictated by the magnitude of channel spacing and

relative birefringence (Ωb). The total optical power of the probe field is given by,

$$\langle A_2 | A_2 \rangle \approx \langle A_{20} | A_{20} \rangle + [\langle A_{20} | A_{21} \rangle + c. c.] \equiv S_0 + \delta S_0 \quad (6.4)$$

where δS_0 is the modulation amplitude, which is a measure of the XPM induced crosstalk. PMD randomly changes the angle between \hat{P} and $\hat{S}(z)$ along the fiber and thus probe field modulation amplitude becomes a random quantity. Solving the equation (6.3) analytically and introducing the normalized modulation amplitude as, $\tilde{\delta}_x(\omega) = \tilde{\delta S_0}(L, \omega) / S_0(L)$; we obtain,

$$\tilde{\delta}_x(\omega) = - \int_0^L \varepsilon_2(z) \tilde{P}_0(z, \omega) [3 + \cos\theta(z)] \sin \left[\frac{1}{2} \int_z^L \omega^2 \beta_{22}(z_1) dz_1 \right] dz \quad (6.5)$$

where a tilde denotes the Fourier transform and $\tilde{P}_0(z, \omega)$ is the Fourier spectrum of the pump power at a distance z inside the fiber and β_{22} is the GVD coefficient of the pump.

Since the pump polarization \hat{P} remains constant and the random variation of $\hat{S}(z)$ responsible for the randomness of $\theta(z)$. Thus to find the pdf of the angle $\theta(z)$ between pump and probe, we assume that it is driven by the white noise process and can be written as,

$$\frac{d\theta}{dz} = \hat{S}(z) \quad (6.6)$$

$$\text{where,} \quad \langle \hat{S}(z) \rangle = 0 \quad (6.7)$$

$$\langle \hat{S}(z_1) \hat{S}(z_2) \rangle = \eta^2 \delta(z_2 - z_1) \quad (6.8)$$

where $\eta = 1/L_d = D_p^2 \Omega^2 / 3$; $\Omega = \omega_2 - \omega_1$ is the channel spacing and D_p is the PMD parameter. This model captures all the essentials of the more realistic case in which both the angle $\theta(z)$ and birefringence vary randomly. From equation (6.8) a diffusion equation for the probability distribution of $\theta(z)$ or

simply θ can be obtained [95],

$$\frac{\partial p}{\partial z} = \frac{1}{2} \eta^2 \frac{\partial^2 p}{\partial \theta^2} \quad (6.9)$$

where $p(\theta, z)$ is 2π periodic in θ and $p(0, z) = \delta(\theta - \theta_0)$. θ_0 is the value of θ at $z = 0$, θ_0 is the relative angle between the pump and probe SOPs at the input end of the fiber. By solving the equation (6.9) we get the pdf $\theta(z)$ and expressed as,

$$p(\theta, z) = \frac{1}{2\pi} + \frac{1}{\pi} \sum_{m=1}^{\infty} \exp\left(-\frac{1}{2} \eta^2 m^2 z\right) \cos m(\theta - \theta_0) \quad (6.10)$$

The SOP of the pump and probe depends on the power and bit pattern of the pump. The SOP fluctuates with time because of its doubly in nature. In the absence of residual birefringence, randomness comes only from the bit pattern. The SOP of pump and probe variance can be obtained by taking the inverse Fourier transform of equation (6.8) along the fiber link length L ,

$$\begin{aligned} \sigma_{sop}^2 &= \int_0^L dz_1 \int_0^L dz_2 F^{-1} \left\{ \hat{S}(z_1) \hat{S}(z_2) \right\} \\ &= \frac{1}{4\pi^2} \int_{-\infty}^{\infty} d\omega_1 \int_{-\infty}^{\infty} d\omega_2 \left[\int_0^L dz_1 \int_0^L dz_2 \eta^2 \delta(z_1 - z_2) \right] \end{aligned} \quad (6.11)$$

To find the $\tilde{P}_0(z, \omega)$, we assume that the effects of dispersion and nonlinearities do not significantly change the pulse shape of the pump channel along the fiber and analytically solving(1), we then obtain,

$$\tilde{P}_0(z, \omega) = \tilde{P}_0(0, \omega) \exp \left\{ \int_0^z [-\alpha_1(z_1) + i\omega \delta\beta_1(z_1)] dz_1 \right\} \quad (6.12)$$

Substituting this expression in (6.5), we obtain the following analytic result for the XPM-induced crosstalk,

$$\tilde{\delta}_x(\omega) = \tilde{P}_0(0, \omega) \int_0^L [3 + \cos\theta(z)] F(z) dz \quad (6.13)$$

where the function $F(z)$ takes into account loss and dispersion variation along the fiber link and is given by,

$$F(z) = -c_2(z) \exp \left\{ \int_0^z [-\alpha_1(z_1) + i\omega \delta\beta_1(z_1)] dz_1 \right\} \sin \left[\frac{1}{2} \int_z^L \omega^2 \beta_{22}(z_1) dz_1 \right] dz \quad (6.14)$$

The crosstalk level changes with time depending on the bit pattern in the pump channel. Thus, $\delta_x(\tau)$ fluctuates with time and the crosstalk variance, also called XPM-induced interference can given by,

$$\begin{aligned} \sigma_m^2 &\equiv \frac{1}{T} \int_{-\frac{T}{2}}^{\frac{T}{2}} [|\delta_x(\tau)|^2] d\tau \\ &= \frac{1}{4\pi^2} \int_{-\infty}^{\infty} d\omega_1 \int_{-\infty}^{\infty} d\omega_2 \tilde{\delta}_x(\omega_1) \tilde{\delta}_x^*(\omega_2) \text{sinc} \left[\frac{(\omega_1 - \omega_2)T}{2} \right] \end{aligned} \quad (6.15)$$

where, T is the time interval of measurement. Usually the measurement time T is small compared with the fluctuation time of PMD and birefringence fluctuations remain frozen during measurement.

6.4 WDM multi-channel system model

The block diagram of a WDM system with EDFA in cascade used for theoretical analysis of PMD and cross phase modulation (XPM) interaction is shown in Fig.1. The different channels are multiplexed by WDM MUX and the composite signal is transmitted through a single mode fiber (SMF). To describe the combined effect of PMD on XPM, we assume that except channel 2 all the other channels act as the pump which modulate the transmitted data of channel 2 from the laser diodes at wavelength, λ_j . We also assume that channel 2 is a low-

power continuous wave (cw) at wavelength, λ_2 . The in-line EDFA's are used in cascade to compensate the fiber losses. Finally, the composite signal is demultiplexed at WDM DEMUX and from the modulated carrier; wavelength λ_2 original signal (channel 2) is recovered through intensity modulation direct detection (IM-DD) method.

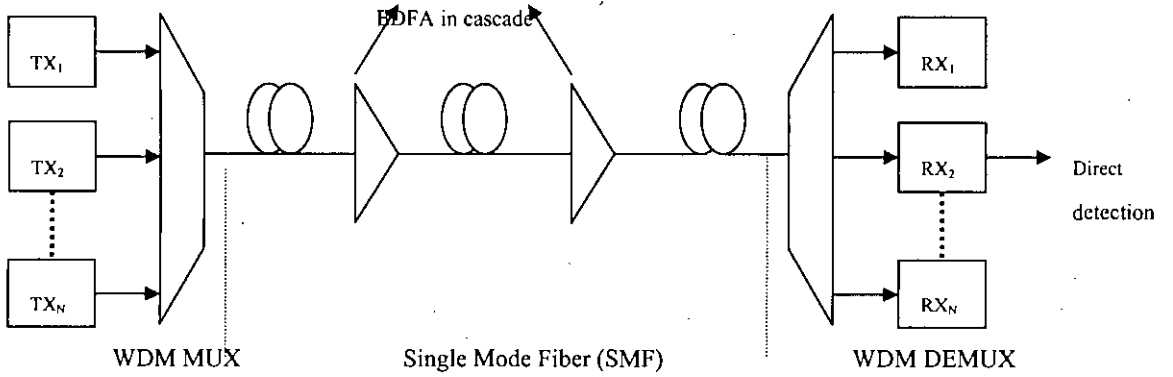


Fig. 6.2: Block diagram of a multi-channel/WDM system with EDFA in cascade

6.5 Theoretical analysis for multi-channel WDM system

In the previous two channel pump-probe configuration research work, we have derived the following two equations that describe the PMD and XPM interaction,

$$\begin{aligned} \frac{\partial |A_2\rangle}{\partial z} = & -\beta_{12} \frac{\partial |A_2\rangle}{\partial t} - \frac{i\beta_{22}}{2} \frac{\partial^2 |A_2\rangle}{\partial t^2} - \frac{\alpha_2}{2} |A_2\rangle - \frac{i}{2} B_2 \cdot \sigma |A_2\rangle \\ & + \frac{2i\gamma_2}{3} [2\langle A_1 | A_1 \rangle + |A_1\rangle\langle A_1| + |A_1^*\rangle\langle A_1^*|] |A_2\rangle \end{aligned} \quad (6.16)$$

$$\begin{aligned} \frac{\partial |A_1\rangle}{\partial z} = & -\beta_{11} \frac{\partial |A_1\rangle}{\partial t} - \frac{i\beta_{21}}{2} \frac{\partial^2 |A_1\rangle}{\partial t^2} - \frac{\alpha_1}{2} |A_1\rangle - \frac{i}{2} B_1 \cdot \sigma |A_1\rangle \\ & + \frac{i\gamma_1}{3} [2\langle A_1 | A_1 \rangle + |A_1^*\rangle\langle A_1^*|] |A_1\rangle \end{aligned} \quad (6.17)$$

where, β_{1j}, β_{2j} and α_j ($j=1,2$) are the inverse group velocities, group velocity dispersion (GVD) coefficient and fiber losses for the two channels and the Jones vectors $|\tilde{A}_1\rangle$ and $|\tilde{A}_2\rangle$ are two-dimensional column vectors representing the two components of the electric field in the x - y plane. In the Jones matrix notations, $\langle A |$ is the Hermitian conjugate of $|A\rangle$. While $|A^*\rangle$ is the complex conjugate of $|A\rangle$. The random vector $B(z, \omega)$ describes the residual fiber birefringence, while the vector σ has the Pauli matrices as its three elements. The vector σ is formed as $\sigma = \sigma_1 \hat{e}_1 + \sigma_2 \hat{e}_2 + \sigma_3 \hat{e}_3$, where \hat{e}_1 , \hat{e}_2 and \hat{e}_3 are three unit vectors in the Stokes space and this vector is used to relate the parameters between Stokes space to Jones space. The σ_1, σ_2 and σ_3 2x2 Pauli spin matrices are given as;

$$\sigma_1 = \begin{pmatrix} 1 & 0 \\ 0 & -1 \end{pmatrix} \quad \sigma_2 = \begin{pmatrix} 0 & 1 \\ 1 & 0 \end{pmatrix} \quad \sigma_3 = \begin{pmatrix} 0 & -i \\ i & 0 \end{pmatrix}$$

It is assumed that interchannel PMD dominates but intrachannel PMD is negligible. The intrachannel PMD barely affect the interchannel XPM interaction because channel spacing typically is much larger than channel bandwidth and the evolution of the SOP of the channels is mainly governed by $B(z, \omega)$.

If now there are more than 2-channels equations (6.16) and (6.17) can be extended as,

$$\begin{aligned} \frac{\partial |A_2\rangle}{\partial z} = & -\beta_{12} \frac{\partial |A_2\rangle}{\partial t} - \frac{i\beta_{22}}{2} \frac{\partial^2 |A_2\rangle}{\partial t^2} - \frac{\alpha_2}{2} |A_2\rangle - \frac{i}{2} B_2 \cdot \sigma |A_2\rangle \\ & + \frac{2i\gamma_2}{3} \sum_j \left[2\langle A_j | A_j \rangle + |A_j\rangle \langle A_j| + |A_j^*\rangle \langle A_j^*| \right] |A_2\rangle \end{aligned} \quad (6.18)$$

$$\begin{aligned} \frac{\partial |A_j\rangle}{\partial z} = & -\beta_{1j} \frac{\partial |A_j\rangle}{\partial t} - \frac{i\beta_{2j}}{2} \frac{\partial^2 |A_j\rangle}{\partial t^2} - \frac{\alpha_{j1}}{2} |A_j\rangle - \frac{i}{2} \mathbf{B}_j \cdot \boldsymbol{\sigma} |A_j\rangle \\ & + \frac{i\gamma_j}{3} \left[2\langle A_j | A_j \rangle + |A_j^*\rangle \langle A_j^*| \right] |A_j\rangle \end{aligned} \quad (6.19)$$

where, we consider the XPM and PMD effects on channel 2 (channel under study), while other channels act as the pump ($j \neq 2$). However, both beat length ($L_b \approx 10m$) and correlation length ($L_c \approx 100m$) associated with residual birefringence are much shorter than the nonlinear length ($L_n > 10 km$ depending on the optical power). As a result, the polarization rotation induced by the residual birefringence is much faster than that induced by nonlinear polarization rotation (NPR). Thus to average over the rapid polarization variation, it is convenient to choose a rotating frame in which the state of polarization (SOP) of channel 2 remain frozen. Adopting a rotation frame through a unitary transformation $|A_j\rangle = \bar{T} |A'_j\rangle$, where the Jones matrix \bar{T} satisfies,

$$\frac{d\bar{T}}{dz} = -\frac{i}{2} \mathbf{B}_1 \cdot \boldsymbol{\sigma} \bar{T} \quad (6.20)$$

The unitary matrix \bar{T} in (5) corresponds to random rotations of the Stokes vector on the Poincare sphere that do not change the vector length. After averaging over the rapid variations induced by \bar{T} and using a reduced time variable a $\tau = (t - \beta_{12}z)$, we obtain,

$$\begin{aligned} \frac{\partial |A_2\rangle}{\partial z} = & -\beta_{12} \frac{\partial |A_2\rangle}{\partial \tau} - \frac{i\beta_{22}}{2} \frac{\partial^2 |A_2\rangle}{\partial \tau^2} - \frac{\alpha_2}{2} |A_2\rangle - \frac{i}{2} \mathbf{B}_2 \cdot \boldsymbol{\sigma} |A_2\rangle \\ & + \frac{2i\epsilon_2}{3} \sum_j P_{0j} [3 + \hat{P}_j \cdot \boldsymbol{\sigma}] |A_2\rangle \end{aligned} \quad (6.21)$$

$$\begin{aligned} \frac{\partial |A_j\rangle}{\partial z} = & -\beta_{1j} \frac{\partial |A_j\rangle}{\partial \tau} - \frac{i\beta_{2j}}{2} \frac{\partial^2 |A_j\rangle}{\partial \tau^2} - \frac{\alpha_{j1}}{2} |A_j\rangle - \frac{i}{2} \mathbf{B}_j \cdot \boldsymbol{\sigma} |A_j\rangle \\ & - \frac{i}{2} \Omega_j \mathbf{b} \cdot \boldsymbol{\sigma} |A_j\rangle + i\varepsilon_j P_{0j} |A_j\rangle \end{aligned} \quad (6.22)$$

where, $P_{0j} = \langle A_j | A_j \rangle$ and $\hat{P}_j = \frac{\langle A_j | \boldsymbol{\sigma} | A_j \rangle}{P_{0j}}$ represents the power and the unit Stokes vector of the j th channel representing the SOP of the channel on the Poincare sphere. Furthermore, $\Omega_j = (\omega_2 - \omega_j)$ is the channel spacing, $\varepsilon_j = \frac{8}{9} \gamma_j$ and $\varepsilon_2 = \frac{8}{9} \gamma_2$ are effective nonlinear parameters for the j th channel and channel 2 respectively and $\delta\beta_j = (\beta_{1j} - \beta_{12})$ group velocity mismatch between the j th channel and channel 2.

Since, the fiber length (L) is typically much longer than the birefringence correlation length (L_c), we model b_j as a three-dimensional (3-D) stochastic process whose first- and second moments are given by,

$$\langle \mathbf{b}_j(z) \rangle = 0, \quad \langle \mathbf{b}_j(z_1) \mathbf{b}_j(z_2) \rangle = \sigma_{0j}^2 \delta_j(z_2 - z_1) \quad (6.23)$$

where, $\sigma_{0j}^2 = \frac{1}{3} D_p^2 \bar{\mathbf{I}}$; $\bar{\mathbf{I}}$ is the second-order unit tensor and D_p is the PMD coefficient of the fiber.

From (6.22) we see that the pumps (all other channel except channel 2) polarization \hat{P}_j remain fixed in the rotating frame. However, PMD changes the relative orientation between the different channels/pumps and channel 2 Stokes vectors at a rate dictated by the magnitude of $\Omega_j \mathbf{b}$. The effectiveness of XPM

depends not only on the group velocity mismatch $\delta\beta_j$, but also on the relative orientation of all the pumps and channel 2 SOPs.

We shall solve (6.22) and (6.23) to study the temporal modulation of channel 2 induced by the combined effect of XPM and PMD of all other channels. Since the modulation amplitude is small in general, we can linearize (6.22) by assuming that $|A_2\rangle = |A_{20}\rangle + |A_{21}\rangle$, where $|A_{20}\rangle$ and $|A_{21}\rangle$ are unperturbed and perturbed channel 2 fields respectively. Substituting this in (6.22) we obtain the following two equations governing the evolution of channel 2 field as,

$$\frac{\partial |A_{20}\rangle}{\partial z} = -\frac{\alpha_2}{2} |A_{20}\rangle - \frac{i}{2} \Omega b \cdot \sigma |A_{20}\rangle \quad (6.24)$$

$$\frac{\partial |A_{21}\rangle}{\partial z} = -\frac{i\beta_{22}}{2} \frac{\partial^2 |A_{21}\rangle}{\partial t^2} - \frac{\alpha_2}{2} |A_{21}\rangle - \frac{i}{2} \Omega b \cdot \sigma |A_{21}\rangle + \frac{i\epsilon_2}{2} \sum_j P_{0j} [\beta + \hat{P}_j \cdot \sigma] |A_{20}\rangle \quad (6.25)$$

where the dispersion term for $|A_{20}\rangle$ was set to zero for a cw input of channel 2.

The total optical power of the channel 2 field is expressed as,

$$\langle A_2 | A_2 \rangle \approx \langle A_{20} | A_{20} \rangle + [\langle A_{20} | A_{21} \rangle + c. c.] \equiv S_0 + \delta S_0 \quad (6.26)$$

here we neglected $\langle A_{21} | A_{21} \rangle$ because of its smallness and introduced the power and SOP of the unperturbed field as,

$$S_0 = \langle A_{20} | A_{20} \rangle \text{ and } \hat{S} = \frac{\langle A_{20} | \sigma | A_{20} \rangle}{S_0} \quad (6.27)$$

To find the modulation amplitude δS_0 , which is the measure of the combined PMD and XPM-induced crosstalk, we first find an equation for $\langle A_{20} | A_{21} \rangle$ only. Using (6.26) and (6.27), this quantity is found to satisfy the following equation,

$$\frac{\partial \langle A_{20} | A_{21} \rangle}{\partial z} = -\frac{i\beta_{22}}{2} \frac{\partial^2 \langle A_{20} | A_{21} \rangle}{\partial \tau^2} - \alpha_2 \langle A_{20} | A_{21} \rangle + \frac{i\varepsilon_2}{2} S_0 \sum_j P_{0j} [3 + \cos[\theta_j(z)]] \quad (6.28)$$

where, $\theta_j(z) = \hat{P}_j \cdot \hat{S}(z)$ is the random angle between the different channels/pumps and channel 2 SOPs. Equation (13) can be solved analytically in the frequency domain because of its linear nature. Using $\delta S_0 \equiv \langle A_{20} | A_{21} \rangle + \langle A_{21} | A_{20} \rangle$ and introducing the normalized modulation

amplitude for the j th channel $\tilde{\delta}_{x_j}(\omega) = \frac{\delta \tilde{S}_0(L, \omega_j)}{S_0(L)}$, where, $\tilde{\delta}_{x_j}(\omega)$ is given by,

$$\tilde{\delta}_{x_j}(\omega) = -\int_0^L \varepsilon_2(z) \tilde{P}_{\theta_j}(z, \omega) [3 + \cos[\theta_j(z)]] \sin\left[\frac{1}{2} \int_z^L \omega_j^2 \beta_{22}(z_1) dz_1\right] dz \quad (6.29)$$

where a tilde denotes the Fourier transform and $\tilde{P}_{\theta_j}(z, \omega)$ is the Fourier spectrum of the different pumps power at a distance z inside the fiber. The effects of PMD enter in this equation through the angle $\theta_j(z)$. More precisely, PMD randomly changes the angle between \hat{P}_j and \hat{S} along the fiber and thus makes $\tilde{\delta}_{x_j}(\omega)$ a random quantity. The total modulation amplitude for channel 2 is just the algebraic sum over all pump channels,

$$\tilde{\delta}_x = \sum_j \delta_{x_j}(\omega) \quad (6.30)$$

To characterize the XPM-induced crosstalk, it is common to introduce the modulation transfer function using the definition,

$$H(L_j, \omega) = \frac{\sum_{j=1}^L \langle \tilde{\delta} S_0(L_j, \omega) \rangle}{\tilde{P}(0, \omega)} = \frac{\sum_{j=1}^L S_0(L_j)}{\tilde{P}(0, \omega)} \langle \tilde{\delta}_x(\omega) \rangle \quad (6.31)$$

The total average crosstalk level $\langle \delta_{x_j}(\tau) \rangle_p$ changes with time depending on the bit pattern in the different pump channels. Thus, $\delta_{x_j}(\tau)$ fluctuates with time because of its doubly random nature. In the absence of residual birefringence, randomness comes only from the bit pattern in the pump channels. In this case, it is common to introduce the crosstalk variance, also called PMD and XPM-induced interference, using the following equation,

$$\begin{aligned} \sigma_j^2 &\equiv \frac{1}{T} \int_{-\frac{T}{2}}^{\frac{T}{2}} [\delta_{x_j}(\tau)]^2 d\tau \\ &= \frac{1}{4\pi^2} \int_{-\infty}^{\infty} d\omega_j \int_{-\infty}^{\infty} d\omega \tilde{\delta}_x(\omega_j) \tilde{\delta}_x^*(\omega_2) \text{sinc} \left[\frac{(\omega_j - \omega_2)T}{2} \right] \end{aligned} \quad (6.32)$$

where, T is the time interval of measurement.

If we assume that bit pattern in different channels are independent of each other, it is easy to show that the variance is also a sum over individual channel such that,

$$\sigma_m^2 = \sum_{j \neq 2} \sigma_j^2 \quad (6.33)$$

6.5.1 Determining the PDF of $\theta_j(z)$ and BER expression

The $\theta_j(z)$ is the sum of all randomly fluctuating angles between the different pumps/channels and the affected channel 2. So, $\theta_j(z)$ can be written as,

$$\theta_j(z) = \theta_1(z) + \theta_2(z) + \theta_3(z) \dots \dots \dots + \theta_N(z) \quad (6.34)$$

Since the different pumps polarization \hat{P}_j remain constant and the random variation of $\hat{S}(z)$ (unit vector of the SOP of channel 2) will be responsible for the angle of $\theta_1(z)$.

We have already analytically determined the pdf of $\theta(z)$ for a 2 channel (pump-probe configuration), which is given by,

$$p(\theta, z) = \frac{1}{2\pi} + \frac{1}{\pi} \sum_{m=1}^{\infty} \exp\left(-\frac{1}{2}\eta^2 m^2 z\right) \cos m(\theta - \theta_0) \quad (6.35)$$

where, $\theta(z) = \hat{P} \cdot \hat{S}(z)$ is the random angle between the pump and probe SOPs and θ_0 is the initial angle.

Now assuming the random variables $\theta_1(z)$, $\theta_2(z)$, $\theta_3(z)$ $\theta_N(z)$ are independent and identically-distributed (iid) in nature, then the combined pdf of SOP fluctuation angles for a multi-channel system can be written as the convolution of all the individual random angle that the channel 2 makes with different pumps SOPs (which results (N-2) folds convolution),

$$p_{combined}(\theta, z) = p(\theta_1, z) \otimes p(\theta_2, z) \otimes p(\theta_3, z) \dots \dots \dots p(\theta_N, z) \quad (6.36)$$

The signal to crosstalk noise ratio (SCNR) can be written as,

$$SCNR = \frac{(R_d S_0)^2}{\sigma_m^2 + \sigma_n^2} \quad (6.37)$$

where σ_m^2 crosstalk variance due to the combined effect of PMD and XPM of all pump channels, σ_n^2 noise variance, $I_s = R_d S_0$, R_d is the responsivity and S_0 is the affected channel 2 power.

Thus,

$$SCNR(\text{for angle } \theta_0) = \frac{I_s^2}{\sigma_m^2(\theta_0) + \sigma_n^2} \quad (6.38)$$

For a given value of θ_0 (which is initial angle), the conditional BER can be

expressed as,

$$BER(\theta_0) = 0.5 \operatorname{erfc} \left(\frac{\sqrt{SCNR(\text{for angle } \theta_0)}}{\sqrt{2}} \right) \quad (6.39)$$

Because of environmental changes (*i.e.*, temperature, pressure, vibration, stress, twisting etc.), PMD fluctuates randomly. Generally, the impact of PMD fluctuations as well as the variation of angle, $\theta_j(z)$ typically occurs on a time scale of milliseconds. Thus, the average BER is given by,

$$BER = \int_{-\pi}^{\pi} BER(\theta_0) p_{combined}(\theta, z) d\theta \quad (6.40)$$

In the case of pump-probe configuration, the BER expression can be written as,

$$BER = \int_{-\pi}^{\pi} BER(\theta_0) p(\theta, z) d\theta \quad (6.41)$$

6.6 Results and discussion

6.6.1 Performance of pump-probe configuration

Following the pump-probe analytical approach, the performance of the 2-channel of IM-DD WDM system is investigated at a bit rate of 10 Gb/s. The pdf of the random polarization angle between pump and probe is evaluated at various length of single mode fiber and shown in Fig.6.3 and Fig. 6.4 for channel spacing of 0.8 and 0.4 nm respectively. From the figure, it is found that for particular channel spacing the pdf is a delta function at $z = 0$ and becomes flat as the link length increases. It is observed that for any lightwave system of fiber length much larger than the diffusion length ($h_E = 280 \text{ m} - 1.5 \text{ km}$), the pdf becomes Gaussian like distribution. Fig. 6.5 shows the variance of pump and probe polarization SOP versus fiber link length for different PMD coefficient. It

is noticed that as the PMD coefficient increases the variance of SOP also increases linearly. Thus the higher value of PMD fibers (usually older fiber) will larger amount of amplitude modulation fluctuations. The Table 6.1 shows the set of parameters and assumption that are made to evaluate the system performance.

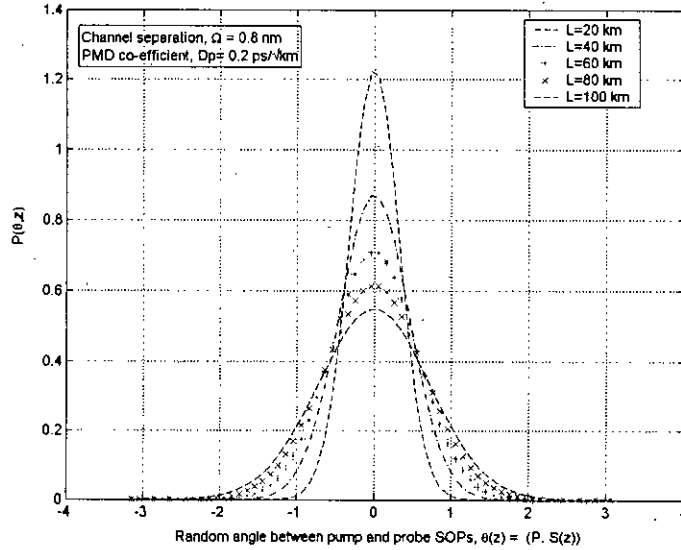


Fig. 6.3: Plots of pdf of $\theta(z)$ at different length of fiber link length with a channel separation 0.8 nm and PMD coefficient 0.5 ps/ $\sqrt{\text{km}}$

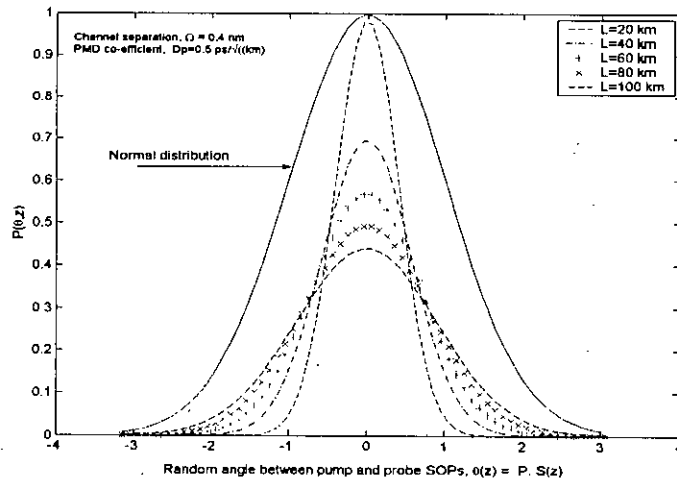


Fig. 6.4: Plots of pdf of $\theta(z)$ at different length of fiber link length with a channel separation 0.4 nm and PMD coefficient 0.2 ps/ $\sqrt{\text{km}}$

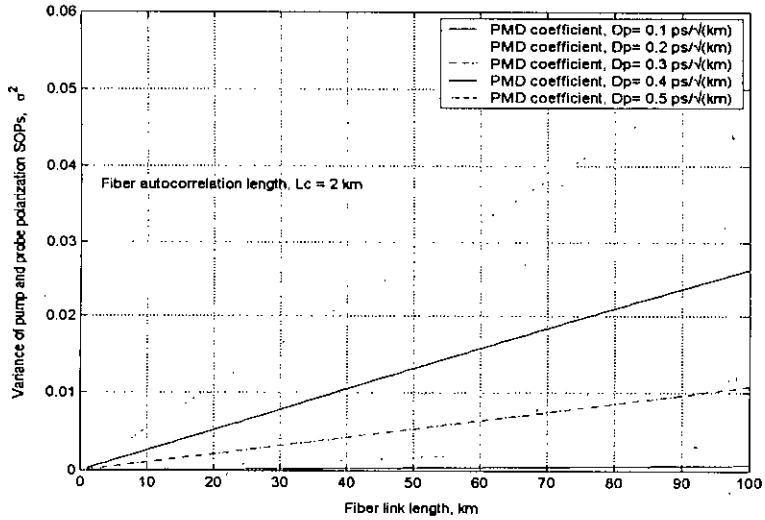


Fig.6.5: Plots of variance of pump and probe polarization SOP vs fiber link length for different PMD parameters.

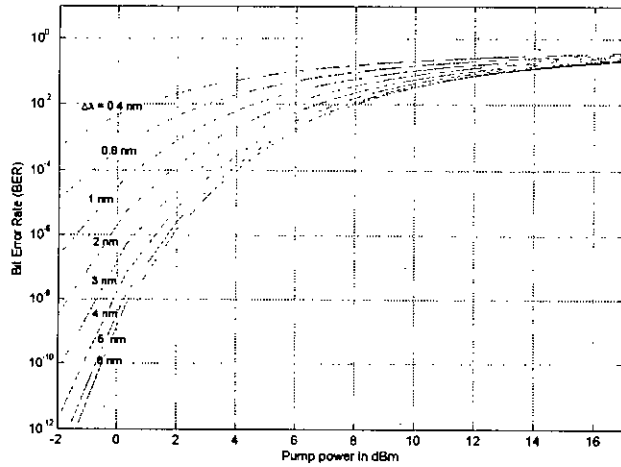


Fig. 6.6: Plots of average BER vs pump power for different channel spacing

The average BER versus pump power is plotted in Fig. 6.6. It is observed that interaction of PMD and XPM increases as the channel spacing decreases for a specific pump power and system suffers a large amount of BER. The significant dependence of XPM effect on BER as a function of channel spacing comes from

the fact that the PMD diffusion length is inversely proportional to the square of the channel spacing. However, at increased pump power the BER increases and when pump power is about 16 dBm the BER curves makes a floor at 10^{-1} irrespective of channel spacing.

The plots of average BER versus probe power is shown in Fig. 6.7. It is seen that at high pump and probe power the BER performance of the fiber link deteriorates sharply. This happens due to the strong interaction of PMD and XPM on each other channel. For example, when the pump power is -15 dBm, we can achieve a BER of 10^{-9} for a 6.25 dBm probe power. Keeping the probe power same, it is found that at 25 dBm pump power the BER drops to a value of 10^{-1} only. This happens due to the higher modulation amplitude fluctuation as a result of high pump power.

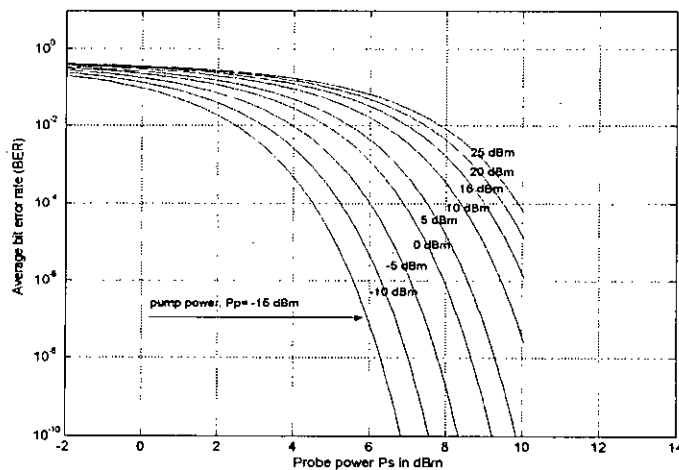


Fig. 6.7: Plots of average BER vs probe power for different pump power

Fig.6.8 depicts the variance of SOP as a function of channel spacing for different length. For smaller channel spacing and short length of fiber link the variance is very negligible. As the link length increases and so does the channel spacing, the variances increases exponentially for larger values of channel spacing.

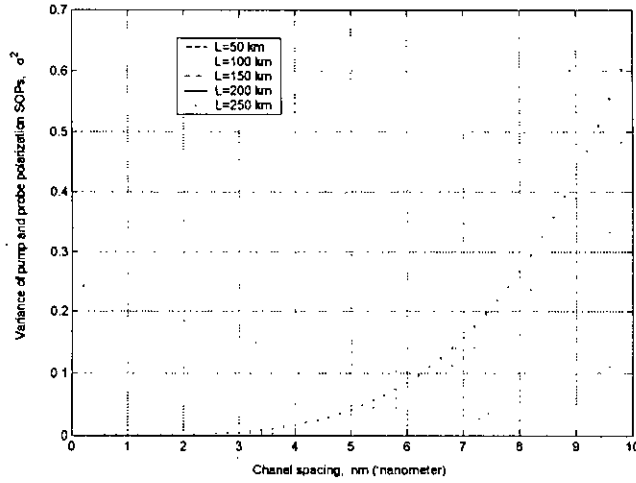


Fig.6.8: Plots of variance of pump and probe polarization SOP vs channel spacing for different link length.

Parameters	Settings
PMD coefficient, D_p	0.1-0.5 ps/ $\sqrt{\text{km}}$
Channel spacing, Ω	0.8 nm
Pump wavelength, λ_1	1550.0 nm
Probe wavelength, λ_2	1550.8 nm
Correlation length, l_c	2 km
Group velocity dispersion, β_{22}	17 ps/nm-km
Bit rate, B	10 Gb/s
Nonlinear coefficient, γ	2.35 W^{-1}/km
Fiber attenuation, α	0.21 dB/km

Table 6.1: Set of parameters and assumptions used in the analysis

6.6.2 Performance of 4-channel WDM system

Following the N-channel analytical approach, the performance of a 4-channel WDM system is investigated at a bit rate of 10 Gb/s per channel. Out of 4-channels, we assume that channel 1, 3 and 4 are pump channel and channel 2 is affected channel, where we observe the effect of XPM and PMD. The channel 2

is in the form of a low-power continuous wave (cw) channel and XPM effect for this channel power is negligible to other channels. We also neglected the effect of intrachannel PMD, as channel spacing typically is much larger than channel bandwidth and evolution of the SOP channels is mainly governed by birefringence.

The combined pdf, $p_{combined}(\theta, z)$ of the random polarization angle between the pumps and channel 2 is evaluated for various length of the single mode fiber and shown in Fig.6.9. From the figure, it is noticed that for channel spacing, $\Delta\lambda = 0.8$ nm and at $z = 0$, the pdf results a delta function. The pdf becomes flat as link length increases. As compared with the pump-probe configuration (2-channel) pdf, the obtained 4-channel random angle pdf is more close to the normal pdf of Gaussian distribution.

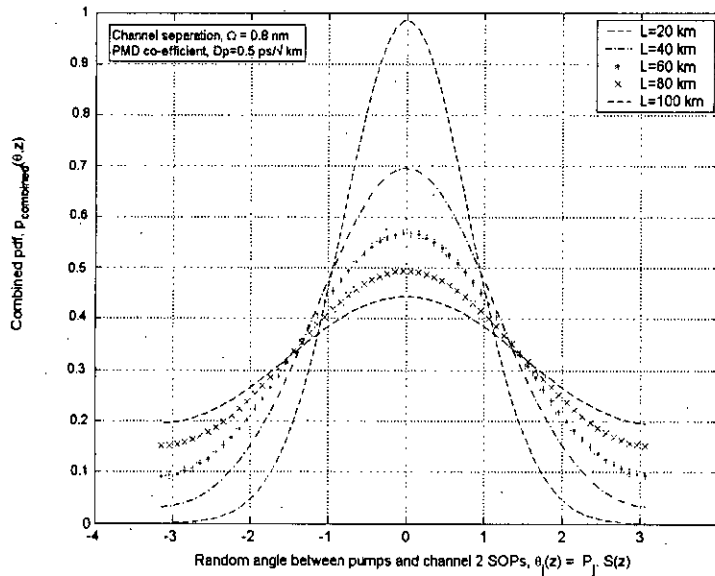


Fig. 6.9: Plots of pdf of $\theta_j(z) = \hat{P}_j \cdot \hat{S}(z)$ at different length of fiber

The average BER vs pump power is plotted in Fig. 6.10 for different channel spacing. We use the wavelengths from 1549.4 nm to 1552.8 nm to accommodate

the 4-channels. It is observed that the interaction of PMD and XPM increases as the channel spacing decreases for specific pump power. For example, when the total pump power is 0 dBm, channel 2 BER is about 10^{-6} and 10^{-10} at channel spacing of 2 nm and 3 nm respectively. However, at increased pump power the BER increases and when pump power is about 18 dBm the BER curves makes a floor at 10^{-1} irrespective of channel spacing.

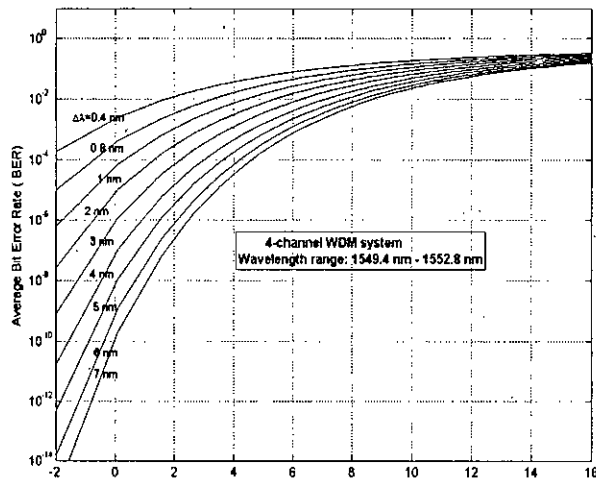


Fig.6.10: Plots of average BER vs pump power for different channel

To evaluate the effect XPM and PMD on channel 2 (affected channel), we vary the channel 2 power from -2 dBm to 16 dBm and the results of this evaluation is shown Fig. 6.11. It is found that at relatively high pump and channel 2 input power the BER performance deteriorates sharply due to the strong interaction of PMD and XPM. For example, when the pump power (each channel) is -15dBm, we can achieve of BER 10^{-10} for a 8 dBm channel 2 power. Keeping the channel 2 power same, it is observed that at 20 dBm pump power the BER drops to 10^{-1} only. This deterioration happens due to the higher modulation amplitude fluctuation as a result of high pump power.

The transfer function for amplitude fluctuation of channel 2 is derived in (16).

We evaluate the average amplitude fluctuations for 3-different channel spacing (in wavelength) as a function of fiber link length and shown in Fig.6.12. It is seen from the figure that for higher channel spacing the fluctuation is less or minimum. For example, at 100 km the amount of average amplitude fluctuation is -33 dB, -27 dB and -23 dB for channel spacing of 4 nm, 1 nm and 4 nm respectively.

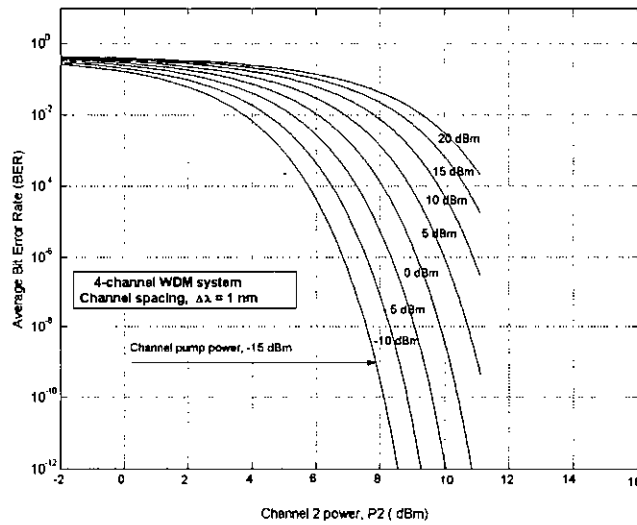


Fig. 6.11: Plots of average BER vs channel 2 power for different pump power

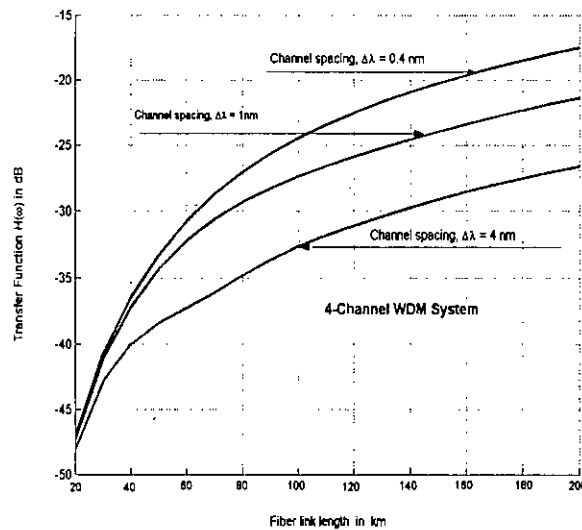


Fig. 6.12: Average amplitude transfer function vs fiber link length

A comparison is established based different parameters between the numerical results of pump-probe WDM configuration and 4-channel WDM system in Table 6.2.

Parameter/description	Pump-probe (2-channel) WDM system	4-channel system WDM system
Channel spacing 1 nm and pump power -2 dBm	Achieves a BER of about 10^{-7}	Achieves a BER of about 10^{-6}
Channel 2 power 8 dBm to attain a BER of 10^{-9}	Allowable pump power -10 dBm	Allowable pump power -15 dBm/channel
Pdf of the random angle	Narrowly flattens as distance of the fiber link increases	As the combined pdf is the convolution other 3-channels, it become flat as distance of fiber link increases and resembles gaussian distribution

Table 6.2: Comparison of results between 2 channel WDM and 4-channel WDM system

6.7 Interaction of PMD and XPM: OptSim software simulation

To simulate the interaction of PMD and XPM, the simulation setup for a 4-channel WDM system is shown in Fig. 6.13. This simulation is carried out in presence of CD. The different simulation parameters that are used in the simulation are shown in Table 1. The 4-WDM channels are launched over two dispersion shifted (DS) fiber span of 100 km each where fiber loss is totally compensated by the EDFA and CD is completely compensated at each span by the fiber Bragg grating. The interaction of XPM and polarization effects also depends upon the fiber's CD due to walk off effects between the pump and probe. So, we varied the CD from 0 - 6 ps/nm-km and observe its effects on the PMD and XPM interaction.

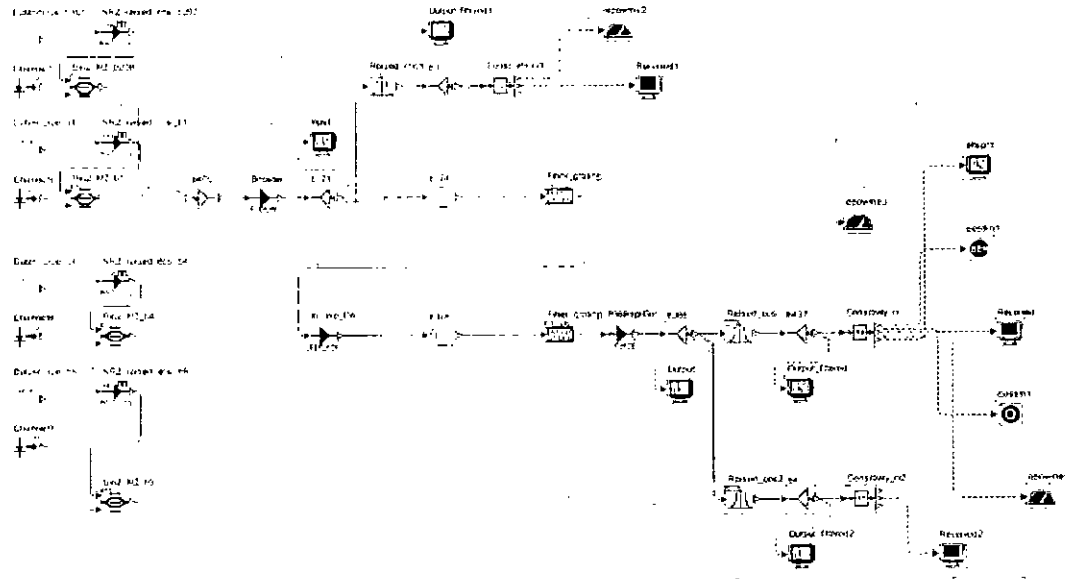
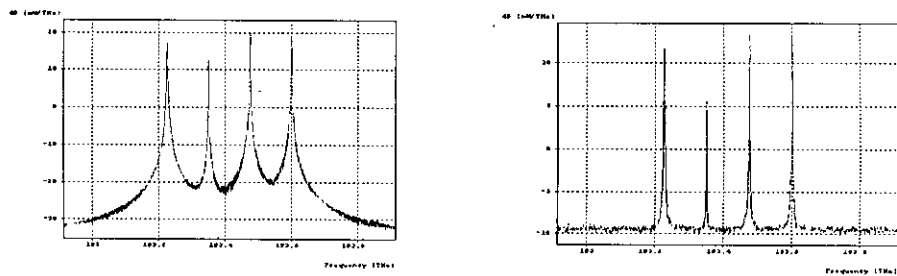


Fig. 6.13: Setup of the system simulation model for a 4-channel WDM/IM-DD for PMD and XPM interaction

Here, we investigate the impact of PMD and XPM on the WDM/IM-DD optical transmission system in terms of eye diagram, BER, Q-value and PMD coefficient. The channels are modulated at 10 Gbit/s data rate using NRZ format and separated by 1 nm, the distance between the inline optical EDFA fiber amplifiers is 100 km (span length). All the 4-incoming channels are multiplexed and transmitted through the fiber. At the receiving end, we demultiplexed the channels and monitor the signal on channel 2 (channel under study) and other channels.



(a)

(b)

Fig.6.14: (a) input optical spectrum, (b) output optical spectrum

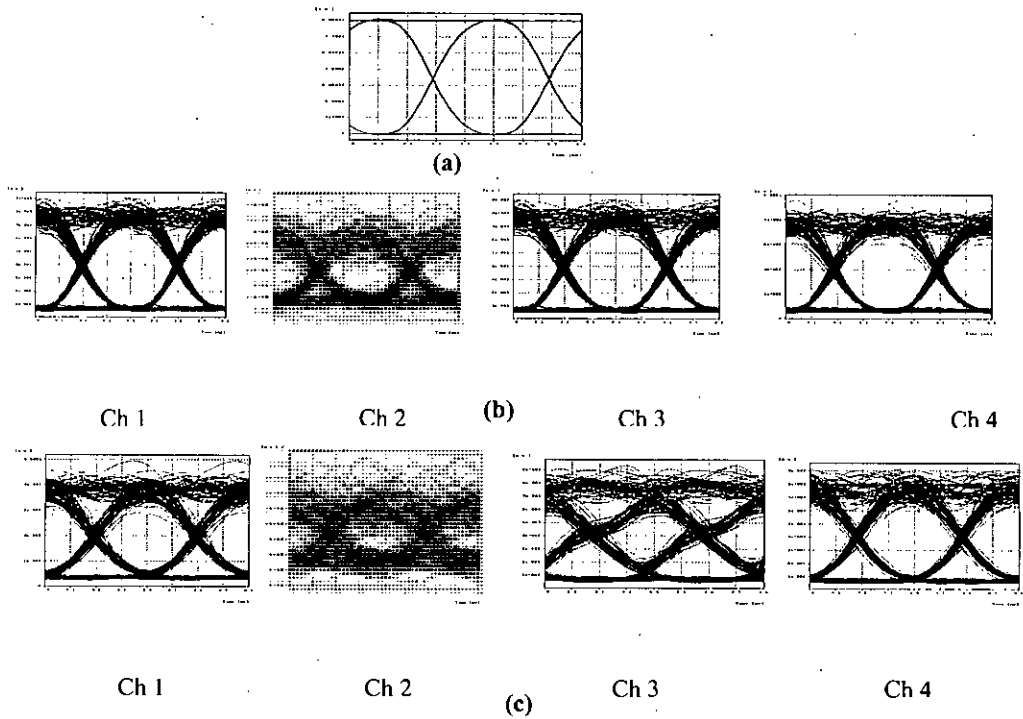


Fig. 6.15: (a) Base line eye diagram (back-to-back), (b) Channel 1- 4 at the output for a PMD coefficient of 0.5 ps/√km; (c) Channel 1- 4 at the output for a PMD coefficient of 1.5 ps/√km

To assess the impact of XPM and PMD on channel in electrical domain we monitor the eye diagram of the channels at the input (back-to-back) as well as at the output for a receiver sensitivity of -24 dBm (at a BER of 10^{-9}). Fig. 6.15 shows the eye diagrams at the input and output of the fiber link of different channels for PMD coefficients of 0.5 ps/√km and 1.5 ps/√km. It is observed that for a fixed channel space (1nm in this case) the channel 2 eye diagram deteriorates more at 1.5 ps/√km than that of 0.50 ps/√km and other channels are also affected due the high value of PMD coefficient. We may calculate the average eye-opening penalty (EOP) due to PMD and XPM for channel 2. Here, we define the parameter of the eye-opening penalty (EOP) as,

$$EOP = -20 \log \left(\frac{B}{B_0} \right) \quad (6.42)$$

where, B is the eye opening without PMD effect and B₀ is the eye-opening with PMD and XPM in channel 2. We found that the EOP (at a probability of 10⁻³) at PMD coefficient 1.5 ps/√km is about 1.85 dB more than that of 0.5 ps/√km

Plot of bit error rate (BER) vs input pump power and Q – value (in dB) vs input pump power are shown in Fig.6.16. It is observed that the maximum interaction occurs between XPM and PMD at zero dispersion co-efficient (*i.e.*, the BER is significantly higher) and as the dispersion coefficient increases the effect is less due to the walk-off phenomenon. On the other hand, as pumps power increases the BER decreases due to the larger effect of PMD and XPM.

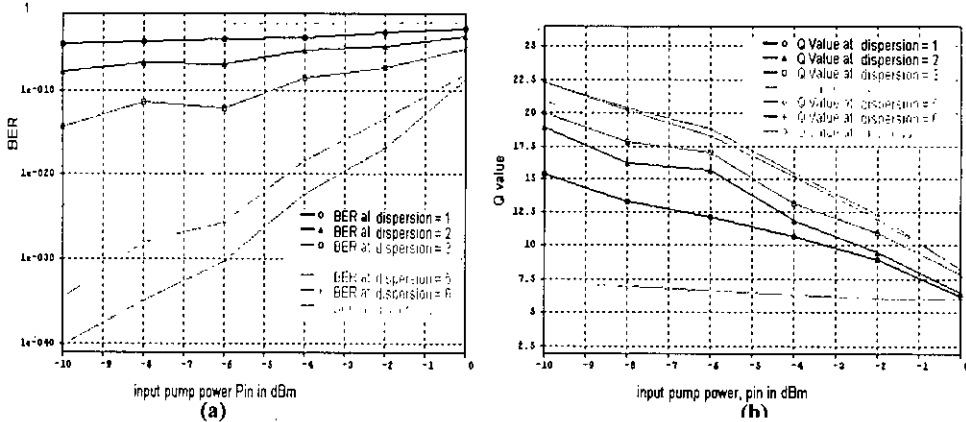


Fig.6.16: (a) BER vs input pump power, (b) Q-value (in dB) vs input pump power (for chromatic dispersion coefficient, D_c = 0 - 6 ps/nm-km)

The effect of PMD coefficient vs BER and Q- value vs PMD coefficient is shown in Fig. 6.17 for a fiber link length of 100 km and dispersion coefficient 3 ps/nm-km. We observe that the relationship between BER or Q value to PMD coefficient is not exactly linear due to presence of mode coupling between the two orthogonal modes.

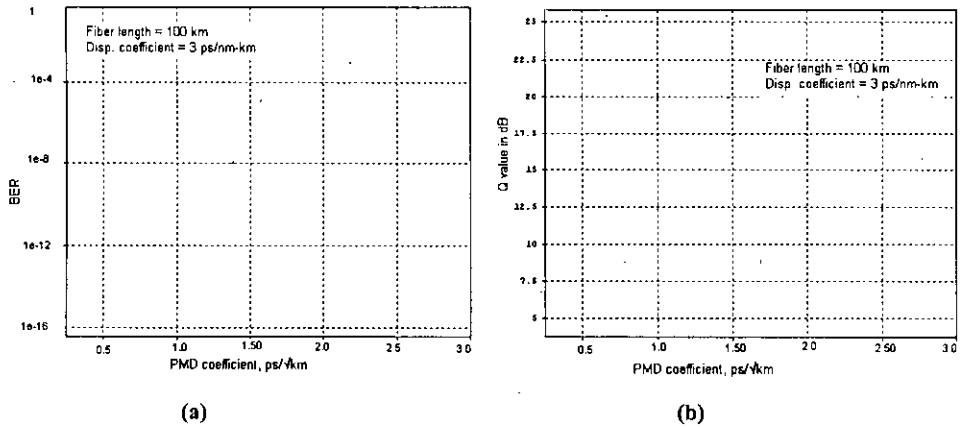


Fig.6.17: (a) BER vs PMD coefficient, (b) Q-value vs PMD coefficient (for chromatic dispersion coefficient, $D_c = 3$ ps/nm-km)

SI no.	Parameters/description	values
1	Fiber loss (dB/km)	0.20
2	Dispersion (ps/km-nm)	0.0 – 6.0
3	Effective core area (μm^2)	80
4	Fiber length (km, 2-span of 100 km)	100
5	PMD co-efficient (ps/ $\sqrt{\text{km}}$)	0.5 – 1.50
7	Bit rate of each channel (Gbit/s)	10
8	No. of channels	4
10	Channel spacing (nm)	1.0
11	Working wavelength range (nm)	1548.5 nm -1551.5 nm
12	Receiver sensitivity (dBm at 10^{-9})	-24
13	Transmitter power for ch. 1, 3& 4 (dBm)	0
14	Booster EDFA output (dBm)	6
15	Transmitter power for channel 2(dBm)	-10

Table 6.3: Different simulation parameters

6.7 Summary

An analytical approach is used to find the pdf of the random SOP angle between the pump and probe in 2-channel and N-channel IM-DD WDM system, which causes the XPM induced modulation amplitude to be random. The strength of the XPM effect is strongly influenced by the evolution of light-polarization of the WDM carriers. We applied the theory for a 4-channel WDM system in which channel 2 in which the weak cw signal is perturbed by other 3 co-propagating channels. The birefringence fluctuations responsible for PMD change the relative orientation $\theta_j(z)$ between the pumps and channel 2 Stokes vectors. Changes in $\theta_j(z)$ affect the XPM interaction among the various channels. We found that effect of XPM and PMD are more pronounced at 4-channel (*i. e.*, channel 2 is more affected) than that of pump-probe configuration. We also observe that, XPM crosstalk becomes polarization independent when channel spacing is large (such as 4 nm or greater) or when the fiber has a relatively large value of PMD co-efficient. It has been demonstrated the interaction of PMD and nonlinear SMF effect XPM by Rsoft OptSim simulation software in terms of eye diagram, BER, Q-value etc. in a 4-channel WDM system. We show that PMD changes the XPM efficiency and affects the interference condition among the XPM-induced nonlinear phase shifts in different sections of the fiber link. Thus at relatively high pump the combination of nonlinearity and PMD can limit the performance of a WDM fiber link significantly.

Chapter 7

CHIRPED FIBER BRAGG GRATING IN PMD COMPENSATION

The chirped fiber grating reflects different wavelength (frequencies) at different points along its length. Effectively, a chirped fiber Bragg grating introduces different delays at different frequencies. Chirped gratings are ideally suited to compensate dispersion for multiple wavelengths. In this chapter, we describe analytical formulations of a variable PMD compensator by using highly birefringent linearly chirped fiber Bragg grating and this compensator is used in a simulation environment for a 4-channel WDM transmission system to compensate PMD without the application of strain.

7.1 Fiber grating in dispersion compensation

The term grating refers to a device whose operation involves interference among multiple optical signals originating from the same source, but with different phase shifts. Fiber Bragg gratings are based on the principle of Bragg reflection. When light propagates by periodically alternating regions of higher and lower refractive index, it is partially reflected at each interface between these regions. If the spacing between those regions is such that all the partial reflections add up in phase – when the round trip of the light between the two reflections is an

integral number of wavelengths – the reflections can grow to nearly 100%, even the individual reflections are very small. That means, the incident wave is reflected from each period of the grating. These reflections add in phase when path length in each period is equal to the half the incident wavelength λ_B (which is actually the Bragg condition, $n_{eff}\Lambda = \lambda_B / 2$). Of course, that condition will only hold for specific wavelength. For other wavelengths, the out of phase reflections end up canceling each other, resulting in high transmission.

In chapter 5, we mentioned that PMD compensation could be accomplished either in the electrical or optical domains and a number of PMD compensation techniques have been presented to overcome PMD limitations. As data rates rise beyond 10 Gb/s, it will be a challenging task to perform electronic equalization because of the difficulty in finding electronic delay stages and filters that can operate at high speed and this technique can not be performed in-line along the larger optical system. On the other hand, conventional optical technique is bulky and its performance may be easily affected by operational environment. Most of electronic or optical domain concepts offer PMD compensation on per-channel basis, because the compensation bandwidth is strongly limited. Hence in a WDM environment, the channels would have to be multiplexed before each channel is individually compensated for PMD. PMD compensation by fiber Bragg grating offers many advantages over other competing technologies, since it is comprise of all fiber geometry, low insertion loss, low return loss, flexible in achieving desired spectral characteristics, low temperature coefficient and also potentially low cost.

Chirped fiber gratings are useful for PMD and chromatic dispersion compensation, for controlling and shaping short pulses in the fiber lasers, and for creating stable continuous-wave and tunable mode-locked external cavity semiconductor lasers [108]-[109]. In a linearly Hi-Bi chirped FBG that is written into a photosensitive fiber by use of a specially designed nonlinearly chirped phase mask or changing the ultra-violet exposure time along the length of the grating with a linearly phase mask. This type of Hi-Bi has a large refractive index difference between its fast and slow polarization axes. The birefringence

Δn causes the orthogonal polarization modes to experience two different couplings with the grating and the Bragg reflection from the birefringence chirped grating for a given signal wavelength occurs at different locations for different polarizations. In essence, the two signal polarizations 'see' two different gratings due to the birefringence. The position difference, ΔL of the reflection produces a differential time delay, Δt , between the two polarizations.

Thus, the delay between the two SOP's can also be achieved by chirped FBG. The Hi-Bi fiber provides different time delay for different SOPs and the chirp of the grating provides the selectability of varying amounts of DGD when the FBG is stretched or compressed [110]-[111]. Since stretching the fiber adjusts DGD without altering the polarization, this device has the potential for compensating variable PMD for long-distance high-speed optical transmission line. S. Lee *et al* [39], experimentally reported a tunable nonlinearity-chirped FBG written into a Hi-Bi fiber to compensate for varying amounts of PMD. Z. Pan *et al* [37], experimentally demonstrated chirp-free tunable PMD compensation for a 10 Gb/s signal by using an adjustable Hi-Bi nonlinearly-chirped FBG in a novel dual-pass configuration that significantly reduces the induced chirp of the FBG. It is shown that a 45-km link interacting with the FBG induced chirp is reduced from 4.0 to 0.5 dB. X. Kun *et al* [112], based on numerical simulations reported that the efficiency of this PMD compensator is assessed for the 10 Gb/s NRZ transmission system with 58.6 ps and 106 ps DGD respectively by applying transverse and uniform distributed force on a linearly chirped FBG (LCFBG).

Unfortunately, the nonlinearly-chirped FBG, by its very nature, induces a chirp into the PMD compensated signal. This chirp may limit the distance of transmission after the compensation due the fiber chromatic dispersion. In this research work, we analytically evaluate the performance of a novel delay element for adjustable PMD compensation based on a tunable Hi-Bi LCFBG. The key feature of this grating is that the linear variation of the DGD is a function of wavelength within the operating bandwidth, without affecting

wavelength outside the bandwidth. The reflection point inside the grating can be moved by several millimeters by stretching the grating by few microns. Results show that a 2 cm long LCFBG allows the DGD to be adjusted from 0 ps to 55 ps by stretching it by 0.2%. It also offers the possibility to adjust the DGD in a continuous way within a 2.4 nm wavelength range. This type of system is well suited for WDM applications since it totally nullifies PMD inside its operational bandwidth. It is an all fiber PMD compensation solution, which is inexpensive, compact, absence of nonlinear effects and feasible for continuously adjustable DGD.

7.2 LCFBG based PMD compensation system model

The system model diagram of the LCFBG based PMD compensation scheme is shown in Fig.7.1. The proposed delay element consists of a 4-port polarization beam splitter (PBS) and a 2 cm length Hi-Bi LCFBG. The PBS splits the incoming optical signal into two orthogonal polarizations: the fast- and slow axis polarization signal respectively. The fast axis signal (P_f) enters the Hi-Bi LCFBG from the longer wavelength port and slow one (P_s) from the shorter wavelength port. The polarization states of the signal (λ_i) within the bandwidth of the grating will be reflected and differently delayed by the grating. By properly tuning the LCFBG, we can adaptively generate required DGD ($\Delta\tau$) for the PMD compensation. The two orthogonally polarized optical signals are then combined without interference and directed to output port 1 of the PBS, where an optical circulator can be used to separate the input signal and the PMD compensated output signal. All light (λ_0) outside the reflection bandwidth of the grating will not be affected and detected to output port 2. In addition, when the grating is tuned, the change in DGD ($\Delta\tau$) will be twice of the change of the grating's group delay. This increases the maximum achievable DGD value and improves the tunable PMD compensation capability of the proposed delay element. The PMD compensation capability of the device is mainly determined

by the characteristics of the Hi-Bi LCFBG and improved capability can be achieved by adopting higher chirp ratio the Hi-Bi grating. In this scheme losses are not a major concern, neither are nonlinear effects.

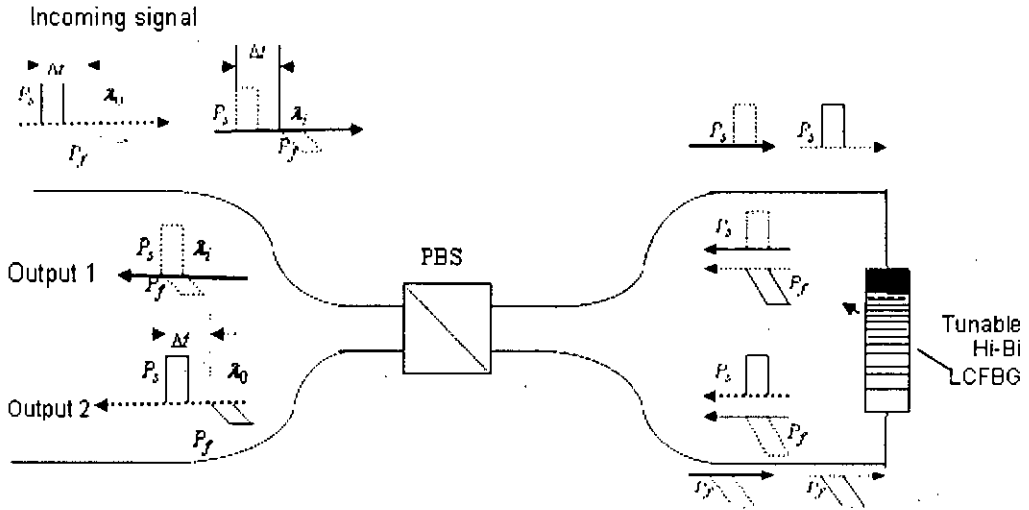


Fig. 7.1: System model of the PMD compensation scheme. The incoming signal has polarization components along both the fast- (P_f) and slow- (P_s) axis. The LCFBG generates the required DGD for the Bragg reflected signal (λ_1), while it does not affect the signal (λ_0) outside the grating bandwidth

7.3.1 Characteristics of birefringent chirped grating

Let us assume that a Bragg grating in a single mode fiber consists of a refractive index that is varied with the period, Λ and the modulation amplitude that is added to the initial refractive index in the fiber. The perturbation to the effective refractive index n_{eff} of the guided mode(s) of interest given by,

$$\delta n(z) = \delta n_{eff} [1 + \nu(z) \cos(Kz + \phi(z))] \quad (7.1)$$

where, $\delta n_{eff} = n_{av} - n_{co}$ is the average index change over one period, ν is the fringe visibility of the index change, $0 \leq \nu \leq 1$. $\cos(Kz + \phi(z))$ is the index perturbation, which has a constant spatial frequency with an additional position

dependent phase variation $\phi(z)$ that represents the change in periodicity. Fig. 7.2 shows a chirped grating of length L and bandwidth $\Delta\lambda_{chirp}$.

The chirp could be viewed as the perturbation with a varying spatial frequency, $\cos((K + \Delta K)(z))$. The relationship between the period, Λ and the spatial frequency can be written as

$$dK = -\frac{2\pi}{\Lambda^2} d\Lambda \quad (7.2)$$

The rate of phase change with distance along the grating, z , can be derived

$$\frac{d\phi(z)}{dz} = \Delta K = -\frac{2\pi}{\Lambda^2} d\Lambda \quad (7.3)$$

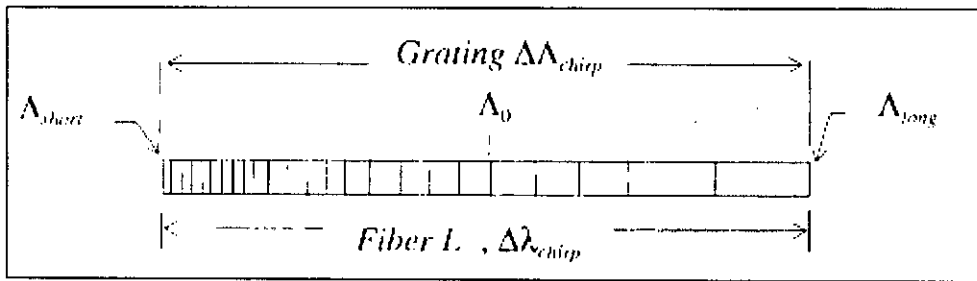


Fig. 7.2: A typical chirped Bragg grating

From the Bragg condition $\lambda_B = 2n_{eff}\Lambda$, then the expression becomes,

$$\frac{d\phi(z)}{dz} = -\frac{2\pi z}{\Lambda^2} \frac{d\Lambda}{dz} = -\frac{4\pi n_{eff}}{\lambda_B^2} \frac{d\lambda_B}{dz} z \quad (7.4)$$

where $\frac{d\lambda_B}{dz}$ is a measure of the rate of change of the design wavelength with position in the grating or simply the rate of the chirp and usually given in units of nanometer / centimeter. Chirp in FBG can be represented by a variation of a periodicity or a variation of mode refractive index along the grating length or a

combination of the two or simply by an additional position dependent phase along the grating.

Birefringence in optical fibers is defined as the difference in refractive index Δn between a pair of orthogonal modes (called the eigenmodes or slow- and fast modes) and results from the presence of circular asymmetries in the fiber section. The refractive index for both the slow- and fast-mode is defined as,

$$n_{eff,s} = n_{eff} + \frac{\Delta n}{2}; \quad n_{eff,f} = n_{eff} - \frac{\Delta n}{2} \quad (7.5)$$

where, n_{eff} is the fiber effective index. In the case of Hi-Bi fibers, the order of magnitude of the birefringence Δn is 3.77×10^{-4} (for a bow tie fiber). To denote the refractive index of both modes from now on we will use notation $n_{eff, f(s)}$

7.3.2 The effect of strain and temperature on LCFBG

The spectra of FBGs are sensitive to both strain and temperature. The spectral behavior of a grating can be controlled by the application of strain and / or temperature gradient. The Bragg wavelength shift of a conventional FBG normally has temperature coefficient of $0.01 \text{ nm}^{\circ} \text{ C}$ [113]. It is therefore necessary to compensate the undesirable temperature sensitivity of a FBG in some applications, such as fiber grating bandpass filters and a chirped FBG as a chromatic dispersion compensator. For using the FBG as a PMD compensator, we determined that temperature compensation is unnecessary. Because the PMD compensation is a dynamic process, the temperature changes could have a minor effect on the range of variable DGD, but its effect on PMD compensation could be negligible

The penetration depth in reflection and the distance traversed in transmission in response to an applied axial strain or temperature changes, because there is a

redistribution of the period as well a change in the refractive index due to photo-elastic or photo-thermal effect. Both of these effects influence the Bragg condition (*i.e.*, $\lambda_B = 2n_{eff,f(s)} \Lambda$). Suppose at constant temperature, under the influence of axial strain (+ve) $\epsilon(z)$, at the grating position z , the FBG will experience a physical elongation of grating period, Λ and a change of refractive index, $n_{eff,f(s)}$ due to the photo-elastic effect. The grating period can be written as,

$$\Lambda(z, \epsilon(z)) = (\Lambda_0 + C_0 z)(1 + \epsilon(z)) \quad (7.6)$$

where, Λ_0 is the grating period at position, $z = 0$ without strain. Constant C_0 denotes the initial chirp of the grating and represented as, $C_0 = \left. \frac{d\Lambda}{dz} \right|_{z=0}$. The

induced change in the fiber index $dn_{eff,f(s)}(z)$ that is due to the photo-elastic

effect is expressed as [113], $\frac{dn_{eff,f(s)}}{n_{eff,f(s)}} = -\rho_e \epsilon(z)$, where we assumed the photo-

elastic contributions into ρ_e , which is defined by

$$\rho_e = \frac{n_{eff,f(s)}}{2} [p_{12} - \mu(p_{11} + p_{12})]$$

in terms of Pockel's coefficients p_{ij} and μ is the Poisson ratio. Together with the Bragg condition the resonance condition can be approximated and becomes dependent on local strain. Thus Bragg wavelength $\lambda_{f(s)}$ at grating position z becomes,

$$\lambda_{f(s)}(z) = 2n_{eff,f(s)} [(\Lambda_0 + C_0 z) + (\Lambda_0 + C_0 z)(1 - \rho_e)\epsilon(z)] \quad (7.7)$$

From (7.7), it is straightforward to observe that the reflection wavelength shift of the grating is proportional to the applied strain. If strain gradient is added to a FBG, the Bragg wavelength varies linearly along the fiber length because of the

change in the effective grating period. The linear relationship between the reflection wavelength and its reflection position determines the group delay characteristics of the grating. Therefore, the expected group delay characteristics of the grating can be obtained by an appropriate design of the strain distribution.

To provide appropriate tuning facility for the required amount of DGD, the grating may be placed in a cantilever structure to induce a linear strain gradient in the grating as shown in Fig.2. The main components of the device consist of a LCFBG and a uniform rectangular beam with length L and thickness h . One end of the beam is free and other end is anchored. A FBG with original length L_g is bonded to the surface of the beam. Deflecting the free end of the beam with displacement Y can induce a strain distribution across the surface of the beam and it can be described by [114],

$$\varepsilon(z) = 3(L - z)hY / (2L^3) \quad (7.8)$$

When a linearly chirped FBG is subjected to axial strain, there is a redistribution of a period as well as a change in the refractive index due to the photo-elastic effect. If the strain field is uniform, the whole chirped bandwidth is simply shifted to the longer wavelength region with increasing strain. The bandwidth of the reflected spectra remain the same, as there is a uniform change of each grating pitch/period and of the refractive index along the grating. This, in accordance with the usual effect of strain/temperature, causes a shift in the Bragg wavelength lie the effective bandwidth remains unaffected. The grating period increases when the displacement of the cantilever beam increases (+ve strain), which results in an increase of the reflection wavelength. Here, we are interested on the spectral properties of the fiber Bragg grating; such as, the group delay and the dispersion of the reflected light. The reflection spectrum and group delay characteristics of Hi-Bi linearly chirped FBGs can be adjusted by applying appropriate strain, $\varepsilon(z)$.

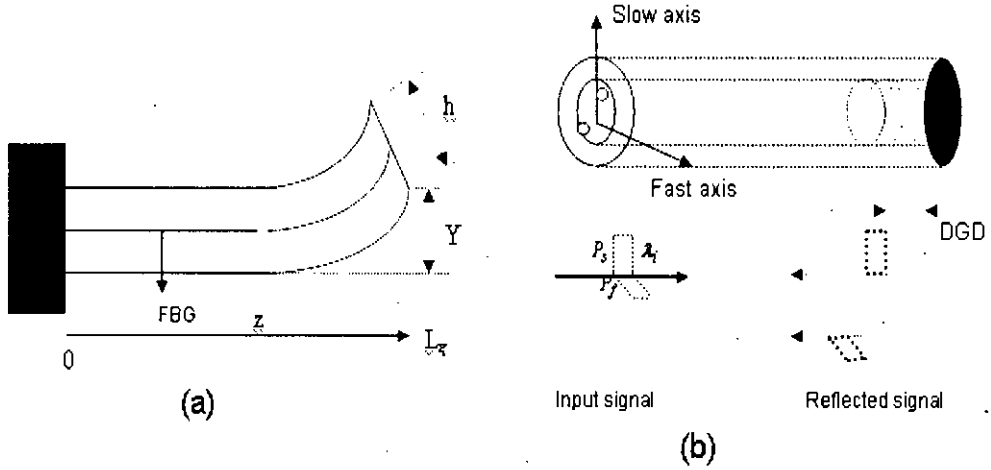


Fig. 7.3: (a) Schematic diagram of the strain gradient cantilever structure, (b) Schematic structure of the Hi-Bi linearly chirped FBG. The reflected signal is introduced as a DGD between the 's' (along the slow axis) and 'f' (along the fast axis) polarization components

7.3.3 Mathematical modeling of the fiber Bragg grating

Coupled-mode theory is a good tool for obtaining quantitative information about the diffraction efficiency and spectral dependence of fiber grating. Generally, Bragg reflection is the interaction between the optical signal and its medium. The optical wave oscillates in space with a period defined by its wavelength and the effective index of the waveguide. This wave interacts with the guiding material by way of the medium's polarization density. Thus, system involving the exchange of energy can be represented by coupled mode equations with appropriate coupling constants. The wave formulation for forward and backward wave amplitudes $F(z)$ and $B(z)$ can be expressed as,

$$\begin{aligned} \frac{dF^+(z)}{dz} &= -i\hat{\sigma}_{f(s)} F^+(z) + i\kappa_{f(s)}^*(z) B^+(z) \\ \frac{dB^+(z)}{dz} &= -i\hat{\sigma}_{f(s)} B^+(z) - i\kappa_{f(s)}^*(z) F^+(z) \end{aligned} \quad (7.9)$$

where, $F^+(z) = F(z) e^{(i\delta z - \varphi/2)}$, $B^+(z) = B(z) e^{(-i\delta z + \varphi/2)}$; $F^+(z)$ (reference) represents the forward propagating mode, $B^+(z)$ (signal) is the identical backward (counter) propagating mode, $\hat{\sigma}_{f(s)}$ and $\kappa_{f(s)}$ are the general dc (period averaged) self-coupling and ac coupling coefficients respectively and can be expressed as,

$$\begin{aligned}\hat{\sigma}_{f(s)} &= \delta_{f(s)} + \sigma_{f(s)} - \frac{1}{2} \frac{d\varphi(z)}{dz} \\ &= \delta_{f(s)} + \frac{2\pi}{\lambda_{f(s)}} \delta n_{eff, f(s)} - \frac{1}{2} \frac{d\phi(z)}{dz}\end{aligned}\quad (7.11)$$

$$\kappa_{f(s)} = \frac{\pi}{\lambda_{f(s)}} \delta n_{eff, f(s)} \nu \quad (7.12)$$

$$\text{again, } \delta_{f(s)} = \beta - \beta_B = 2\pi n_{eff, f(s)} \left(\frac{1}{\lambda_{f(s)}} - \frac{1}{\lambda_B} \right) \quad (7.13)$$

$\delta_{f(s)}$ is the detuning (which is independent of z for all gratings) from the Bragg wavelength λ_B related to period Λ_0 . Here $\delta n_{eff, f(s)}$ is the dc index spatially averaged over a grating period (index modulation of the FBG). The derivative $1/2(d\varphi(z)/dz)$ describes the possible chirp of the grating. For single mode fiber (*i.e.*, where cut off frequency, $V \leq 2.405$) the dc coupling coefficient is denoted by $\sigma_{f(s)}$, ν is the fringe visibility of the index changes (contrast of the interference pattern, or the fraction of energy in the core, $\nu = 1 - V^{-2}$) and the chirp of the grating can be expressed with the grating period function along length z by the following equation,

$$\frac{d\phi(z)}{dz} = -\frac{2\pi z}{\Lambda_0^2} \frac{d\Lambda}{dz} \quad (7.14)$$

7.3.4 Analytical solution of coupled mode equations

The coupled mode equations for the forward and the backward propagating modes, when applied to a uniform period grating, can be solved using

appropriate boundary conditions. Consider Fig.3, where the grating has a length of L_g and the boundary conditions assume a forward propagating mode with $F^+(0)=1$ and that the backward propagating mode, at the end of the grating, will be zero, $B^+(L_g)=0$ as there are no perturbing beyond the end of the grating.

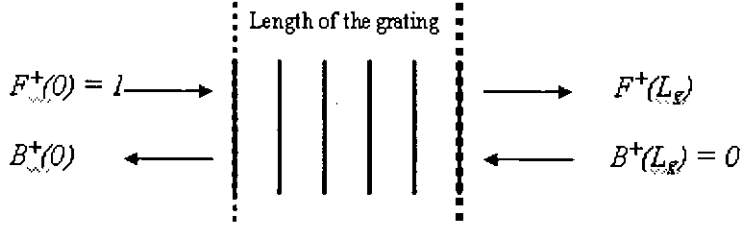


Fig.7.4: schematic of the grating with boundary conditions

For a grating that is uniform along z , $\delta n_{eff, f(s)}$ is constant and $d\phi(z)/dz = 0$. As a result the parameters $\kappa_{f(s)}$, $\sigma_{f(s)}$ and $\hat{\sigma}_{f(s)}$ are all constants. Under these conditions, the coupled mode equations are simplified into first order differential equations with constant coefficients. The solutions to these equations can be found by applying appropriate boundary conditions. Thus we can easily find the analytical solution of the coupled mode equations. The analytical solution of the uniform Bragg grating will be seen to be an important building block in the prediction of the optical response of arbitrary complex intra-grating structure. The solution of the coupled mode equation (7.9) can be best expressed by,

$$\begin{bmatrix} F^+(0) = 1 \\ B^+(0) \end{bmatrix} = [T] \begin{bmatrix} F^+(L_g) \\ B^+(L_g) = 0 \end{bmatrix} \quad (7.15)$$

where T is the transfer matrix and given by,

$$T = \begin{bmatrix} T_{11} & T_{12} \\ T_{21} & T_{22} \end{bmatrix} \quad (7.16)$$

$$\text{where, } T_{11} = \cosh(\gamma L_g) - i \frac{\hat{\sigma}_{f(s)}}{\gamma} \sinh(\gamma L_g) \quad (7.17)$$

$$T_{12} = -i \frac{\kappa_{f(s)}}{\gamma} \sinh(\gamma L_g) \quad (7.18)$$

$$T_{22} = \cosh(\gamma L_g) + i \frac{\hat{\sigma}_{f(s)}}{\gamma} \sinh(\gamma L_g) \quad (7.19)$$

$$T_{21} = i \frac{\kappa_{f(s)}}{\gamma} \sinh(\gamma L_g) \quad (7.20)$$

γ is the parameter relating to coupling coefficient as $\gamma = \sqrt{\kappa_{f(s)}^2 - \hat{\sigma}_{f(s)}^2}$

Reflectivity is the percentage of light reflected at the Bragg wavelength, the wavelength outside of the reflected bandwidth is transmitted without disturbance. For the case of uniform grating, the complex amplitude reflection coefficient at the beginning of the FBG at $z = 0$ is defined as,

$$\rho_{f(s)}(\lambda) = \frac{B^+(\hat{\sigma}_{f(s)})}{F^+(\hat{\sigma}_{f(s)})} = \frac{T_{12}}{T_{11}} \quad (7.21)$$

$$\rho_{f(s)}(\lambda) = -\frac{\kappa_{f(s)} \sinh(\gamma L_g)}{\hat{\sigma}_{f(s)} \sinh(\gamma L_g) + i \gamma \cosh(\gamma L_g)} \quad (7.22)$$

and the reflectivity or the power reflection coefficient, $R_{f(s)}(\lambda)$ is given by,

$$R_{f(s)}(\lambda) = |\rho_{f(s)}(\lambda)|^2 = \frac{\sinh^2(\gamma L_g)}{\cosh^2(\gamma L_g) - \frac{\hat{\sigma}_{f(s)}^2}{\kappa_{f(s)}^2}} \quad (7.23)$$

The reflectivity in equation (7.23) has a decay nature and drops off exponentially along the perturbation region as power is transferred from the forward to the backward propagation mode. The maximum reflectivity R_{max} is then obtained

from the equation when $\hat{\sigma}_{f(s)} = 0$, i.e., at the phase matching condition,

$$\lambda_B = 2n_{eff, f(s)}\Lambda.$$

$$R_{\max} = \tanh^2(\kappa_{f(s)}L_g) \quad (7.24)$$

The full bandwidth over which the maximum reflectivity prevails is

$$\Delta\lambda = \frac{\lambda_B^2}{\pi n_{eff, f(s)}} \left[(\kappa_{f(s)}L_g)^2 + \pi^2 \right]^{\frac{1}{2}} \quad (7.25)$$

The condition for weak grating corresponds to $\kappa_{f(s)}L_g \ll \pi$, in which case the bandwidth is an inverse function of the grating length,

$$\Delta\lambda = \frac{\lambda_B^2}{2n_{eff, f(s)}L_g} \quad (7.26)$$

Thus, for weak grating the bandwidth is length limited, if the converse is true i.e., $\kappa_{f(s)}L_g \gg \pi$; for strong grating the bandwidth becomes,

$$\Delta\lambda = \frac{\lambda_B^2 \kappa_{f(s)}}{2n_{eff, f(s)}} \quad (7.27)$$

and the bandwidth is depended on the ac coupling coefficient.

7.3.5 Relative group delay and DGD of the reflected wavelength

Light reflected from a FBG contains both phase and amplitude information. To determine the magnitude of the penetration depth and path traversed, FBGs have been modeled and the phase response is analyzed. The complex reflectivity, $\rho_{f(s)}(\lambda)$ can be written as,

$$\rho_{f(s)}(\lambda) = \left| \frac{B^+(0)}{F^+(0)} \right| e^{-i\varphi_p} \quad (7.28)$$

where, $B^+(z)$ (signal) is the reflected wave, $F^+(z)$ (reference) is the incident wave, and $\varphi_p(\lambda)$ is the relative phase of the reflected waveform.

The group delay of the reflected light can be determined from the phase of the complex amplitude reflection coefficient $\rho_{f(s)}(\lambda)$. If we denote $\varphi_\rho \equiv \text{phase}(\rho_{f(s)}(\lambda))$, then the local frequency ω_0 may be expanded $\varphi_\rho(\lambda)$ in Taylor series about ω_0 .

$$\varphi_\rho = \varphi_0 + \frac{d\varphi_\rho}{d\omega}(\omega - \omega_0) + \frac{1}{2} \frac{d^2\varphi_\rho}{d\omega^2}(\omega - \omega_0)^2 + \frac{1}{6} \frac{d^3\varphi_\rho}{d\omega^3}(\omega - \omega_0)^3 + \dots \quad (7.29)$$

Since the first derivative $\frac{d\varphi_\rho}{d\omega}$ is directly proportional to the frequency ω , this quantity can be identified as a time delay. Thus, the time delay τ_R for light reflected off of a grating is,

$$\tau_{R, f(s)} = \frac{d\varphi_\rho}{d\omega} = -\frac{\lambda_{f(s)}^2}{2\pi c} \frac{d\varphi_\rho}{d\lambda_{f(s)}} \quad (7.30)$$

$\tau_{R, f(s)}$ is usually given in picoseconds.

where, ω is the angular frequency and c is the velocity of light. Thus an optical wave traveling through a medium of length L and refractive index n will undergo a phase change, $\varphi_\rho = \frac{2\pi n_{\text{eff}, f(s)} L_g}{\lambda}$; The derivative of the phase with respect to wavelength is an indication of the delay experienced by the wavelength component of the reflected light;

$$\frac{d\varphi_\rho}{d\lambda_{f(s)}} = -\frac{2\pi n_{\text{eff}, f(s)} L_g}{\lambda_{f(s)}^2} \quad (7.31)$$

The time delay, $\tau_{R, f(s)}$ equation (7.30) imparted to an incident light is related to the change in phase with wavelength which in turn is related to the distance traveled, equation (7.31). For the reflected light, it is the distance to its resonance position inside the FBG at which the Bragg resonance condition is satisfied. Therefore, each wavelength can be associated with a reflection point along the length of the FBG and a concomitant wavelength dependent penetration depth

into the FBG. The time delay also provides information regarding the optical path traversed for the transmitted wave.

The reflected spectrum is characterized by a main peak at the wavelength defined as, $\lambda_{\max, f(s)} = 2(n_{\text{eff}, f(s)} + \delta n_{\text{eff}, f(s)})\Lambda(z)$. In case of a FBG written in a Hi-Bi fiber, we can define reflection coefficients $\rho_s(\lambda)$ and $\rho_f(\lambda)$ for the slow and fast modes respectively and two wavelengths ($\lambda_{\max, s}$ and $\lambda_{\max, f}$) for the corresponding main peaks. Thus, with a large refractive-index difference Δn between the fast and slow polarization axes; this results in a shift in Bragg wavelength $\Delta\lambda_B = |\lambda_{\max, s} - \lambda_{\max, f}| = 2\Delta n \Lambda_0$ at the same location for two polarizations. In other words, for a fixed signal wavelength the Bragg reflection occurs at different locations for different polarizations. Therefore, the Hi-Bi linearly chirped FBG can be seen as two different chirped FBGs because of the birefringence. The position difference of the reflection produces a DGD:

$$DGD(\lambda) = |\tau_{R, f}(\lambda) - \tau_{R, s}(\lambda)| \quad (7.32)$$

7.4 Results and discussion

7.4.1 Performance of the LCFBG based PMD compensator

Following the analytical formulations, performance of a 2 cm long LCFBG is investigated in terms of relative group delay, DGD, stretching, length etc. to determine the tuning range and maximum amount of PMD that can be compensated. To avoid the power loss due to the leakage of the grating, the reflectivity was greater than 99% within the grating bandwidth is assumed. The different parameters used for the performance analysis of the FBG are listed in Table 7.1.

To examine the bandwidth change with the grating length, FWHM values of the FBG is considered for various lengths and plotted in Fig. 7.5. The FWHM denotes the bandwidth with 50% reflectivity (3-dB bandwidth) of the signals peak. The 3-dB bandwidth showed an exponentially decrease over the elevation of the grating lengths, and when the grating length 95 mm, the 3-dB bandwidth is 1.11 and maintained subsequently for longer lengths. So, it is confirmed that for some defined parameters the LCFBG can attain stability for a fix bandwidth when the grating length is 2 cm.

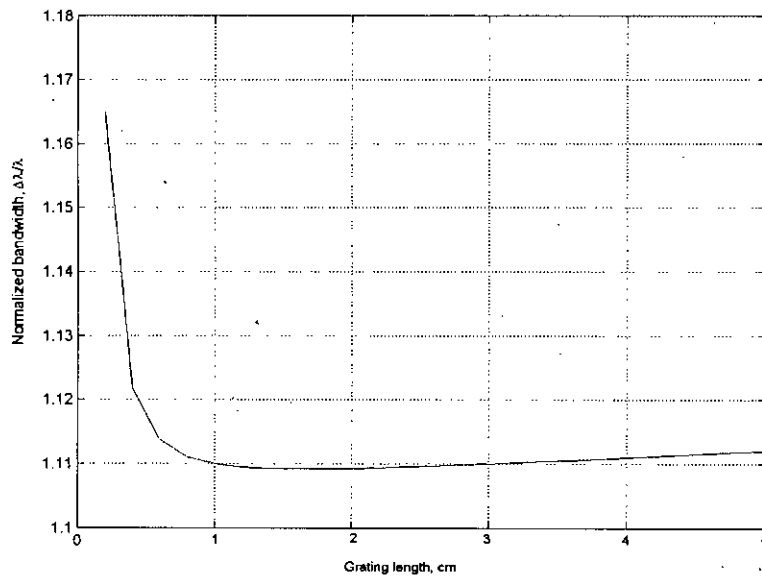


Fig.7.5: The relationship between fiber grating bandwidth and grating length

The reflectivity as well as the bandwidth of FBG changes, if they are under different grating lengths. Fig.7.6 indicates the reflectivity change of the FBG with an increase of grating lengths. As shown in Fig.7.6, the reflectivity increases with the elevation of the grating length. The fiber grating achieves 100% reflection when the grating length is 0.6 cm and maintained this value for the longer length. This tendency is very similar with the results of 3-dB bandwidth change but in an inverse direction where the reflectivity showed an exponential increase over the elevation of the grating signals. So, it is found that

LCFBG showed greater performance as the grating length increased and achieves 100% reflection at the length of 1.4 cm. Fig. 7.6 can be compared with the simulated work of a 20 cm long uniform grating of Ref. [115], where it is reported that the reflectivity increased with the elevation of the grating length in which it achieves 100% in reflection at grating length 10 mm and maintained its value for longer lengths.

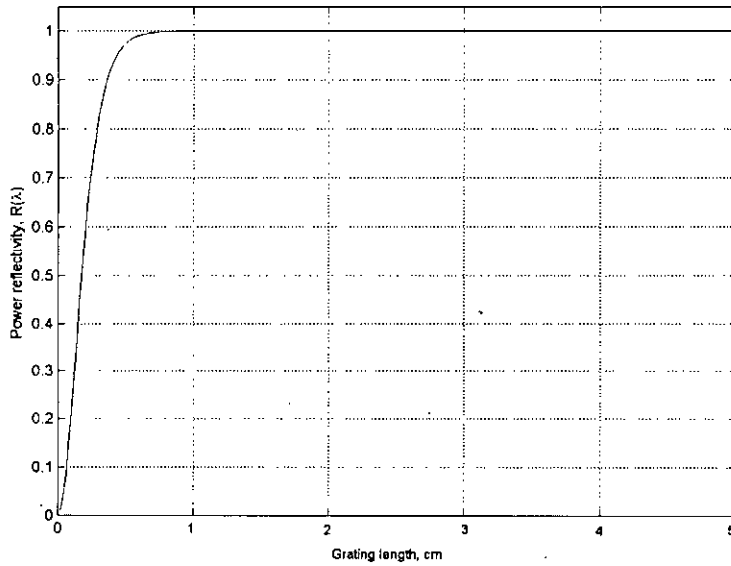


Fig. 7.6: The relationship between fiber grating reflectivity and grating length

Fig. 7.7 shows the relative time delay for the fast- and slow axis polarization reflected signals inputting from the long- and short wavelength ports of the unstressed FBG respectively as a function of wavelength. From the plots, it is seen that the group delay of the grating reveals good linearity and the delay curves for the two polarization axes are shifted by 0.25 nm at wavelength 1550.5 nm relative to each other due to the high birefringence of the fiber. Since the group delay of the grating is shifted to longer or shorter wavelength by stretching or compressing the grating, the DGD between fast- and slow axes are increased or decreased for a given wavelength. The linear variation makes it easy for the

adjustment of the DGD to any given value.

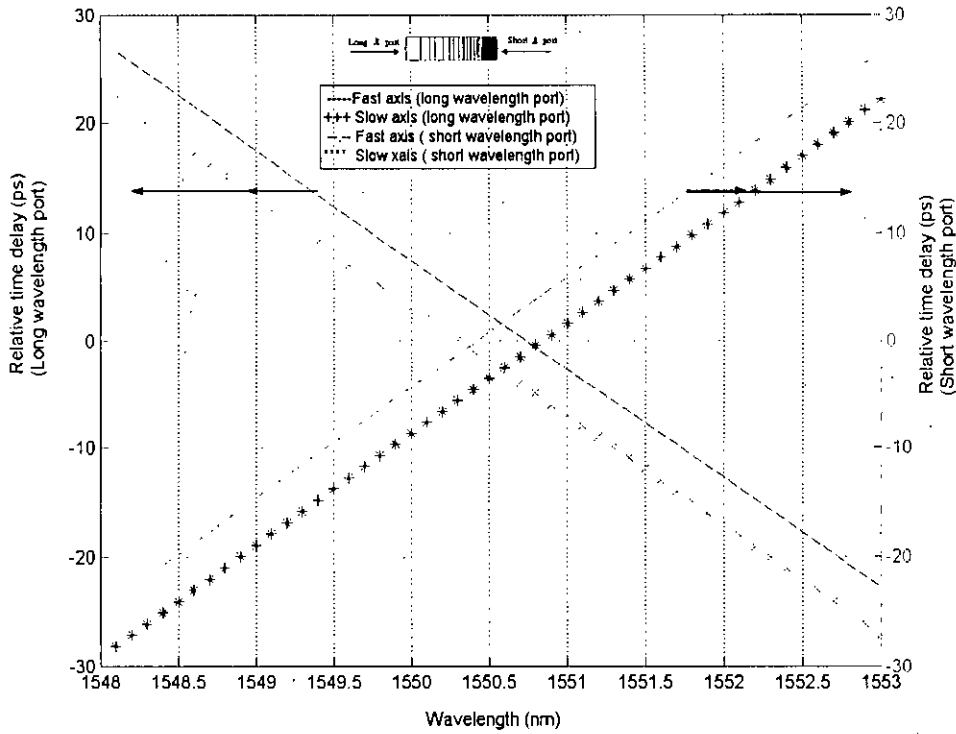


Fig. 7.7: Reflected relative time delay for the fast- and slow axis of polarization

The reflection spectrum of the grating is shown in Fig. 7.8. It is observed that the bandwidth of the grating is 1548.9 nm to 1551.02 nm at unstressed condition. When the grating is stretched, the amplitude and the group delay spectrum shifts to longer wavelength. As we mounted the grating on a cantilever beam tuning structure (Fig. 7.3), it provides about ± 2.4 nm linear tuning capability through stretching and compression. Note that due to tuning, though the passband shifts to shorter or longer wavelength but the polarization of the reflected signal remains same. S. Lee *et.al* [39], experimentally achieved reflection wavelength ranging from 1547.2 nm to 1550.5 nm at unstressed condition and a tuning range of 2.32 nm for a 5 cm long nonlinearly chirped grating. The simulation work in Ref. [37] obtained a bandwidth ranging from 1548.2 nm to 1550.5 nm and 2.1

nm of tuning range using a 1cm LCFBG.

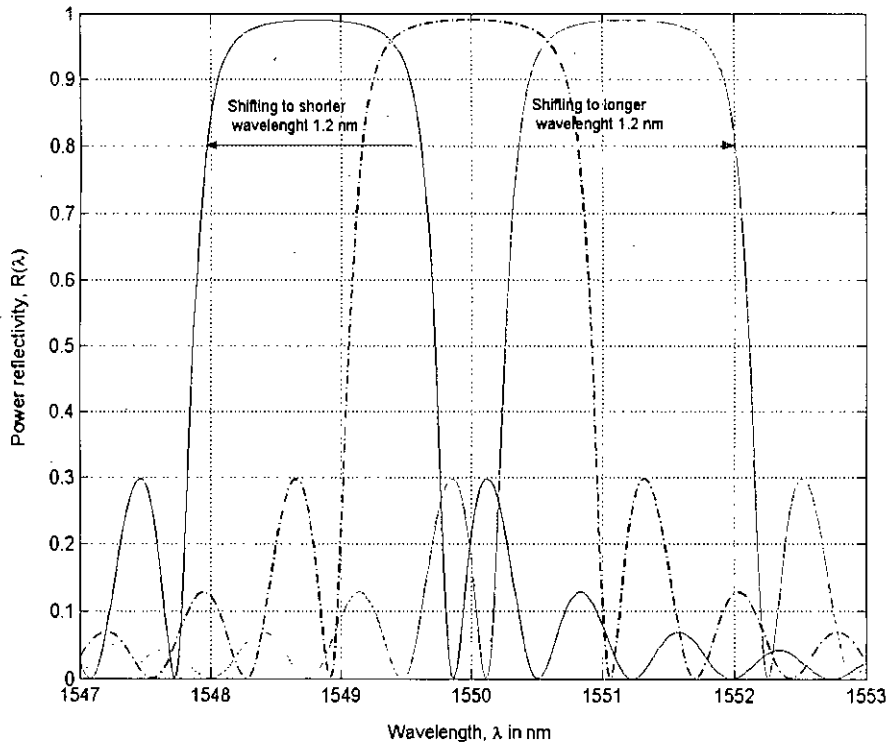


Fig.7.8: Reflection spectrum for the LCFBG under stretching and compression. Wavelength tuning shifts the passband to longer- or shorter wavelength regime without changing the shape of the spectrum

The grating period increases when the displacement of the cantilever beam increases, which results in an increase of the reflected wavelength. The period difference at two points of grating also increases with increase of displacement Y , which ultimately results unchanged reflected passband and the higher tuning range of DGD. The plots of DGD versus wavelengths (from the fast wavelength port) under stretched and compressed condition of the LCFBG are shown Fig. 7.9 It is seen that for a maximum vertical displacement of the free end of the cantilever structure is 6 mm assumed which corresponds to a maximum value of the strain is $3800 \mu\epsilon$ [114] and the PMD compensator has a adjustable range from -55 ps to 55 ps.

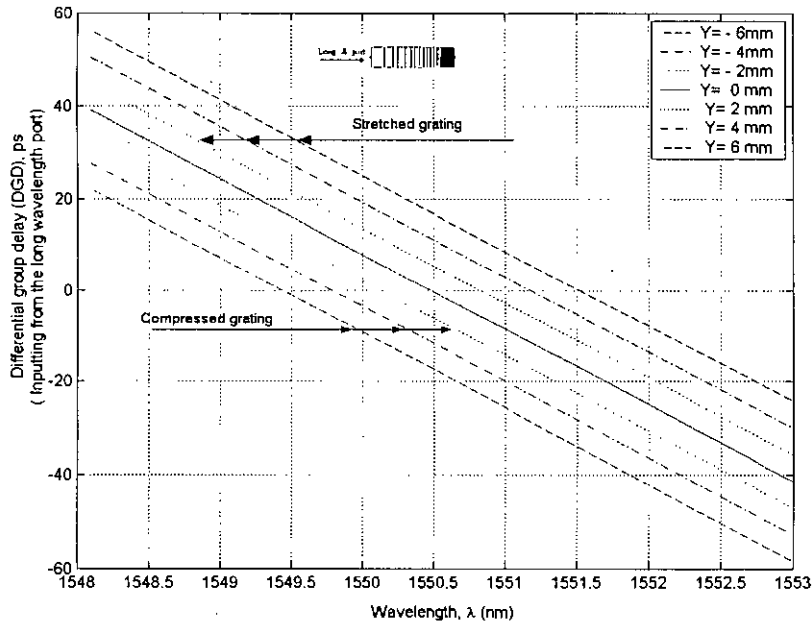


Fig. 7.9: Plots of DGD versus wavelength under stretched- and compressed condition of the LCFBG inputting from the fast wavelength port.

Fig. 7.10 shows the change in the differential time delay (ps) as a function of the grating stretching ratio. By changing the strain ϵ from 0% to 0.2% the DGD can be continuously adjusted from 3 ps to 58 ps. As mentioned earlier, all light outside the reflection bandwidth λ_0 can be directed to the output port without adding any PMD. For this system we have a residual DGD of 3 ps. It is also observed that a maximum DGD is varied over a 55 ps range by a 0.2 % stretch of the grating at 1552.2 nm. Ref. [117] experimentally demonstrates a variable polarization delay line exhibits an adjustable amount of PMD within its operating bandwidth that the DGD can be continuously adjusted from 0 to 80 ps (from 1330.4 nm to 1531 nm wavelength range) under mechanical strain applied by a piezo driven translator.

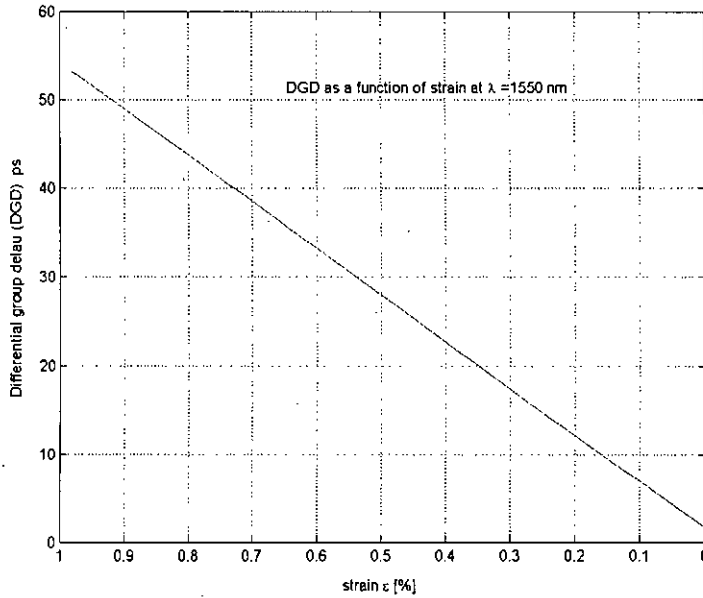


Fig.7.10: Variation of the DGD between two polarizations as the LCFBG stretched (the stretching ratio is the change in the length of the fiber grating divide by its original length ($\epsilon = \Delta L/L$)).

The relation between the DGD of the Hi-Bi linearly chirped FBG and the wavelength tuning of the grating (due to the displacement Y of the cantilever beam) is illustrated in Fig. 7.11. Here, it is noted that the maximum tolerated strain of the FBG is assumed at $3800 \mu\epsilon$; corresponds to a Bragg wavelength shift of approximately 2.8 nm at 1550.5 nm. From Fig.7.11, it can be seen that when the grating is tuned 1.4 nm to the longer or shorter wavelength, the DGD between the two polarizations states continuously increases or decreases by approximately 60 ps respectively. Thus, 1 nm wavelength tuning gives approximately 42.85 ps change in DGD.

Fig. 7.12 depicts the grating length dependence of the DGD within the reflection bandwidth of the length of the grating. When the first axis polarization signal at input wavelength λ_i enters the Hi-Bi LCFBG from the longer wavelength port,

it is reflected and experiences a time delay t_1 ; whereas, the slow axis polarization signal is reflected and has a time delay t_2 ; when enters from the shorter wavelength port. The time delay difference, $\Delta t = t_1 - t_2$, is the DGD between the two axes of polarizations. This is a good agreement with the relative group delay curve of the LCFBG shown in Fig. 7.7. It is observed that about 135 ps DGD can be compensated with a 5 cm long grating.

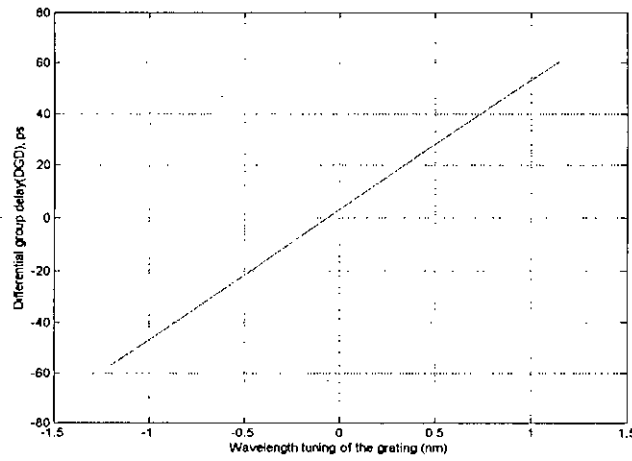


Fig. 7.11: DGD as a function of wavelength tuning (as a result of the displacement Y) at a given signal wavelength $\lambda_B = 1550.5$ nm

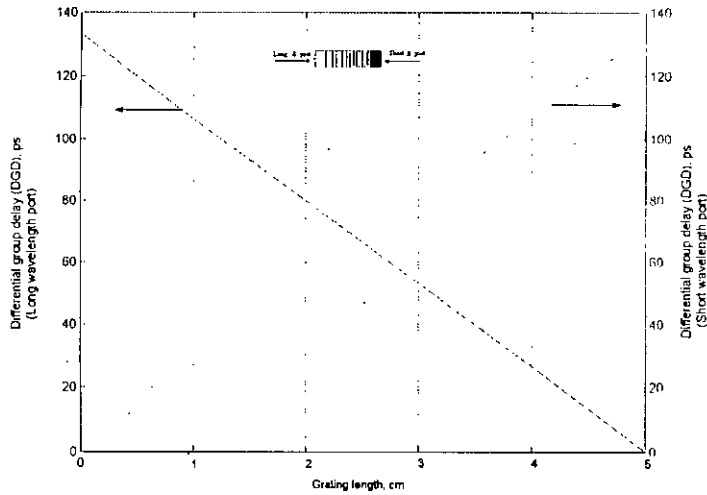


Fig. 7.12: DGD as function of grating length for short- and long wavelength ports

Parameters	Settings
Index modulation, δn	2.15×10^{-4}
Birefringence, Δn	3.77×10^{-4}
Core index, n_{eff}	1.46
Central wavelength, λ_H	1550.5 nm
Grating length, L_g	2.00 cm
Pockel's coefficient, ρ_e	0.22
Initial grating period, Λ_0	530 nm
Initial grating chirp, C_0	1×10^{-8}
Maximum ac index, $\nu \delta n_{eff}$	2×10^{-4}
Cantilever beam length, L	2.20 cm
Beam thickness, h	15 mm

Table 7.1: Set of LCFBG parameters

7.4.2 LCFBG based PMD compensator in a WDM/IM-DD system

To demonstrate the capability of this device, we carried simulation with Rsoft OptSim simulation software. Fig.7.13 shows a 4-channel WDM/IM-DD transmission system model and the placement of the PMD compensator along the transmission path. Fig. 7.14 shows the typical module of the compensation scheme. It shows the power penalty (at the input and output) for different DGD values when the input power is evenly divided between the two PSPs. The power penalty for small (such as 10 ps) DGD is usually negligible or within the power margin of the system and therefore be tolerated. It is the high values that cause significant degradation when signal power splits almost equally between the two PSPs.

The simulation diagram for a 4-channel PMD compensation using Hi-Bi linearly chirped fiber Bragg grating (LCFGBG) is shown in Fig. 7.15. Here, we use two span of 200 km fiber where fiber loss is totally compensated by EDFA. The different parameters used in the simulation are shown in Table 7.2. Here, we

used a 2-cm long customized LCFBG as a compensation element after 400 km of fiber length. In the simulation environment, we have not applied any strain the LCFBG. Without strain, the compensation device can compensate about 25 ps of DGD.

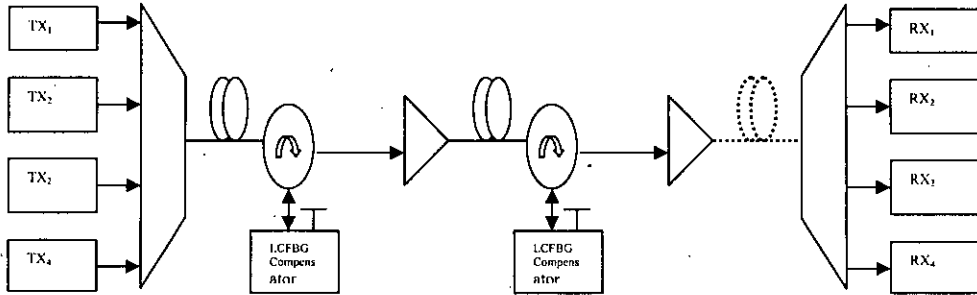


Fig.7.13: Hi-Bi LCFBG based 4-channel PMD compensation fiber-optic WDM transmission system model

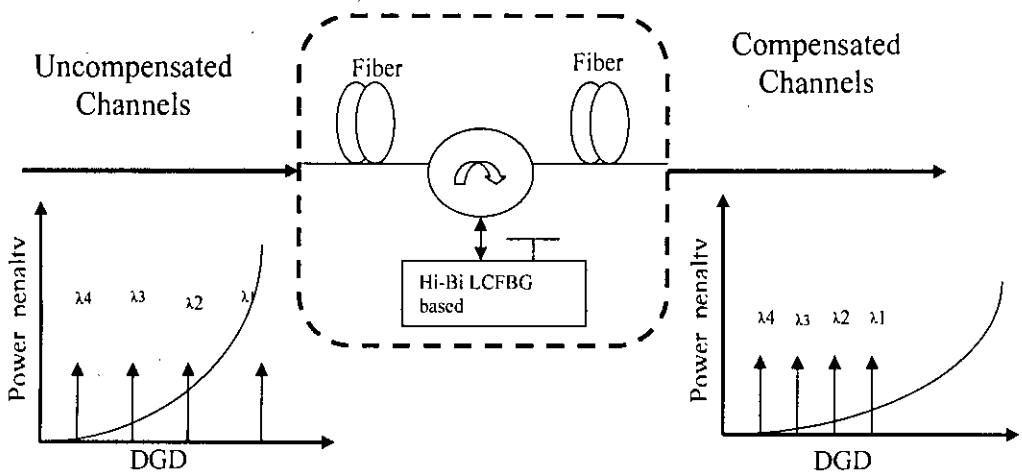


Fig.: 7.14 Hi-Bi LCFBG based WDM-PMD compensation module

Here, we investigate the impact of PMD on the WDM/IM-DD optical transmission in terms eye diagram. At the receiving end we demultiplexed all the 4-channel and monitor their eye diagram without and with applying the PMD compensation scheme. A typical measurement of the eye diagram of the accumulated DGD for 4-channels before and after compensation is shown in Fig. 7.16. At 10 Gbit/s data rate each channel produces (200 km span) about 28 ps of DGD and our designed LCFBG compensator can compensate only 25 ps DGD

without any external strain. We observe that channel 4 has been improved significantly after compensation without impacting the other channels and about 6 ps DGD of each channel remain uncompensated which is also within tolerance level or power margin of the system.

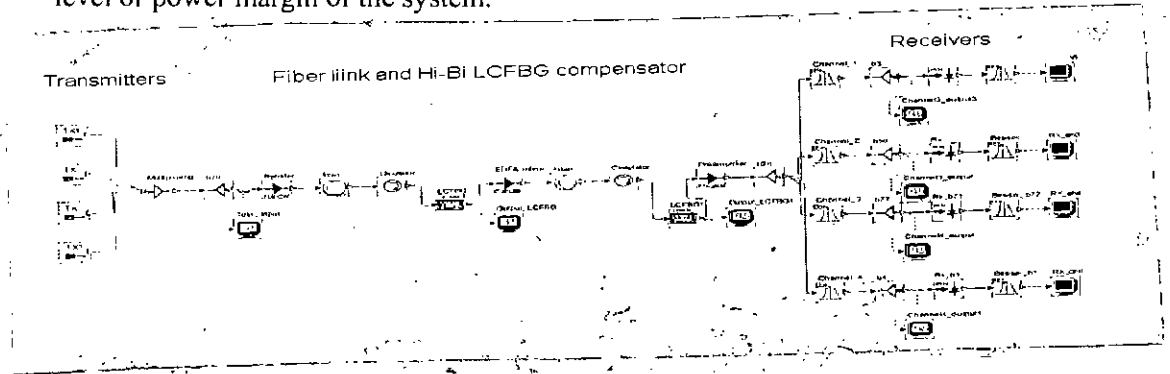


Fig. 7.15: Simulation diagram of a 4-channel WDM-PMD compensation scheme

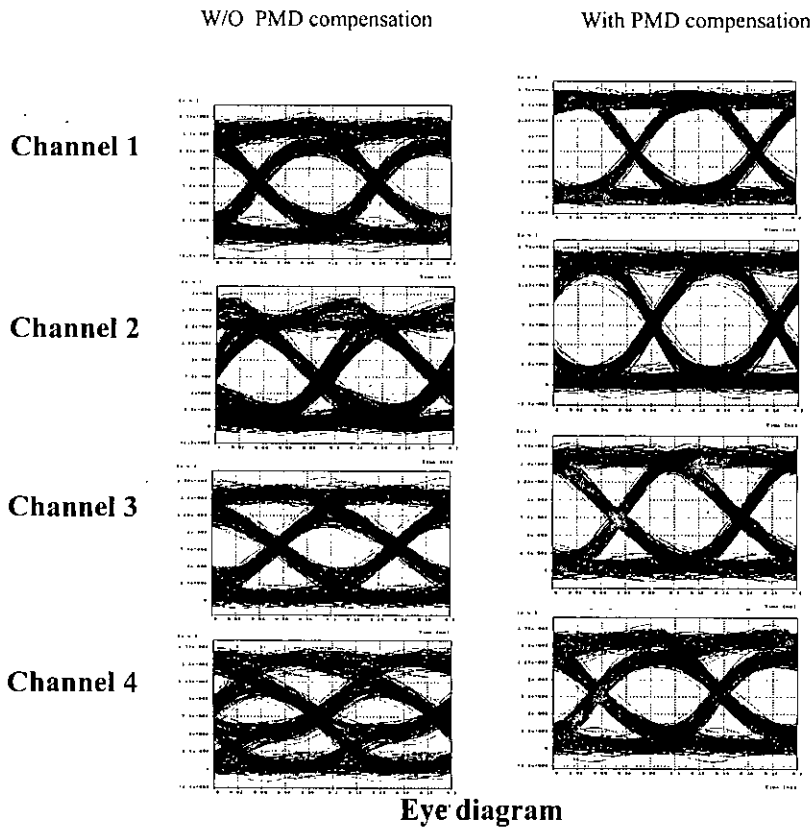


Fig.:7.16 Eye diagram for a 4-channel (each channel at 10 Gbps, NRZ modulation) with and without WDM-PMD compensation. The output signal is received after 400 km transmission

Finally we calculate the average eye-opening penalty (EOP) due to PMD for 4-channel. Here, we define the parameter of the eye-opening penalty (EOP) as,

$$EOP = -20 \log\left(\frac{B}{B_0}\right) \quad (7.33)$$

where, B is the eye opening without PMD effect and B₀ is the eye-opening with PMD.

Fig. 7.17 shows a comparison of EOP penalty between our 4-channel simulated transmission system and with single channel LCFBG based compensation system as a function of DGD. From the curve we found that about 2.5 dB of EOP reduction is obtained at 40 ps by the compensation scheme. The performance of the single channel is 0.55 dB better for values of fiber DGD > 40 ps and this happens due to channel crosstalk in 4-channel WDM system.

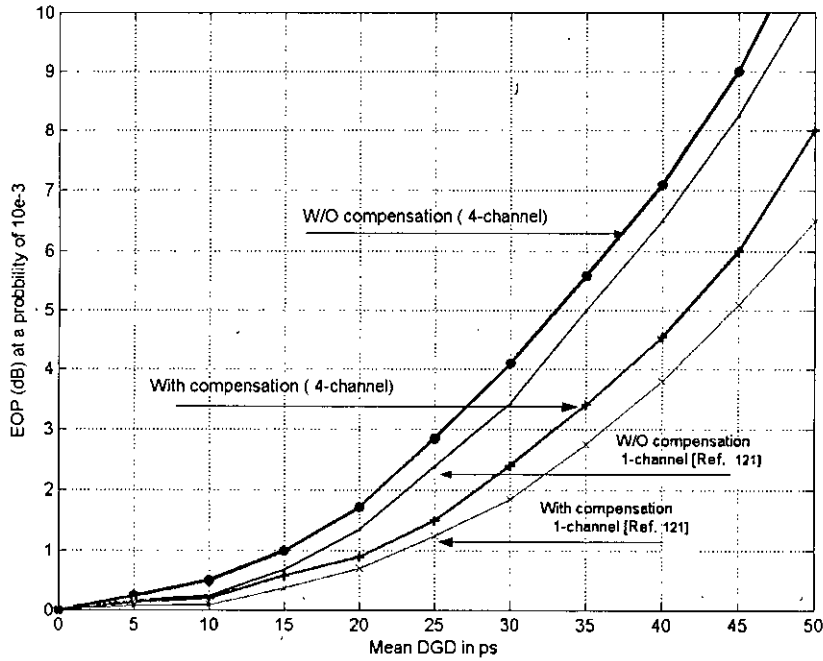


Fig.: 7.17: Eye opening penalty (EOP) at a probability of 10⁻³ in the dependence of the mean DGD for 4-channel and single transmission system.

Sl no.	Parameters/description	values
1	Fiber loss (dB/km)	0.25
2	Dispersion (ps/km-nm)	0
3	Effective core are (μm^2)	80
4	Fiber length (km, 2-span of 200 km)	400
5	PMD co-efficient (ps/ $\sqrt{\text{km}}$)	2
6	Birefringence of the Hi-Bi LCFBG	3.77×10^{-4}
7	Bit rate of each channel (Gb/s)	10
8	No. of channels	4
9	Compensation bandwidth without strain (nm)	2
10	Channel spacing (nm)	0.4
11	Working wavelength range (nm)	1549 nm -1551 nm
12	Receiver sensitivity (at 10^{-9})	-24
13	Transmitter power (dBm) for each channel	-10
14	Booster EDFA output (dBm)	9

Table 7.2: Simulation parameters of Hi-Bi LCFBG based PMD-WDM compensation scheme

7.5 Summary

The performance analysis of a novel PMD compensation scheme using a 2-cm long LCFBG is carried out, which can be tuned mechanically to provide linearly continuous DGD. By deflecting one free end of the beam, we obtained a linear strain gradient on the grating. The various properties of reflectivity, relative group delay and DGD of the Hi-Bi LCFBG have been discussed in detail. With an optimal design of the grating and cantilever beam parameters, this PMD compensation method is well suited for WDM applications over a significant range of operating wavelength, where a number of channels can be compensated together. Larger amount PMD can be compensated by concatenating several of these devices in cascade.

We found that the performance of our simulated compensation scheme achieved a significant improvement in quality of eye pattern of the received signal for a link length of 400 km at a bit rate of 10 Gb/s and it compensates about 50 ps of DGD per channel. It is also observed that the amount eye power penalty for a single channel is about 0.55 dB less than that of 4-channel WDM system (at 40 ps of DGD) and that happens due to absence of channel crosstalk in a single channel system. Thus proposed PMD compensator can be potentially useful; because it is inexpensive to simple structure, low cost and flexibility to adjust compensated DGD.

Chapter 8

CONCLUSIONS AND FUTURE WORK

Since the advent of optical communications, a great technological effort has been devoted to the exploitation of the huge bandwidth of optical fibers. Starting from a few Mb/s single channel systems, a fast technological development yielded the present 10 Gbit/s per channel dense WDM systems. Such a pace in technological progress must be supported or better preceded, by an analogous evolution of the theory. Our mission in this research work to analyze the optical system from strict communication theory point of view to understanding the effects of PMD and its compensation on the performance of optical fiber communication systems using different types of modulation scheme. For this purpose, we have studied the following in detail:

- IM-DD, DD- and heterodyne CPFSK transmission system modeling and analysis.
- Determination of pdf of the random output phases of DD- and heterodyne CPFSK system and random SOPs of the pump-probe angle.
- Performance evaluation in terms of conditional and average BER

considering Maxwellian distribution for the DGD in single- and multi-channel system.

- Passive PMD compensation using optical linecodes in single channel and all optical LCFBG based in multi-channel respectively.
- Comparing the obtained analytical results with other recently reported available simulation and/or experimental works.

8.1 Summary of major contributions

The main motivation of this work was to obtain and compare analytical models to characterize the effects of PMD and its compensation on fiber optic communication system. Fiber PMD has been found to be one of the limiting factors for optical fiber communication systems as channel capacity requirement continues to grow beyond 10 Gbit/s. Therefore, understanding of fiber PMD is crucial to optimize system performance of optical fiber transmission links. Accurate models are needed to describe the propagation and performance evaluation of the transmitted signal through a transmission media like optical fiber. In this respect analytical models are very helpful for a deeper comprehension and overall view of the system can be used to drastically reduce computation time. Keeping this in mind, several analytical models have been presented to give better physical insight of the effect of fiber PMD and its compensation on optical transmission system. The major results obtained from each approach are summarized as follows:

1. An analytical model is developed to evaluate the effect of PMD for IM-DD transmission system. Based on the model analytical formulations are established from which the conditional and average BER expression is derived considering the effects of ISI up to fourth approximation interference among the adjacent bits due to PMD. Based on instantaneous DGD (for conditional BER), the amount of power penalty is about 7.75

dB for a DGD of 160 ps. It is shown that BER floors occur at about 2×10^{-9} , 10^{-7} and 10^{-5} corresponding to mean DGD of 45 ps, 50 ps and 60 ps respectively at 10 Gbit/s. The power penalty due to PMD is significant at higher mean DGD; for example, at 20 ps DGD the penalty is 0.27 and at 60 ps it is about 5.25 dB. It is observed that analytical and simulation results the same power penalty up to 35 ps DGD and above it the simulation gives little bit better result than that of analytical approach.

2. A low pass equivalent direct detection CPFSK system model is developed considering PMD, chromatic dispersion and the signal components in the output PSPs propagate independently through the entire system. Due the presence of PMD the output phase of the balanced detector is random; pdf of this phase is determined by evaluating the moments of the characteristic function of the signal. Performance of the system is evaluated in terms of conditional BER, average BER considering with- and without Maxwellian distribution for the mean DGD. It is shown that with modulation index $h=0.5$ suffers less penalty than that of $h=1.0$ and at mean DGD of 40 ps the amount of penalty is 1.75 dB. A direct detection CPFSK system with $h=1$ suffers almost same amount of power penalty as NRZ IM-DD system (which is 5.15 dB at 60 ps). Results are also compared with other analytical work. It is found that power penalty of IM-DD DPSK is lower than DD CPFSK system due to the high spectral efficiency (*i.e.*, >0.4) of DPSK. But in terms of implementation complexity and cost DD CPFSK is superior to DPSK system.
3. As the coherent optical transmission using heterodyne or homodyne detection are attractive due to their improved receiver sensitivity compared with direct detection, we assessed the BER performance limitations of an optical heterodyne CPFSK with delay-demodulation

receiver. The characteristic function of the random output phase is analytically derived and using the characteristic function we calculate the pdf of the output phase. It is shown that BER floors occur at about 2×10^{-8} , 10^{-5} and 2.5×10^{-4} corresponding to mean DGD of 60 ps, 70 ps and 80 ps respectively at 10 Gb/s and modulation index of 0.50. The CPFSK heterodyne transmission system is more sensitive to the effect of PMD than DD CPFSK system. For example, the amount of penalty is approximately 6.80 dB when the mean DGD is 40 ps at modulation index of $h=1.0$ (in DD CPFSK, it is 1.75 dB). Again the penalty due to PMD is significant at higher modulation index and higher values of DGD. For instance, at $h=0.5$ and mean DGD of 40 ps the amount of penalty is 3.50, which is 6.80 dB for the same value of DGD.

4. A detailed theoretical analysis is presented for three linecodes to determine their ability to mitigate the effect PMD. Three optical line codes (*i.e.* AMI, DM and order 1) are used to increase the PMD tolerance in optical transmission. It is shown that for lower values of PMD the compensation effect of linecoding is more pronounced than higher values of DGD. As a result, the power penalty improvements above 30 ps mean DGD is almost constant for all linecodes and the amounts are about 0.30 dB, 0.80 dB and 1.65 dB corresponding to DM, AMI and order-1 respectively for a heterodyne CPFSK system. Among the three linecodes order-1 linecoding is superior to AMI and DM. It is found that order-1 is the best, AMI is better than DM. For example, at 30 ps mean DGD, order-1 effects is 0.80 dB and 1.40 dB higher than AMI and DM respectively.
5. At high bit rates the effect from both PMD and fiber nonlinearity are pronounced due to high power and large signal bandwidth used. To assess the effect on system performance, the interaction of PMD and

XPM; first a two channel WDM system model (pump-probe configuration) is developed is analyzed and secondly a model for multi-channel is developed and analyzed in detail. Nonlinear effect XPM causes amplitude modulation to the co-propagating channel and due to PMD this fluctuation becomes random. The pdf of the random SOP angle between pump and probe is determined and BER performance is evaluated. Results show that the XPM induced crosstalk becomes polarization independent when channel spacing is large ($\Delta \lambda = 6$ nm and above) or when the fiber has a relatively large value of PMD coefficient ($D_p = 4$ ps/ $\sqrt{\text{km}}$ or above). Simulation is carried out using the OptSim software for a 4-channel WDM system to study the performance limitation due to the combined effect of XPM and PMD. The results are presented in terms of eye diagram, BER, Q-value and PMD coefficient. It is shown that the EOP (at a probability of 10^{-3}) at PMD coefficient 1.5 ps/ $\sqrt{\text{km}}$ is about 1.85 dB more than that of 0.5 ps/ $\sqrt{\text{km}}$. A comparison is also established between the pump-probe configuration and 4-channel WDM system. It is found that for a fixed amount of pump power (-2 dBm) and channel spacing (1 nm) the effect of XPM and PMD is about 2.5 times more in 4-channel system to achieve the same BER of 10^{-9} .

6. Finally, a Hi-Bi LCFBG based analytical approach is developed to compensate PMD in optical domain. Theoretical analysis is carried out to derive the different parameter of interest; such as reflectivity, DGD, relative group delay in the short- and long wavelength port, of the grating. We focus on the robustness of system performance and PMD compensation optimization with respect to different device parameters. It is found that a 2 cm long LCFBG allows the DGD to be adjusted from 0 ps to 55 ps by stretching it by 0.2%. The analytically developed Hi-Bi LCFBG device is used in a WDM transmission; where multiple

wavelengths could be compensated simultaneously. Using OptSim, simulation is carried out at normal situation (at unstretched condition) in a 4-channel WDM system of 400 km length of fiber link (consists of 2 span of 200 km) in terms of eye diagram. Results are compared with single channel system and found that about 2.5 dB of EOP reduction is obtained at 40 ps. It is also observed that the performance of the single channel is 0.55 dB better for values of fiber DGD > 40 ps and this happens due to channel crosstalk in 4-channel WDM system. The proposed PMD compensator can be potentially useful; because it is inexpensive to simple structure, low cost and flexibility to adjust compensated DGD.

It is worth recalling that each of the above mentioned developed analytical model for studying the impact and compensation of PMD has its own valid range of parameters or valid systems.

8.2 Suggestions for future research

Approximations have been used throughout the works in this thesis to simplify the problems. We have neglected the influence of higher order PMD introduced by the fiber and the influence of this factor should be incorporated in a more through analysis.

We also assumed zero polarization dependent loss (PDL). PDL refers to energy loss that is preferential to one polarization state. In the Jones picture, one axis suffers more loss than the other. The combination of PDL and PMD creates effects which are quite complicated and which can impair a communication system more than either effect alone. PDL is generally wavelength independent while PMD is generally wavelength dependent. Therefore, it should be a great interest to see how analytical models developed in this thesis can be modified in the presence of PDL.

In the multi-channel PMD analysis, we confined ourselves with the interaction of PMD and XPM only. In our developed model, other nonlinear effects like SPM, FWM etc., could be incorporated to analyze the performance degradation due to PMD and the other nonlinear crosstalk.

For occurrences of high instantaneous DGD, signal quality may be intolerable and results a PMD-induced outage. Such outages may significantly affect network availability for higher bit rates (*i.e.* 10 Gb/s, 40 Gb/s and higher). One can estimate the probability that the system no longer functions properly; the outage probability, which must be very low, typically $10^{-6} - 10^{-5}$, corresponding to a few seconds to a few minutes per year. The maximum link DGD that a receiver can tolerate before the signal degradation become unacceptable depends on a variety of factors; including modulation format, optical SNR and receiver design. So, in the design of robust long-haul fiber-optic network, the system outage probability due to PMD could be done as further extension of this thesis work.

The PMD compensation capability of the FBG based device is mainly determined by the characteristics of the Hi-Bi LCFBG and improved capability could be achieved by adopting higher chirp ratio phase mask to fabricate the Hi-Bi grating. However, this performance improvement would be limited by the induced distortion due to the existence of CD at the fast- and slow axis of the compensator. The CD induced pulse broadening would decrease the receiver sensitivity due to the increase in the ISI and the reduction in the SNR. This unwanted CD effect of the Hi-Bi LCFBG based compensator may be included in the analysis to reflect its actual performance.

Further research can be initiated to develop analytical model for probability of bit error/packet error rate in an IP over WDM network and optical burst

switching networks considering the influence of above mentioned system impairments. Still, a lot of room is available for the researchers in the area of fiber optics. The impact of PMD and other nonlinear effects like stimulate Raman scattering and stimulated Brillouin scattering may be considered in a WDM system.

BIBLIOGRAPHY

- [1] K. C. Kao and G. A. Hockham, "Dielectric fiber surface waveguides for optical frequencies," *Proceedings of IEE*, vol. 133, pp. 1151-1158, July 1966.

- [2] C. D. Poole and R. E. Wagner, "Phenomenological approach to polarization mode dispersion in long single mode fibers", *Electronics Lett.*, vol.22, no. 19, pp.1029-1030, September 11, 1986.

- [3] C. D. Poole, R. W. Tkach, A. R. Chraplyvy and D. A. Fishman, "Fading in lightwave systems due to polarization mode dispersion", *IEEE Photon. Technol. Lett.*, vol.3, no. 1, pp.68-70, January 1991

- [4] C. D. Poole and R. C. Giles, "Polarization-dependent pulse compression and broadening due to polarization dispersion in dispersion shifted fiber", *Optics Lett.*, vol.13, no. 2, pp. 155-157, February 1988.

- [5] F. Curti, B. Daino, Q. Mao and F. Matera, "Concatenation of polarization dispersion in single-mode fibers", *Electronics Lett.*, vol. 25, no. 4, pp.290-292, February 1989.

- [6] N. Gisin and J. P. Pellaux, "Polarization mode dispersion: time versus frequency domains", *Optics Communications*, vol. 89, pp. 316-323, May 1992.

- [7] C. D. Poole and J. Nagel, "Polarization effects in lightwave systems", Chapter 6, *Optical Fiber Telecommunication*, volume III A, Edited by I. P. Kaminow and T. L. Koch, Academic Press, San Diego, CA, 1997.

- [8] H. Kogelnik, R. M. Jopson and L. E. Nelson, "Polarization-mode dispersion", Chapter 15, *Optical Fiber Telecommunications*, volume IV B, Edited by I. P. Kaminow and T. Li, Academic Press, San Diego, CA 2002.

- [9] A. F. Elrefie and R. E. Wagner, "Chromatic dispersion limitations in coherent optical fiber transmission systems", *Electron. Lett.*, vol. 23, no. 14, pp. 756-758, July 1987.

- [10] G. J. Foschini and C. D. Poole, "Statistical theory of polarization dispersion in single mode fibers", *IEEE J. of Lightwave Technol.*, vol.9, no. 11, pp. 1439-1456, November 1991.

- [11] F. Curti, B. Daino, G. De Marchis and F. Matera, " Statistical treatment of the evolution of the principal states of polarization in single-mode fiber", *J. of Lightwave Technol.*, vol. 8, no. 8 pp. 1162-1165, August 1990.

- [12] C. De Angelis, A. Galtarosa, G. Gianello, F. Matera and M. Schiano, "Time evolution of polarization mode dispersion in long terrestrial links", *J. of Lightwave Technol.*, vol. 10, no. 5, pp.552-555, May 1995.
- [13] N. Gisin, R. Passy, J. C. Bishoff and B. Perney, "Experimental investigation of the statistical properties of polarization mode dispersion in single mode fibers", *IEEE Photon. Technol. Lett.*, vol. 5, no. 7 pp. 819-821, July 1993.
- [14] T. Tahashi, T. Imai and M. Aiki, "Time evolution of polarization mode dispersion in 120 km installed optical submarine cable", *Electronics Lett.*, vol. 29, no. 18, pp. 1605-1606, September 1993.
- [15] J. P. Gordon, and H. Kogelnik, "PMD fundamentals: polarization mode dispersion in optical fibers," *Proceedings of the National Academy of Sciences*, vol. 97, no. 9, pp. 4541-4550, 2000.
- [16] S. J. Savory and F. P. Payne, "Pulse propagation in fibers with polarization mode dispersion," *J. of Lightwave Technol.*, vol. 20, no.12, pp. 350-359, 2001.
- [17] M. Puzio, Z. Zhu, R. S. Blum, P.A. Andrekson and T. Li, "Channel coding for polarization-mode dispersion limited optical fiber transmission" *Optic Express*, vol.12, no.18, pp. 4333-4338, 2004.
- [18] J. S. Garcia, A. G. Gonzalez and M. L. Iribas, "Polarization mode dispersion power penalty: influence of rise/fall time, receiver Q and amplifier noise", *IEEE Photon. Technol. Lett.*, vol.8, no.12, pp.1719-1721, 1996.

Bibliography

- [19] A. E. Willner, S. M. R. M. Nizam, L. Yan, Z. Pan, Z. and M. C. Hauer, "Monitoring and control of polarization-related impairments in optical fiber systems", *J. of Lightwave Technol.*, vol. 22, no.1, pp. 106-125, 2004.
- [20] B. Liu, "Simulation of optical fiber communication system with polarization mode dispersion", *M. Sc. Engineering thesis*, University of New Brunswick, Canada, 2000.
- [21] B. Christos, E. Marc and B. Keith, "Polarization mode dispersion correlations with the coarse-step method", *Optics Communications*, vol.26, no.2, pp. 135-139, 2006.
- [22] I. T. Lima, A. O. Lima, Y. Sun, J. Zweck, B. S. Marks, G. M. Carter and C. R. Menyuk, "Computation of the outage probability due to the polarization effects using importance sampling," *Optical Fiber Communication Conference and Exhibit, 2002, OFC 2002*, pp.56 – 57, 2002.
- [23] X. Liu, C. Xie and A. J. Van Wijngaarden, "Multichannel PMD mitigation and outage reduction through FEC with sub-burst-error-correction period PMD scrambling", *IEEE Photon. Technol. Lett.*, vol.16, no.9, pp. 2183-2185, 2004.
- [24] H. Bulow, "PMD mitigation Techniques and their effectiveness in installed fiber", (*in paper ThH1*), *Proc. Optical Fiber Conference*, 3, Baltimore, MD, pp. 110-112, 2000.
- [25] H. Sunnerud, M. Karlsson, C. Xie, and P. A. Andrekson, "Polarization mode dispersion in high speed fiber-optic transmission system," *J. of Lightwave Technol.*, vol.20, no.12, pp.2204-2219, 2002.

- [26] J. Wang and J. M. Kahn, "Impact of chromatic and polarization mode dispersion on DPSK system using interferometric demodulation and direct detection," *J. of Lightwave Technol.*, vol. 15, no.12, pp. 1779-1781, 2003.
- [27] C. Xie, L. Moller, H. Hauntein and S. Hunsche, "Comparison of System tolerance to polarization mode dispersion between different modulation format," *IEEE Photon. Technol. Lett.*, vol.15, no. 8, pp. 1168-1170, 2003.
- [28] N. Kikuchi, "Analysis of signal degree of polarization degradation used as control signal for optical polarization mode dispersion compensation," *J. of Lightwave Technol.*, vol.19, no.4, pp.480-486, 2001.
- [29] R. Noe, D. Sandel and V. Mirvoda, "PMD in high-bit-rate transmission and means for its mitigation," *IEEE J. of Selected Topic Quantum Electronics*, vol.10, no.2, pp. 341-355, 2004.
- [30] H. F. Haunstein, W. S. Greff, A. Dittrich, K. Sticht and R. Urbansky, "Principles of electronic equalization of polarization mode dispersion," *J. of Lightwave Technol.*, vol.22, no.4, pp.1169-1181, 2004.
- [31] C. Xie and L. Moller, "Evaluation and mitigation of polarization mode dispersion impairments in high speed transmission system," *APOC 2006, Proc. of SPIE*, 6353 (2006), South Korea, pp. 635310-1- 635310-8., 2006.
- [32] H. Sunnerud, J. Li, P. A. Andrekson and C. Xie, "Experimental quantification of soliton robustness to polarization-mode dispersion in dispersion managed systems," *IEEE Photon. Technol. Lett.*, vol.13, no.2, pp.118-120, 2000.

- [33] A.O. Lima, I. T. Lima, Jr. T. Adali and C. R. Menyuk, "A novel polarization diversity receiver for PMD mitigation," *IEEE Photon. Technol. Lett.*, vol.14, no.3, pp.465-467, 2002.
- [34] M. Rao, L. Li, Y. Tang, M. Zhang. And X. Sun, "Novel C-IPDM signal format for suppression of polarization mode dispersion." *Photonic Network Communications*, vol. 7, no.1, p. 97-104, 2004.
- [35] W. Kaiser, W. Otte, T. Wuth and W. Rosenkranz, "Experimental verification of reduced sensitivity of optical duobinary to higher order PMD," *OFC 2003*, Anaheim, CA, Tu15, pp. 53-55., 2003.
- [36] S. Kim, "Analytical calculation of pulse broadening in optical higher order PMD compensation", *J. of Lightwave Technol.*, vol. 20 no. 7, pp. 1118-1123, July 2002.
- [37] Z. Pan, Y. Xie, S. Lee, A. E Willner, "Tunable compensation for polarization-mode dispersion using a birefringent nonlinearly-chirped Bragg grating in a dual-pass configuration," *U. S. Patent* 6,400,869 B2, 2002.
- [38] X. Yi, C. Lu, X. Yang, W. -De Zhong, F. Wei and Y. wang, "High-birefringence linearly chirped grating based optical device for PMD compensation ," *Optics Express*, vol. 11, no. 20, pp. 2634-2640 ,2003.
- [39] S. Lee, R. Khoeravani, J. Peng, A. E. Wilner, V. Grubsky, D. S. Starodubov, J. Feinberg, "High-birefringence nonlinearly-chirped fiber Bragg grating for tunable compensation of polarization mode dispersion", *TuS3, OFC*, San Diego, 1999.

- [40] K. Iwashita. and T. Matsumoto, "Modulation and Detection characteristics of optical continuous-phase frequency shift keying transmission system," *J. of Lightwave Technol.*, vol.5, no. 2, pp.452-460, 1998.
- [41] G. P. Agrawal, "Fiber-Optic Communication Systems", 3rd Edition, *Wiley*, New York, 2002.
- [42] M. Cvijetic, "Coherent and Nonlinear Lightwave Communications", *Artech House*, Boston, USA 1996.
- [43] C. D. Poole and Nagel, "Polarization effects in lightwave systems," Chapter 15: *Optical Fiber Telecommunications IIIA*, I. P. Kaminow and T. L. Koch. Eds San Diego, CA: Academic press, 1997.
- [44] E. Iannone, F. Matera, A. Galtarossa, "Effect of polarization dispersion on the performance of IM-DD communication systems", *IEEE Photon. Technol. Lett.*, vol. 5 , no. 10, pp. 1247-1249, 1993.
- [45] A.O. Lima, I.T. Lima, Jr., C.R. Menyuk, T. Adali, "Comparison of penalties resulting from first-order and all-order polarization mode dispersion distortions in optical fiber transmission systems", *Optics Lett.*, vol.28, no. 5, pp. 310-312 , 2003.
- [46] K. Iwashita and T. Matsumoto, "Modulation and detection characteristics of optical continuous-phase FSK transmission system", *J. of Lightwave Technol.*, vol. LT-5, pp. 452-460, April 1987.

- [47] N. S. Bergano, C. D. Poole, and R.E. Wagner, "Investigation of polarization dispersion in long lengths of single-mode fiber using multilongitudinal mode lasers," *J. of Lightwave Technol.*, vol. LT-5, pp. 1618-1622, Nov. 1987.
- [48] R.E. Wagner and A.F. Elrefaie, "Polarization dispersion limitations in lightwave systems," *Tech. Dig. OFC'88*, p37, New Orleans, LA, 1988.
- [49] A. F. Elrefaie and R. E. Wagner, "Chromatic dispersion limitations for FSK and DPSK systems with direct detection receivers", *IEEE Photon. Technol. Lett.*, vol. 8, no. 1, January 1991.
- [50] E. Iannone, F. Matera, A. Galtarossa, G. Gianello and M. Schiano, "Effect of polarization dispersion on the performance of IM-DD communication system", *IEEE photon. Technol. Lett.*, vol. 5, no. 10, pp.1247-1249, Oct. 1993.
- [51] F. Bruyere and O. Audouin, "Assessment of system penalties in a 5 Gb/s optically amplified transoceanic link", *IEEE Photon. Technol. Lett.*, vol. 6, no. 3, pp.443-445, March 1994.
- [52] C. D. Angelis, A. Galtarossa, C. Campanile and F. Matera, "Performance evaluation of ASK and DPSK optical coherent systems affected by chromatic dispersion and polarization mode dispersion", *J. of optical comm.*, vol.16, no. 5, pp.173-178, 1995.

- [53] H. Bulow, "Operation of digital optical transmission system with minimal degradation due to polarization mode dispersion." *Electronics Lett.*, vol. 3, no.3 , pp. 214-215, 1995.
- [54] B.W. Hakki, "Polarization mode dispersion in a single mode fiber," *J. of Lightwave Technol.*, vol. 14, no. 10, pp. 2202-2208, 1996.
- [55] F. Bruyere, "Impact of first and second order PMD in optical digital transmission systems," *Optical Fiber Technol.*, vol. 2, no. 3, pp. 269-280, July 1996.
- [56] M. Karlsson, " Polarization mode dispersion-induced pulse broadening in optical fibers," *Optics Lett.*, vol. 23, no. 9, pp. 688-690, May 1998.
- [57] S. P. Majumder, M. Z. Yusoff, A. F. Muhammad and H.T. Chuah, " Effect of polarization mode dispersion on optical heterodyne CPFSK system", *Proc. of GLOBECOM'00*, vol.2, pp. 1233-1236, 2000.
- [58] F. Buchali and H. Bülow, "Adaptive PMD Compensation by Electrical and Optical Techniques", *J. of Lightwave Technol.*, vol.22, no. 4, pp. 1116-1126 , 2004.
- [59] C. Antonelli, A. Mecozzi, "Pulse broadening due to polarization mode dispersion with first-order compensation", *Optics Lett.*, vol. 30. no. 13, pp. 1626-1628, 2005.
- [60] H. Yoon, N.Y. Kim, N. Park, "Study on the PMD Impairment of Optical Multilevel DPSK Systems and its Mitigation Methods" *IEEE Photon. Technol. Lett.*, vol. 17, no. 12, pp. 2577-2579, 2005.

- [61] S.P Majumder et al, "Performance of linecoded optical heterodyne FSK systems with nonuniform laser FM response", *J. of Lightwave Technol.*, vol 13, No. 4, pp. 628-638, April 1995.
- [62] V.K Prabhu, "Some considerations of error bounds in digital systems", *Bell Syst. Tech., J.*, vol 50, pp. 3127-3150, 1971.
- [63] R. Noe, H. Heidrich and D. Hoffman, "Endless polarization control systems for coherent optics", *J. of Lightwave Technol.*, vol. 6, no. 7, pp. 1199-1208, 1988.
- [64] T. Okoshi, "Polarization state control schemes for heterodyne or homodyne optical fiber communications", *J. of Lightwave Technol.*, vol. 3 no.6, pp.1232-1237, 1985.
- [65] N. G. Walker and G. R. Walker, "Polarization control for coherent communications", *J. of Lightwave Technol.*, vol.8, no. 3, pp.438-458, 1990.
- [66] J. H. Winters and R. D. Gitlin, "Electrical signal processing techniques in long-hual fiber-optic systems", *IEEE Trans. of Commun.* , vol.38, no.9, pp.1439-1453, 1990.
- [67] H. Kim, C. R. Doerr, R. Pafchek, L.W. Stulz and P. Bernasoconi, "Polarization mode dispersion impairments in direct detection differential phase shift keying systems", *Electron Lett.*, vol. 38, no.18, pp.1047-1048, 2002.

- [68] Z. Pan, Y. Wang, Y. Song, R. Motaghian, S. Havstad and A. E. Willner, "Monitoring chromatic dispersion and PMD impairments in optical differential phase shift-keyed (DPSK) systems," *Proc. of optical fiber commun. Conf.*, Optical Society of America, Washington, DC, Paper WP1, 2003.
- [69] B. Fu and R. Hu, "Fiber Chromatic dispersion and polarization mode dispersion monitoring using coherent detection", *IEEE photon. Technol. Lett.*, vol.17, pp. 1561-1563, 2005.
- [70] S. P. Majumder, R. Gangopadhaya, E. Forestieri and G. Prati, "Sensitivity penalty for AMI coded CPFSK in heterodyne delay demodulation receiver," *IEEE Photon. Technol. Lett.*, vol. 7, no.10, pp.1207-1209, 1995.
- [71] H. F. Haunstein, W. Sauer-Greff, A. Dittrich, K. Stich and R. Urbansky, "Principles for Electronic equalization of polarization-mode dispersion", *J. of Lightwave Technol.*, vol. 22, pp. 1169-1182, 2004.
- [72] D. A. Nolan, X. Chen and M. -J. Li, "Fibers with low polarization mode dispersion", *J. of Lightwave Technol.*, vol. 22, pp. 1066-1077, 2004.
- [73] A. Galtarossa, L. Palmieri and A. Pizziant, "Optimized spinning design for low PMD fibers: An analytical approach", *J. of Lightwave Technol.*, vol. 19, pp.1502-1512, pp. 2001.

- [74] P. C. Chou, J. M. Fini and H. A. Haus, "Demonstration of feed-forward PMD compensation technique", *IEEE Photon. Technol. Lett.*, vol. 14, no. 2, pp. 161-163, 2002.
- [75] W. Kaiser, W. Otte, T. Wuth and W. Rosenkranz, "Experimental verification of reduced sensitivity of optical duobinary modulation to higher order PMD", *OFC 2002*, Anaheim, CA, Tu15, pp. 53-54, 2002.
- [76] E. Forestieri and G. Prati, "Novel optical line codes tolerant to fiber chromatic dispersion", *J. of Lightwave Technol.*, vol. 19, no. 11, pp.1675-1684, November 2001.
- [77] J. Rasmussen, "Automatic PMD compensation at 43 Gb/s utilizing an accurate DOP monitor," in *Tech. Dig. ECOC 2002*, 11.1.4, 2002.
- [78] M. Shtaif, M. Mecozzi, M. Tur and J. Nagel, "A compensator for the effects of high-order polarization mode dispersion in optical fiber", *IEEE Photon. Technol. Lett.*, vol.12, pp. 434-436, 2000.
- [79] T. Kudou, M. Iguchi, M. Masuda and T. Ozeki, "Theoretical basis of polarization mode dispersion equalization up to the second order", *J. of Lightwave Technol.*, vol. 18, no. 4, pp. 614-617, April 2000.
- [80] H. Bülow and G. Thielecke, "Electronic PMD mitigation- from linear equalization to maximum-likelihood detection", *Proc. OFC'2001*, Los Angeles, CA, paper WAA3, 2001.

- [81] S. Sarkimukka, A. Djupsjobacka, A. Gavler and G. Jacobsen, "Mitigation of polarization mode dispersion in optical multichannel systems", *J. of Lightwave Technol.*, vol. 18, no.10, pp.1374-1380, October 2000.
- [82] R. Khosravani and A. E. Wilner, "Comparison of different modulation formats in terrestrial systems with high polarization mode dispersion", *Proc. OFC 2000*, Baltimore, paper WL5, pp. 201-203, 2000.
- [83] M. S. Islam and S. P. Majumder, "Performance limitations of an optical heterodyne continuous phase frequency shift keying transmission system affected by polarization mode dispersion in a single mode fiber", *Optical Engineering*, SPIE, vol. 46, no. 6, pp. 065008-1 – 065008-6, June 2007.
- [84] G. P. Agrawal, "*Nonlinear Fiber Optics*", San Diego, CA, Academic Press, 2001.
- [85] S. Betti and M. Giaconi, "Effect of cross phase modulation on WDM optical systems: analysis of fiber propagation", *IEEE Photon. Technol. Lett.*, vol. 13, pp. 305-307, April 2001.
- [86] R. Hui, K. R. Demarest and C. T. Allen, "Cross-phase modulation in multispan WDM optical fiber systems", *J. of Lightwave Technol*, vol. 17, no. 6 pp. 1018-1026, June 1999.
- [87] G. Goeger, M. Wrange and W. Fischler, "Cross-phase modulation in multi-span WDM systems with arbitrary modulation formats, " *IEEE photon. Technol. Lett.*, vol. 16, no. 8, pp. 18058-1060, August 2004.

- [88] P. I. Killey, H. J. Thiele, V. Mikhailove and P. Bayvel, "Prediction of transmission penalties due to cross-phase modulation in WDM systems using simplified Technique", *IEEE Photon. Technol. Lett.*, vol. 12, no. 7, pp. 804-806, July 2007.
- [89] M. Shtaif, M. Eiselt and L. D. Garrett, "Measurement of cross-phase modulation distortion in multispan WDM systems", *IEEE Photon. Technol. Lett.*, vol.12, pp. 88-90, January 2000.
- [90] G. Bellotti, A. Bertaina and S. Bigo, "Dependence of self-phase modulation impairments on residual dispersion in 10 Gb/s based terrestrial transmission using standard fiber", *IEEE Photon. Technol. Lett.*, vol. 11, pp. 824-826, 1999.
- [91] D. van den Borne, N. E. Hecker-Denschlag, G. D. Khol and H. de Waardt, "Cross-phase modulation induced depolarization penalties in 2x10 Gbit/s polarization-multiplexed transmission", *Proc. ECOC 2004*, 1, Mo4.5.5, 5-9 September 2004, pp. 191-194, ECOC Stockholm, Sweden 2004.
- [92] Q. Lin and G. P. Agrawal, "Effects of polarization mode dispersion on cross-phase modulation in dispersion managed wavelength-division-multiplexed systems", *J. of Lightwave Technol.*, vol. 22, no. 4, pp. 977-987, April 2004.
- [93] N. Hanik "Influence of polarization mode dispersion on the effect of cross-talk modulation in optical WDM transmission", *Proc. of the 6th International Conference on Transparent Optical Networks*, vol. 1, pp. 190-194, July 2004.

- [94] G. Zhang, J. T. Stango, X. Zhang and C. Xie, "Impact of fiber nonlinearity on PMD penalty in DWDM transmission systems", *IEEE Photon. Technol. Lett.*, vol. 17, no. 2, pp. 501-503, February 2005.
- [95] C. R. Menyuk and B. S. Mark, "Interaction of polarization mode dispersion and nonlinearity in optical fiber transmission systems", *J. of Lightwave Technol.*, vol. 24, no. 7, pp. 2806-2826, July 2006.
- [96] P. K. A Wai and C. R. Menyuk, "Polarization mode dispersion, decorrelation and diffusion in optical fibers with randomly varying birefringence," *J. of Lightwave Techno.*, vol. 14, pp. 148-157, 1996.
- [97] E. Ibragimov, C. R. Menyuk and W. L. Kath, "PMD-induced reduction of nonlinear penalties in terrestrial optical fiber transmission", *Proc. OFC, 2000*, pp. 195-197, Paper WL3, 2000.
- [98] L. Moller, Y. Su, G. Raybon, S. Chandrasekar and L. L. Buhl, "Penalty interference of nonlinear intra-channel effect and PMD in ultra-high speed TDM systems", *Electron Lett.*, vol. 38, no. 6, pp. 281-283, March 2002.
- [99] B. S. Marks and C. R. Menyuk, "Polarization mode dispersion enhancement of nonlinear propagation", *Proc. ECOC'03*, Rimini, Italy, 2003, Paper Mo3.7.1, 2003.
- [100] R. Khosravani, Y. Xie, L. -S. Yan, A. E. Willner and C. R. Menyuk, "Bit pattern dependent polarization rotation in the first-order PMD-compensated WDM systems", *Optics Comms.*, pp. 191-196, July 2005..

Bibliography

- [101] Z. Pan, Q. Yu and A. E. Willner, "Fast XPM-induced polarization-state fluctuation in WDM systems and their mitigation", *Proc. OFC, 2002*, pp. 379-381, Paper ThA7, 2002.
- [102] Q. Lin and G. P. Agrawal, "Vector Theory of cross-phase modulation: role of nonlinear polarization rotation", *J. of Lightwave Technol.*, vol. 40, no. 7, pp. 958-964, July 2004.
- [103] A. Bononi, A. Vanocci, A. Orlandini, E. Corbel, S. Lanne and S. Bigo, "Degree of polarization degradation due to cross-phase modulation and its impact on polarization mode dispersion", *J. of Lightwave Technol.*, vol. 21, no. 9, pp. 1903-1913, 2003.
- [104] S. Song, "The impact of polarization-mode dispersion on four-wave wave mixing in WDM systems", *Proc. of OFC 2001*, Page(s): ThA7-1 - ThA7-3 vol.4, 2001.
- [105] B. C. Collings and L. Boivin, "Nonlinear Polarization evolution induced by cross-phase modulation and its impact on transmission system", *IEEE Photon. Technol. Lett.*, vol. 12, no. 11, November 2000.
- [106] J. H. Lee, K. J. Park, C. H. Kim and Y. C. Chung, "Impact of nonlinear crosstalk on optical PMD compensation", *IEEE Photon. Technol. Lett.*, vol. 14, no. 8, pp. 1082-1084, August 2002.
- [107] S. Pachnicke, J. Reichert, E. Voges, "Impact of polarization mode dispersion and fiber nonlinearities on four-wave mixing efficiency", *Proc. of 11th OptoElectronics and Communication Conference (OECC) 2006*, Kaohsiung, Taiwan, July 2006.

- [108] R. Kashyap, "Fiber Bragg Grating, Chapter 7: *Chirped fiber Bragg gratings*", Academic Press, San Diego, USA (1999)
- [109] "Fiber Bragg gratings," USA: Furukawa Electric North America, *Lightwave Inc.*, 2005.
- [110] M. Schiano and G. Zaffiro, "Polarization mode dispersion in chirped fiber gratings", in *proc. ECOC (1998)*, pp. 403-404, 1998.
- [111] M. Wang, T. Li and S. Jian, "Tunable PMD compensator based on high-birefringence linearly chirped FBG with cantilever beam", *Optics Express*, vol. 11, no. 19, pp.2354-2362, 2003.
- [112] X. Kun, F. Jia, X. Chen, Mao Jin, M. Chen, X. Li and S. Xie, "A novel adjustable PMD compensation using sampled Bragg gratings with uniform grating period," *Optics Commun.*, vol. 202, no. 4-6, pp. 297-302, 2002.
- [113] A. D. Kersey, M. A. Devis, H. J. Patrick, M. Le Blanc, K. P. Koo, C. G. Askins, M. A. Putnam and E.J. Friebele, "Fiber Grating Sensors," *J. of Lightwave Technol.*, vol.15, pp. 1442-1461, 1997.
- [114] D. Roylance, "*Mechanics of Materials*", Wiley & sons, New York, 1996.
- [115] W. Du, X. Tao and H. Tam, "Fiber Bragg grating cavity sensor for simultaneous measurement of strain and temperature", *IEEE Photon. Technol. Lett.*, vol. 11, pp. 105-107, 1999.

- [116] H. S. Phing, J. Ali, R. A. Rhaman and B. A. Tahir, "Fiber Bragg grating modeling, simulation and characteristics with different grating length," *J. of Fundamental Sc.*, UTM, Malaysia, July 2007.
- [117] H. Rosenfeldt, Ch. Knothe, E. Brinkmeyer, "Component for Optical PMD-Compensation in a WDM Environment," *Proc. Europ. Conf. on Opt. Comm. (ECOC)*, Munich, Germany, vol. I (3.4.1), pp. 135-136, 2000.
- [118] L. N. Binh and D. Perera, "Multi-level line coding for ultra-high speed long haul optical fiber communication systems", *Department of Electrical and Computer Systems Engineering*, Monash University, Clayton Victoria 3168 Australia, 2006.
- [119] Ivan B. Djordjevic, "PMD compensation in fiber-optic communication systems with direct detection using LDPC-coded OFDM", vol. 15, no. 7, *OPTICS EXPRESS*, pp. 3692-3701. 2007.
- [120] M. Rao, L. Li, Y. Tang, M. Zhang and X. Sun, "Novel C-IPDM signal format for suppression of polarization mode dispersion", *Photonics Networks Communications*, vol. 7, no. 1, pp. 97-104, 2004.
- [121] M. Wang, T. Li and S. Jian, "Tunable PMD compensator based on high-birefringence linearly chirped FBG with cantilever beam", *Optics Express*, vol. 11, no. 19, pp. 2354-2363, 2003.
- [122] B. W. Hakki, "Polarization mode dispersion by phase diversity detection", *IEEE Photon. Technol. Lett.*, vol. 9, pp. 121-123, 1997.

Bibliography

- [123] F. Heismann, D. A. Fishman and D. L. Wilson, "Automatic compensation of first-order polarization mode dispersion in a 10 Gb/s transmission system", in *Proc. ECOC'98*, pp.529-530, 1998.
- [124] L. Yan, X. S. Yao, M. C. Hauer, A. E. Willner, "Practical solutions to polarization-mode-dispersion emulation and compensation

APPENDIX A

Derivation of output optical signal, $g_1(t)$

The filtered output signal of the 1st pair of MZI is given by,

$$g_1(t) = \text{Re}[p(t) \otimes h_1(t)] \quad (\text{A-1})$$

$$H_{pmd1}(f) = \exp[-j2\pi f(-\frac{\Delta\tau}{2})] \quad (\text{A-2})$$

$$\begin{aligned} h_{pmd1}(t) &= \int_{-\infty}^{\infty} H_{pmd1}(f) \exp(j2\pi ft) df \\ &= \int_{-\infty}^{\infty} \exp[-j2\pi f(-\frac{\Delta\tau}{2})] \exp(j2\pi ft) df \end{aligned} \quad (\text{A-3a})$$

$$= \delta(t - \frac{\Delta\tau}{2}) \quad (\text{A-3b})$$

Fiber transfer function due to chromatic dispersion,

$$H_{cd}(f) = \exp[-j\gamma(\pi T)^2] \quad (\text{A-4})$$

where, $\gamma = \frac{\lambda^2}{\pi c} DR_b L$ = Chromatic dispersion index

$$h_{cd}(t) = \int_{-\infty}^{\infty} H_{cd}(f) \exp(j2\pi ft) df \quad (\text{A-5a})$$

$$= \frac{1}{T\sqrt{\pi\gamma}} \exp[-j\{\frac{1}{\gamma}\left(\frac{t}{T}\right)^2 - \frac{\pi}{4} \text{sgn } \gamma\}] \quad (\text{A-5b})$$

$$H_1(f) = H_{pmd1}(f) H_{cd}(f) \quad (\text{A-6})$$

$$h_1(t) = h_{pmd1}(t) \otimes h_{cd}(t) \quad (\text{A-7a})$$

$$= \delta(t - \frac{\Delta\tau}{2}) \otimes \frac{1}{T\sqrt{\pi\gamma}} \exp[-j\{\frac{1}{\gamma}\left(\frac{t}{T}\right)^2 - \frac{\pi}{4}\}] \quad (\text{A-7b})$$

$$= \int_{-\infty}^{\infty} \delta(t - \frac{\Delta\tau}{2} - \tau) \frac{1}{T\sqrt{\pi\gamma}} \exp[-j\{\frac{1}{\gamma}\left(\frac{\tau}{T}\right)^2 - \frac{\pi}{4}\}] d\tau \quad (\text{A-7c})$$

$$h_1(t) = \frac{1}{T\sqrt{\pi}} \exp\left[-j\left\{\frac{1}{\gamma} \left(\frac{t - \frac{\Delta\tau}{2}}{T}\right)^2 - \frac{\pi}{4} \operatorname{sgn} \gamma\right\}\right] \quad (\text{A-7d})$$

Again, we can write the output pulse $g_1(t)$ can be written as the convolution of the input pulse $p(t)$. Now,

$$g_1(t) = \operatorname{Re}[p(t) \otimes h_1(t)] \quad (\text{A-8a})$$

$$= \int_{-\infty}^{\infty} p(\tau) h_1(t - \tau) d\tau \quad (\text{A-8b})$$

$$h_1(t) = \frac{1}{T\sqrt{\pi}} \exp\left[-j\left\{\frac{1}{\gamma} \left(\frac{t - \frac{\Delta\tau}{2}}{T}\right)^2 - \frac{\pi}{4} \operatorname{sgn} \gamma\right\}\right] \quad (\text{A-9})$$

$$\text{Now, } g_1(t) = \operatorname{Re}[p(t) \otimes h_1(t)] \quad (\text{A-10a})$$

$$= \int_{-\infty}^{\infty} p(\tau) h_1(t - \tau) d\tau$$

$$= \int_{-\infty}^{\infty} p(\tau) \frac{1}{T\sqrt{\pi}} \exp\left[-j\left\{\frac{1}{\gamma} \left(\frac{t - \frac{\Delta\tau}{2} - \tau}{T}\right)^2 - \frac{\pi}{4} \operatorname{sgn} \gamma\right\}\right] d\tau \quad (\text{A-10b})$$

Let

$$\tau = \gamma \pi f T^2$$

$$d\tau = \gamma \pi T^2 df$$

$$g_1(t) = \frac{1}{T\sqrt{\pi\gamma}} \int_{-\infty}^{\infty} p(\pi\gamma T^2) \exp\left[-j\left\{\frac{1}{\gamma} \left(\frac{t - \frac{\Delta\tau}{2} - \gamma\pi f T^2}{T}\right)^2 - \frac{\pi}{4} \operatorname{sgn} \gamma\right\}\right] \gamma\pi T^2 df \quad (\text{A-11a})$$

$$g_1(t) = T\sqrt{\gamma\pi} \exp\left[-j\left\{\frac{1}{\gamma}\left(\frac{t-\Delta\tau/2}{T}\right)^2 - \frac{\pi}{4} \operatorname{sgn} \gamma\right\}\right] \quad (\text{A-11b})$$

$$\int_{-\infty}^{\infty} p(\gamma\pi f T^2) \exp\left[-j\left\{\frac{1}{\gamma}(\gamma\pi f T)^2 - 2\pi f t + \Delta\tau f\pi\right\}\right] df$$

$$\text{Let, } TT = T\sqrt{\gamma\pi} \exp\left[-j\left\{\frac{1}{\gamma}\left(\frac{t-\Delta\tau/2}{T}\right)^2 - \frac{\pi}{4} \operatorname{sgn} \gamma\right\}\right] \quad (\text{A-12})$$

$$g_1(t) = TT \int_{-\infty}^{\infty} p(\gamma\pi f T^2) \exp[-j\gamma(\pi f T)^2] \exp(j2\pi f t) \exp[-j2\pi f (\frac{\Delta\tau}{2})] df \quad (\text{A-13a})$$

$$g_1(t) = TT \int_{-\infty}^{\infty} p(\gamma\pi f T^2) \exp[j2\pi f (t - \frac{\Delta\tau}{2})] \left[1 + \sum_{n=1}^{\infty} \frac{(j\gamma T^2)^n}{2^n n!} (j2\pi f)^{2n}\right] df \quad (\text{A-13b})$$

Expanding in Taylor series the term, $\exp[-j\gamma(\pi f T)^2]$ we get,

$$\exp[-j\gamma(\pi f T)^2] = 1 + \sum_{n=1}^{\infty} \frac{(j\gamma T^2)^n}{2^n n!} (j2\pi f)^{2n} \quad (\text{A-14})$$

Which is in the form of an inverse Fourier transform, we obtain

$$g_1(t) = \frac{1}{T\sqrt{\pi\gamma}} \exp\left[-j\left\{\frac{1}{\gamma}\left(\frac{t-\Delta\tau/2}{T}\right)^2 - \frac{\pi}{4} \operatorname{sgn} \gamma\right\}\right] \times \left[P\left(-\frac{t}{\pi\gamma T^2}\right) + \sum_{n=1}^{\infty} \frac{(j\gamma T^2)^n}{2^n n!} \times \frac{d^{2n} P\left(-\frac{t}{\gamma\pi T^2}\right)}{dt^{2n}} \right] \quad (\text{A-15})$$

It can be easily seen that each term in the summation on the right-hand-side of (A-15) vanishes for increasing γ , as

$$\frac{d^{2n} p\left(-\frac{t}{\gamma\pi T^2}\right)}{dt^{2n}} = \left(\frac{-1}{\gamma\pi T^2}\right)^{2n} P^{(2n)}\left(\frac{-t}{\pi\gamma T^2}\right)$$

$$\text{where, } P^{(2n)}(f) \cong \frac{d^{2n} p(f)}{df^{2n}}$$

and then,

$$\lim_{\gamma \rightarrow \infty} \frac{(j\gamma T^2)^n}{2^{2n} n!} \frac{d^{2n} P(-\frac{t}{\gamma\pi T^2})}{dt^{2n}} = \lim_{\gamma \rightarrow \infty} \frac{1}{n!} \left(\frac{-j}{4\pi^2 \gamma T^2} \right)^2 P^{(2n)} \left(\frac{-t}{\pi\gamma T^2} \right) = 0 \quad (\text{A-15})$$

Which is found to be valid for $\gamma \gg \frac{1}{(\pi B_m T)^2}$, B_m being the input pulse bandwidth. Thus the output pulse $g_1(t)$ corresponding to the input pulse $p(t)$ with Fourier transform $P(f)$ can be approximated as,

$$g_1(t) \cong \frac{1}{T\sqrt{\pi\gamma}} \exp[-j\{ \frac{1}{\gamma} (\frac{t-\Delta\tau}{T})^2 - \frac{\pi}{4} \text{sgn } \gamma \}] P \left(\frac{-t}{\gamma\pi T^2} \right), \quad (\text{A-16})$$

for $\gamma(\pi B_m T)^2 \gg 1$

Considering the second term only:

$$g_{12}(t) \cong \frac{1}{T\sqrt{\pi\gamma}} \exp[-j\{ \frac{1}{\gamma} (\frac{t-\Delta\tau}{T})^2 - \frac{\pi}{4} \text{sgn } \gamma \}] \times -\frac{j}{4\pi^2 \gamma T^2} P^2 \left(\frac{t-\Delta\tau}{\gamma\pi T^2} \right) \quad (\text{A-17})$$

for $\gamma(\pi B_m T)^2 \gg 1$

Let us consider as an example, the input pulse $p(t) = \text{rect}(\frac{t}{T})$, to which corresponding approximate output pulse $g_1^a(t)$ given by,

$$g_1^a(t) = \frac{1}{\sqrt{\pi\gamma}} \exp[-j\{ \frac{1}{\gamma} (\frac{t-\Delta\tau}{T})^2 - \frac{\pi}{4} \text{sgn } \gamma \}] \sin c \left(\frac{t-\Delta\tau}{\gamma\pi T} \right) \quad (\text{A-18})$$

APPENDIX B

Coupled vector and pump-probe equations

In a dielectric medium where an external electric field is applied, the effective electric field $D(\mathbf{r}, t)$ is linked with the apparition of elementary bipolar moments $p(t)$ induced by the opposite movement of the equilibrium position of the linked charges. The macroscopic polarization field $P(\mathbf{r}, t)$ is the average bipolar moment per unit volume. The nonlinear response of the medium is expressed by a nonlinear polarization field P which satisfies the development,

$$P = \varepsilon_0 \bar{\chi}^{(1)} \cdot E + \varepsilon_0 \bar{\chi}^{(2)} : EE + \varepsilon_0 \bar{\chi}^{(3)} : EEE \quad (\text{B-1})$$

where $\bar{\chi}^{(i)}$ is the $(i+1)$ th tensor.

The amorphous characteristics of silica make all the even order nonlinear polarization zero. In particular, $\bar{\chi}^{(2)} = 0$, we will consider the terms of higher than 3rd order as negligible, we have than,

$$P = \varepsilon_0 \bar{\chi}^{(1)} \cdot E + \varepsilon_0 \bar{\chi}^{(3)} : EEE \quad (\text{B-2})$$

$$P_L(\mathbf{r}, t) \quad P_{NL}(\mathbf{r}, t)$$

Although $\bar{\chi}^{(3)}$ is small, it will be responsible for most of the nonlinear effects occurring during the electric field propagation. Highly confined in the core of the fiber, it will create high power densities. Moreover, the large interaction distances (around 20 km for a 0.2 dB/km attenuation) play a key role in the manifestation of the nonlinear effects.

Assuming that the instantaneous electronic response dominates for the XPM process, the third-order nonlinear polarization in a medium such as silica glass given by,

$$P^{(3)}(\mathbf{r}, t) = \varepsilon_0 \bar{\chi}^{(3)} : E(\mathbf{r}, t) E(\mathbf{r}, t) E(\mathbf{r}, t) \quad (\text{B-3})$$

where, $\tilde{\chi}^{(3)}$ is a measure of the instantaneous electronic response of the nonlinear medium.

In the case of two distinct optical fields propagating simultaneously inside an optical fiber, the total electric field can be written as,

$$\mathbf{E} = \text{Re}[\mathbf{E}_1 \exp(-i\omega_1 t) + \mathbf{E}_2 \exp(-i\omega_2 t)] \quad (\text{B-4})$$

where Re stands for the real part and \mathbf{E}_1 and \mathbf{E}_2 are the slowly varying (complex) amplitudes for the fields oscillating at frequencies ω_1 and ω_2 respectively.

Now writing $\mathbf{P}^{(3)}$ also in the same form as the electric field we get,

$$\mathbf{P}^{(3)} = \text{Re}[\mathbf{P}_1 \exp(-i\omega_1 t) + \mathbf{P}_2 \exp(-i\omega_2 t)] \quad (\text{B-5})$$

The nonlinear polarization at the pump and signal frequencies found to be,

$$\begin{aligned} \mathbf{P}_j(\omega_j) = & \frac{\epsilon_0 \chi_{1111}^{(3)}}{4} [(\mathbf{E}_j \cdot \mathbf{E}_j) \mathbf{E}_j^* + 2(\mathbf{E}_j^* \cdot \mathbf{E}_j) \mathbf{E}_j] + \\ & \frac{\epsilon_0 \chi_{1111}^{(3)}}{2} [(\mathbf{E}_m^* \cdot \mathbf{E}_m) \mathbf{E}_j + (\mathbf{E}_m \cdot \mathbf{E}_j) \mathbf{E}_m^* + (\mathbf{E}_m^* \cdot \mathbf{E}_j) \mathbf{E}_m] \end{aligned} \quad (\text{B-6})$$

where $j, m = 1, 2$ ($j \neq m$) and electronic response is assumed to be isotropic for the silica such that $\chi_{1111}^{(3)} = 3\chi_{1122}^{(3)} = 3\chi_{1212}^{(3)} = 3\chi_{1221}^{(3)}$

The two optical fields \mathbf{E}_1 and \mathbf{E}_2 evolve along the fiber length as dictated by the combination of GVD, SPM and XPM.

If we use (B-5) and (B-6) in the Maxwell equation [41], we find that \mathbf{E}_1 and \mathbf{E}_2 satisfy in the frequency domain a nonlinear Helmholtz equation of the form

$$\nabla^2 \tilde{\mathbf{E}}_j + \frac{\omega_j^2}{c^2} \tilde{\epsilon}_j(\omega) \tilde{\mathbf{E}}_j = -\frac{\omega_j^2}{\epsilon_0 c^2} \mathbf{P}_j \quad (\text{B-7})$$

where the tilde denotes Fourier transform ϵ_0 is the vacuum permittivity and $\tilde{\epsilon}_j(\omega)$ is the linear part of the dielectric constant resulting from the linear response of silica glass. Its tensorial nature is important to account for the PMD effects that have their origin in the birefringence of silica fibers, while its frequency dependence leads to chromatic dispersion.

Both $\tilde{\mathbf{E}}_1$ and $\tilde{\mathbf{E}}_2$ evolve along the fiber length. It is common to choose the z axis along the fiber axis and assume that $\tilde{\mathbf{E}}_1$ and $\tilde{\mathbf{E}}_2$ lie in the x - y plane. This assumption amounts to neglecting the longitudinal components of the two vectors and is justified in practice as long as the spatial size of the fiber mode is larger than optical wavelength. We follow the notation of [15] and employ the ket vector $|\tilde{\mathbf{A}}\rangle$ for representing a Jones vector polarized along the x - y plane. In this notation, two fields at any point \mathbf{r} inside the fiber can be written as,

$$\tilde{\mathbf{E}}_1(\mathbf{r}, \omega - \omega_1) = F_1(x, y) |\tilde{\mathbf{A}}_1(z, \omega - \omega_1)\rangle \exp[i\beta(\omega_1)z] \quad (\text{B-8})$$

$$\tilde{\mathbf{E}}_2(\mathbf{r}, \omega - \omega_2) = F_2(x, y) |\tilde{\mathbf{A}}_2(z, \omega - \omega_2)\rangle \exp[i\beta(\omega_2)z] \quad (\text{B-9})$$

where $F_1(x, y)$ and $F_2(x, y)$ represent the fiber mode field profile, $\beta(\omega_1)$ and $\beta(\omega_2)$ are propagation constants at the two carrier frequencies and the Jones vectors $|\tilde{\mathbf{A}}_1\rangle$ and $|\tilde{\mathbf{A}}_2\rangle$ are two-dimensional column vectors representing the two components of the electric field in the x - y plane. Since, $F_1(x, y)$ and $F_2(x, y)$ do not change with z , we only need to consider the evolution of $|\tilde{\mathbf{A}}_1\rangle$ and $|\tilde{\mathbf{A}}_2\rangle$ along the fiber.

Now substitute (B-8) and (B-9) back into (B-7) integrate over the transverse mode distribution in the x - y plane and assume that $|\tilde{\mathbf{A}}_1\rangle$ and $|\tilde{\mathbf{A}}_2\rangle$ to be slowly

varying function of z so that we can neglect their second-order derivatives with respect to z . The fiber mode profiles can be taken to be nearly the same for typical channel spacing i.e., $F_1(x, y) \approx F_2(x, y) \cong F(x, y)$, which amounts to assuming the same effective core area a_{eff} for the two channels. With these simplifications, the equation governing the evolution $|\tilde{A}_1\rangle$ and $|\tilde{A}_2\rangle$ taken the form,

$$\frac{\partial |\tilde{A}_j\rangle}{\partial z} + \left(\frac{\omega_j^2 \tilde{\epsilon}_j(\omega)}{2i\beta(\omega_j)c^2} + \frac{i}{2} \beta(\omega_j) \sigma_0 \right) |\tilde{A}_j\rangle = \frac{i\gamma_j}{3} \langle \tilde{P}_j \rangle_F \quad (\text{B-10})$$

where F denotes the average over the mode profile, σ_0 is a unit matrix and the nonlinear parameter at the carrier frequency ω_j is defined in the usual meaning and nonlinear coefficient γ_j is given by,

$$\gamma_j = \frac{n_2 \omega_j}{c a_{eff}} = \frac{3\omega_j^2 \chi_{1111}^{(3)}}{[8c^2 \beta(\omega_j) a_{eff}]} \quad (\text{B-11})$$

To proceed further, we write the dielectric constant tensor $\tilde{\epsilon}_j(\omega)$ in the basis of Pauli matrix as [18].

$$\left(\frac{\omega_j^2}{c} \right) \tilde{\epsilon}_j(\omega) = \left[\beta_j(\omega) + \frac{i\alpha_j(\omega)}{2} \right]^2 \sigma_0 - \beta_j(\omega) \mathbf{B}(\omega) \cdot \boldsymbol{\sigma} \quad (\text{B-12})$$

The vector $\boldsymbol{\sigma}$ is formed as $\boldsymbol{\sigma} = \sigma_1 \hat{e}_1 + \sigma_2 \hat{e}_2 + \sigma_3 \hat{e}_3$, where \hat{e}_1 , \hat{e}_2 and \hat{e}_3 are three unit vectors in the stokes space and the Pauli matrices are given as;

$$\sigma_1 = \begin{pmatrix} 1 & 0 \\ 0 & -1 \end{pmatrix} \quad \sigma_2 = \begin{pmatrix} 0 & 1 \\ 1 & 0 \end{pmatrix} \quad \sigma_3 = \begin{pmatrix} 0 & -i \\ i & 0 \end{pmatrix} \quad (\text{B-13})$$

The vector $\mathbf{B}(\omega)$ account for fiber birefringence. Its frequency dependence produces PMD.

If the channel bandwidth is not too large, we can assume $\alpha_j(\omega) \approx \alpha(\omega_j)$ and expand $\beta_j(\omega)$ and $B(\omega)$ around ω_j in Taylor series as,

$$\beta(\omega) \approx \beta_0(\omega_j) + \beta_1(\omega - \omega_j) + \beta_2 \frac{(\omega - \omega_j)^2}{2} + \dots \quad (\text{B-14})$$

$$B(\omega) \approx B(\omega_j) + (\omega - \omega_j)\delta + \dots \quad (\text{B-15})$$

Using these expansions in (B-12) and substituting them into (B-10) we obtain the following vector equation in the frequency domain,

$$\begin{aligned} \frac{\partial \langle \tilde{A}_j \rangle}{\partial z} = & \left[-\frac{\alpha_j}{2} + i\beta_1(\omega - \omega_j) + \frac{i\beta_2}{2}(\omega - \omega_j)^2 \right] \langle \tilde{A}_j \rangle \\ & - \frac{i}{2} [B(\omega_j) + (\omega - \omega_j)\delta] \cdot \sigma \langle \tilde{A}_j \rangle + \frac{i\gamma_j}{3} \langle \tilde{P}_j \rangle_F \end{aligned} \quad (\text{B-16})$$

Now we write (B-16) in the time domain by using $(\omega - \omega_j) \rightarrow i \left(\frac{\partial}{\partial t} \right)$, use the form of nonlinear polarization (B-6) and denote $B(z, \omega)$ as simply B_j . We obtain the following complete vector equation governing the XPM process in optical fiber,

$$\begin{aligned} \frac{\partial \langle A_j \rangle}{\partial z} = & -\beta_{1j} \frac{\partial \langle A_j \rangle}{\partial t} - \frac{i\beta_{2j}}{2} \frac{\partial^2 \langle A_j \rangle}{\partial t^2} - \frac{\alpha_j}{2} \langle A_j \rangle - \frac{i}{2} B_j \cdot \sigma \langle A_j \rangle + \frac{1}{2} \delta \cdot \sigma \frac{\partial \langle A_j \rangle}{\partial t} \\ & + \frac{i\gamma_j}{3} \left[2 \langle A_j | A_j \rangle + |A_j^* \rangle \langle A_j^* | + 2 \langle A_m | A_m \rangle + 2 |A_m^* \rangle \langle A_m^* | + 2 |A_m^* \rangle \langle A_m^* | \right] \langle A_j \rangle \end{aligned} \quad (\text{B-17})$$

where $j, m = 1, 2$ ($j \neq m$), $\omega_j, \beta_{1j}, \beta_{2j}$ and α_j are the optical carrier frequencies, inverse group velocities, GVD coefficient and fiber losses for the two channels. These parameters are generally z dependent for dispersion-managed periodically amplified systems.

In the Jones matrix notations, $\langle A |$ is the Hermitian conjugate while $|A^* \rangle$ is the complex conjugate of $|A \rangle$. The random vector $B_j = B(z, \omega)$ describes the residual fiber birefringence, while the vector σ has the Pauli matrices as its three

elements. Because of a frequency difference between the two channels, the state of polarizations (SOP) of the two channels evolve on the Poincare sphere at different rates as dictated by the magnitudes of B_1 and B_2 . The vector δ describe the intrachannel PMD effects resulting from random change in group velocities of the two polarization components of the channel and providing pulse broadening [15], [96]. The effects of both the SPM and XPM are included in (B-17) through the nonlinear parameter γ_j .

Equation (B-17) describes the XPM interaction between two channels in its most general form. It can be simplified considerably when we consider the pump-probe configuration and assume that the probe act as channel 2 and is in the form of a low-power continuous wave (CW), while the pump act as channel 1 and imposes the XPM-induced phase shift on channel 2. Two approximations can then be made to simplify the following analysis:

- (i) The probe is assumed to be weak enough that the XPM and SPM induced by it can be neglected.
- (ii) We neglect the δ term responsible for intrachannel PMD.

Although the above two terms broadens pulse in each channel, they barely affect the intrachannel XPM interaction because channel spacing typically is much larger than channel bandwidth and the evolution of the SOP of the channels is mainly governed by B . This approximation corresponds to the case when interchannel PMD dominates but intrachannel PMD is negligible. With these simplification (B-17) can be written in the following two equations:

$$\begin{aligned} \frac{\partial |A_1\rangle}{\partial z} = & -\beta_{11} \frac{\partial |A_1\rangle}{\partial t} - \frac{i\beta_{21}}{2} \frac{\partial^2 |A_1\rangle}{\partial t^2} - \frac{\alpha_1}{2} |A_1\rangle - \frac{i}{2} B_1 \cdot \sigma |A_1\rangle \\ & + \frac{i\gamma_1}{3} \left[2\langle A_1 | A_1 \rangle + |A_1^*\rangle \langle A_1^*| \right] |A_1\rangle \end{aligned} \quad (\text{B-18})$$

$$\begin{aligned} \frac{\partial |A_2\rangle}{\partial z} = & -\beta_{12} \frac{\partial |A_2\rangle}{\partial t} - \frac{i\beta_{22}}{2} \frac{\partial^2 |A_2\rangle}{\partial t^2} - \frac{\alpha_2}{2} |A_2\rangle - \frac{i}{2} \mathbf{B}_2 \cdot \boldsymbol{\sigma} |A_2\rangle \\ & + \frac{2\gamma_1}{3} \left[2\langle A_1 | A_1 \rangle + |A_1\rangle \langle A_1| + |A_1^*\rangle \langle A_1^*| \right] |A_2\rangle \end{aligned} \quad (\text{B-19})$$

The XPM induces not only a time dependent phase shift in the probe channel, but also a nonlinear polarization rotation of the probe channel [18].

However, both beat length ($L_B \approx 10m$) and correlation length ($L_c \approx 100m$) associated with residual birefringence are much shorter than the nonlinear length ($L_n > 10 km$ depending on the optical power). As a result, the polarization rotation induced by the residual birefringence is much faster than that induced by nonlinear polarization rotation (NPR). Rapid variation of SOP's average over the SPM and XPM effects in (B-19) and eventually the nonlinear PMD becomes negligible. Thus, we can average over such rapid polarization variations to study the evolution of XPM on a length scale much longer than the correlation length (L_c) by adopting a rotation frame through a unitary transformation $|A_j\rangle = \vec{T} |A'_j\rangle$, where the Jones matrix \vec{T} satisfies,

$$\frac{d\vec{T}}{dz} = -\frac{i}{2} \mathbf{B}_1 \cdot \boldsymbol{\sigma} \vec{T} \quad (\text{B-20})$$

The unitary matrix \vec{T} in (B-20) corresponds to random rotations of the Stokes vector on the Poincare sphere that do not change the vector length. In Jones space, an arbitrary unitary matrix can be written in the form

$$\vec{T} = \begin{pmatrix} a_1 & -a_2^* \\ a_2 & a_1^* \end{pmatrix} \quad (\text{B-21})$$

where $|a_1|^2 + |a_2|^2 = 1$. If we introduce a Jones vector $|a_1\rangle$ with its two elements a_1 and a_2 this vector satisfies,

$$\frac{d|a_1\rangle}{dz} = -\frac{i}{2} \mathbf{B}_1 \cdot \boldsymbol{\sigma} |a_1\rangle \quad (\text{B-22})$$

Since random residual birefringence makes all SOPs equally likely, $|a_1\rangle$ can be expressed in its most general form as

$$|a_1\rangle = e^{-\frac{i\varphi_0}{2}} \begin{pmatrix} \cos(\frac{\theta}{2}) e^{-\frac{i\varphi}{2}} \\ \sin(\frac{\theta}{2}) e^{-\frac{i\varphi}{2}} \end{pmatrix} \quad (\text{B-23})$$

where φ_0 and φ are uniformly distributed in the range $[0, 2\pi]$ and $\cos\theta$ is uniformly distributed in the range $[-1, 1]$. Thus, the most general form of the transformation matrix \bar{T} is given by,

$$\bar{T} = \begin{pmatrix} \cos(\frac{\theta}{2}) e^{-\frac{i(\varphi+\varphi_0)}{2}} & -\sin(\frac{\theta}{2}) e^{-\frac{i(\varphi+\varphi_0)}{2}} \\ \sin(\frac{\theta}{2}) e^{-\frac{i(\varphi-\varphi_0)}{2}} & \cos(\frac{\theta}{2}) e^{-\frac{i(\varphi-\varphi_0)}{2}} \end{pmatrix} \quad (\text{B-24})$$

We make the use of the following relation,

$$|A^*\rangle \langle A^*| = |A\rangle \langle A| - \langle A|\sigma_3|A\rangle \sigma_3 \quad (\text{B-25})$$

$$|A\rangle \langle A| = \frac{||A\rangle \langle A| + \langle A|\sigma|A\rangle \cdot \sigma}{2} \quad (\text{B-26})$$

Now (B-18) and (B-19) becomes,

$$\begin{aligned} \frac{\partial |A'_1\rangle}{\partial z} = & -\beta_{11} \frac{\partial |A'_1\rangle}{\partial t} - \frac{i\beta_{21}}{2} \frac{\partial^2 |A'_1\rangle}{\partial t^2} - \frac{\alpha_1}{2} |A'_1\rangle \\ & + \frac{i\gamma_1}{3} [3\langle A'_1|A'_1\rangle - \langle A'_1|\bar{T}'\sigma_3\bar{T}|A'_1\rangle \bar{T}'\sigma_3\bar{T}] |A'_1\rangle \end{aligned} \quad (\text{B-27})$$

$$\begin{aligned} \frac{\partial |A'_2\rangle}{\partial z} = & -\beta_{12} \frac{\partial |A'_2\rangle}{\partial t} - \frac{i\beta_{22}}{2} \frac{\partial^2 |A'_2\rangle}{\partial t^2} - \frac{\alpha_2}{2} |A'_2\rangle - \frac{i}{2} \Omega \mathbf{b} \cdot \sigma |A'_2\rangle \\ & + \frac{2i\gamma_2}{3} [2\langle A'_1|A'_1\rangle + \langle A'_1|\sigma|A'_1\rangle \cdot \sigma - \langle A'_1|\bar{T}'\sigma_3\bar{T}|A'_1\rangle \bar{T}'\sigma_3\bar{T}] |A'_2\rangle \end{aligned} \quad (\text{B-28})$$

where \mathbf{b} is related to \mathbf{B} by a rotation as,

$$b = \bar{R}^{-1} \frac{[B(z, \omega_2) - B(z, \omega_1)]}{\Omega} \equiv \bar{R}^{-1} \frac{dB}{d\omega} \quad (\text{B-29})$$

where \bar{R} is the three dimensional (3-D) rotation matrix in the Stokes space that is isomorphic to T in the Jones space *i.e.*, $\bar{R}\sigma = \bar{T}'\sigma\bar{T}$

We now average over (B-28) and (B-29) over θ , φ and φ_0 to obtain the evolution of the field on a length scale much longer than the birefringence correlation length. It can be also showed that

$$\langle \langle A_1 | \bar{T}' \sigma_3 \bar{T} | A_1 \rangle \bar{T}' \sigma_3 \bar{T} \rangle = \frac{1}{3} \langle A_1 | \sigma | A_1 \rangle \cdot \sigma \quad (\text{B-30})$$

Substituting (B-30) into (B-28) and (B-29) and using the reduced time as $\tau = (t - \beta_{12}z)$ as the new temporal variable and writing A_1 and A_2 instead of A_1' and A_2' respectively, we obtain the following two equations,

$$\frac{\partial |A_1\rangle}{\partial z} = -\delta\beta_1 \frac{\partial |A_1\rangle}{\partial \tau} - \frac{i\beta_{21}}{2} \frac{\partial^2 |A_1\rangle}{\partial \tau^2} - \frac{\alpha_1}{2} |A_1\rangle - i\varepsilon_1 P_0 |A_1\rangle \quad (\text{B-31})$$

$$\frac{\partial |A_2\rangle}{\partial z} = -\frac{i\beta_{22}}{2} \frac{\partial^2 |A_2\rangle}{\partial \tau^2} - \frac{\alpha_2}{2} |A_2\rangle - \frac{i}{2} \Omega b \cdot \sigma |A_2\rangle + \frac{i\varepsilon_2}{2} P_0 (3 + \hat{P} \cdot \sigma) |A_2\rangle \quad (\text{B-32})$$

where, $P_0 = \langle A_1 | A_1 \rangle$ is the pump power, $\hat{P} = \langle A_1 | \sigma | A_1 \rangle / P_0$ is the unit vector representing the SOP of the pump on the Poincare sphere, $\Omega = (\omega_2 - \omega_1)$ is the channel spacing, $\varepsilon_1 = 8/9\gamma_1$ and $\varepsilon_2 = 8/9\gamma_2$ are effective nonlinear parameters for the two channels, $\delta\beta_1 = (\beta_{11} - \beta_{12})$ group velocity mismatch between the two channels.

To study the temporal modulation of a CW probe field induced by the combination of XPM and PMD as a consequence of pump field, we have to solve the (B-31) and (B-32). We can linearize (B-32) by assuming that $|A_2\rangle = |A_{20}\rangle + |A_{21}\rangle$, where $|A_{20}\rangle$ and $|A_{21}\rangle$ are unperturbed and perturbed probe fields respectively and simply we obtain the equations (6.1), (6.2) and (6.3).

LIST OF PUBLICATIONS

a) Journal

1. **M. S. Islam** and S. P. Majumder, "Impact of Polarization Mode Dispersion on CPFSK Transmission Systems using MZI Based Direct Detection Receiver", *Journal of Optical Communications*, vol. 28, pp. 46-51, 2007, Germany.
2. **M. S. Islam** and S. P. Majumder, "Performance Limitations of an Optical Heterodyne Continuous Phase Frequency Shift Keying Transmission System Affected by Polarization Mode Dispersion in a Single Mode Fiber", *Optical Engineering*, vol. 46(6), pp. 065008-1- 065008-8, 2007, SPIE (The International society for Optical Engineering), USA.
3. **M. S Islam** and S. P. Majumder, "Bit Error Rate and Cross Talk Performance in Optical Cross Connect with Wavelength Converter", *Journal of Optical Networking*, vol. 6 no. 3 March 2007, pp. 295-303, USA.
4. **M. S. Islam** and S. P. Majumder, "Performance of Lincoded Optical Heterodyne CPFSK Transmission System Affected by Polarization Mode Dispersion", *IEEE Transactions on Communications*, submitted for publication, February 2008.
5. **M. S. Islam** and S. P. Majumder, "Performance Limitations of Optical Cross Connect without Wavelength Converter Due to Crosstalk", *Journal of Optical Communications*, submitted for publication, February 2008.

6. **M. S. Islam** and S. P. Majumder, "Analytical Performance Evaluation of an Adjustable PMD Compensator Using High-Birefringence Linearly Chirped FBG", *OPTIK - International Journal for Light and Electron and Optics*, submitted for publication, March 2008.
7. **M. S. Islam** and S. P. Majumder, "Performance of Line Codes in Optical Direct Detection Continuous Phase Frequency Shift Keying Transmission System Impaired by Polarization Mode Dispersion", *Journal of Modern Optics*, Submitted for publication, March 2008.
8. **M. S. Islam** and S. P. Majumder, "Influence Of Polarization Mode Dispersion on Cross-Phase Modulation in Intensity Modulation-Direct Detection WDM Transmission System", *Journal of Optics and Laser Technology*, Elsevier, Submitted for publication, March 2008

b) Conference

1. **M. S. Islam** and S. P. Majumder, "Performance Evaluation of an Optical Direct Detection CPFSK Transmission System Affected by Polarization Mode Dispersion", *Proceedings of Asia-Pacific Conference on Communications (APCC'06)*, 31 Aug. – 1 Sept. 2006, Busan, Republic of Korea.
2. **M. S. Islam** and S. P. Majumder, "Performance Limitations of an Optical IM-DD Transmission System Due to Polarization Mode Dispersion", *Proceedings of the SPIE Symposium on Optics East ITCOM*, 1– 4 October 2006, Boston, Massachusetts, USA.

3. **M. S. Islam** and S. P. Majumder, "Impact of Polarization Mode Dispersion on CPFSK Transmission Systems using MZI Based Direct Detection Receiver", *Proceedings of the IEEE INDICON 2006*, 15-17 September 2006, New Delhi, India.
4. **M. S. Islam** and S. P. Majumder, "Performance Limitations of an Optical Heterodyne CPFSK Transmission System Affected by Polarization Mode Dispersion in a Single Mode Fiber", *Proceedings of the IEEE INDICON 2006*, 15-17 September 2006, New Delhi, India.
5. **M. S Islam** and S. P. Majumder, "Effect of Polarization Mode Dispersion on Direct Detection CPFSK Optical Transmission System in a Single Mode Fiber", *Proceedings of tenth IEEE Conference on Communication Systems (IEEE ICCS 2006)*, 30 Oct. – 1 Nov., Singapore, 2006..
6. **M. S. Islam** and S. P. Majumder, "Analytical Performance Evaluation of an Optical Heterodyne CPFSK System Impaired by Polarization Mode Dispersion in a Single Mode Fiber", *Proceedings of the 4th International Conference on Electrical and Computer Engineering (ICECE 2006)*, 19-21 December 2006, Dhaka, Bangladesh
7. Ngee Thiam Sim, S. P. Majumder and **M. S. Islam**, "Bit Error Rate and Crosstalk Performance in Optical Cross Connect with Wavelength Converter", *Proceedings of the 4th International Conference on Electrical and Computer Engineering (ICECE 2006)*, 19-21 December 2006, Dhaka, Bangladesh

8. Ngee Thiam Sim, S. P. Majumder and **M. S. Islam**, "Bit Error Rate and Crosstalk Performance in Optical Cross Connect without Wavelength Converter", *Proceedings of International Conference on Information and Communication Technology (ICICT 2007)*, 7-9 March 2007, Bangladesh, pp.217-222, 2007.
9. **M. S. Islam** and S. P. Majumder, "Performance of Lincoded Optical Heterodyne CPFSK Transmission System Affected by Polarization Mode Dispersion in a Single Mode Fiber", *Proceedings of IEEE Global Communication Conference (GLOBECOM 2007)*, 26-30 November 2007, Washington DC, USA.
10. **M.S. Islam**, J.B. Alam and S.M.L. Kabir, "Satellite Based Internet Education Delivery and E-Learning Objects Evaluation: SOI Asia And Codewitz Perspective", *Proceeding of International Conference on Teaching and Learning (ICTL 2007)*, 14-16 November 2007, Malaysia
11. **M. S. Islam** and S. P. Majumder, "Optical Line Codes Tolerant to Polarization Mode Dispersion in a Direct Detection Continuous Phase Frequency Shift Keying Transmission System", *Accepted in 7th Asia-Pacific Symposium on Information and Telecommunication Technologies (APSITT 2008)*, will be held 22-24 April 2008, Bandos Island. Maldives.
12. **M. S. Islam** and S. P. Majumder, "Influence Of Polarization Mode Dispersion on the Effect of Cross-Phase Modulation in Intensity Modulation-Direct Detection WDM Transmission System", *Accepted in the International Conference on Computer and Communication Engineering (ICCCE 2008)*, will be held 13-15 May 2008, IIUM, Malaysia

13. **M. S. Islam** and **S. P. Majumder**, "Analytical Performance Evaluation of an Adjustable Polarization Mode Dispersion Compensator Using High-Birefringence Linearly Chirped Fiber Bragg Grating", *Accepted in the second International Conference on Communication and Electronics (HUT-ICCE 2008)*, will be held in 04-06 June 2008, Hanoi, Vietnam.

14. **M. S. Islam** and **S. P. Majumder**, "Analytical Performance Evaluation of a Tunable Polarization Mode Dispersion Compensator Based on High-Birefringence Linearly Chirped FBG in a WDM System", *Accepted in the SPIE Symposium on Optical Engineering and Applications*, will be held 10-14 August 2008 in San Diego, CA, USA.

